2018-05-07

Post-ictal hypoperfusion detected by CT Perfusion

Li, Emmy

UNIVERSITY OF CALGARY

Post-ictal hypoperfusion detected by CT Perfusion

by

Emmy Li

A THESIS

SUBMITTED TO THE FACULTY OF GRADUATE STUDIES

IN PARTIAL FULFILMENT OF THE REQUIREMENTS FOR THE

DEGREE OF MASTER OF SCIENCE

GRADUATE PROGRAM IN NEUROSCIENCE

CALGARY, ALBERTA

May, 2018

Abstract

Background: Seizures are often followed by a period of transient neurological dysfunction whereby sensory, cognitive, or motor abilities are impaired. Alterations in cerebral blood flow (CBF) during the postictal period has been proposed as a possible mechanism for this phenomenon. Recent animal studies have shown reduced local CBF at the seizure onset zone (SOZ) lasting up to one hour following seizures (Farrell, et al., 2016). Using arterial spin labeling magnetic resonance imaging (ASL MRI), we have observed postictal hypoperfusion at the SOZ in 75% of patients lasting up to one hour (Gaxiola-Valdez, 2017). The clinical implementation of ASL as a novel tool to identify the SOZ is hampered by the limited availability of MRI on short notice. Computed tomography perfusion (CTP) also measures CBF changes and may circumvent the logistical limitations of MRI.

Methods: Fifteen patients with drug resistant focal epilepsy admitted for pre-surgical evaluation were prospectively recruited and underwent CTP scanning within 80 min of a habitual seizure. Patients underwent a second scan in the interictal period after they were seizure-free for at least 24 hours. The acquired scans were visually assessed for perfusion differences and quantitatively assessed to identify areas of significant postictal hypoperfusion.

Results: Postictal reductions of >15 CBF units ($ml/100g^{-1}/min^{-1}$) were seen in 12/15 patients. In 10 of these patients, the location of the hypoperfusion was partially or fully concordant with the presumed SOZ, and all patients localized additional areas of seizure propagation concordant with their electroencephalography (EEG).

Conclusions: Postictal hypoperfusion can be measured by CTP. Thus, CTP has the potential to be a cost-effective and readily available tool in localizing the SOZ by measuring postictal CBF changes.

Acknowledgements

The work contained in this thesis represents the time, dedication, effort, and support of so many wonderful people and I am eternally grateful for all their help throughout this journey.

To my supervisor, Dr. Paolo Federico, thank you for all your guidance, support, and supervision. I am grateful for all the opportunities you have provided me and your support in both my academic and professional endeavors. You have been a wonderful mentor.

To Ismael Gaxiola, thank you for showing me the ropes around the lab and always being there to catch me during all my trials and tribulations of data collection.

To Chris d'Esterre, thank you for being so immensely generous with your time with me throughout my whole project. This project would not have been possible without all your insight and guidance. I've learnt so much from you.

To Ting Lee, thank you for taking the time to review so many CTP images with me and providing so much constructive insight and guidance throughout the pipeline development process.

To the clinical assistants, Dr. Salma Hanna and Dr. Ray Avendano, SMU staff and EEG techs, thank you for being so cooperative and supportive of this project during the data collection process.

To my wonderful lab mates, Negar Mohammadi for all the laughs we've had in the "Testoster-zone" in which we eventually changed to an "Estro-gym", and Daniel Pittman for all your enthusiastic input and incredibly educational and enjoyable learning sessions.

To my amazing family, your love and support is always felt. Luca and Patrick, you two are the best older brothers a little sis could ask for and the two of you are always a source of inspiration and giggles for me. To Jing Bai and Qing Li, my amazing parents, thank you for your

unwavering love, encouragement and support in all my endeavors. You make me stronger every day. To Rummy, the best doggo roommate, thanks for the snuggles and keeping my feet warm under the table when I worked late into the night.

And lastly, to my partner in crime, John Coburn, thank you for being an infinite pool of love and support in my life, catching me when I fell both emotionally and physically, and chasing me with a gigantic snowball.

Dedication

To my parents,

You’re the strongest people I know.

Table of Contents

List of Tables

List of Figures and Illustrations

List of Symbols, Abbreviations and Nomenclature

Symbol	Definition
ADC	Apparent Diffusion Coefficient
ASD	Anti-Seizure Drug
AIF	Arterial Input Function
ANTs	Advanced Normalization Tools
ASL	Arterial Spin Labeling
BET	Brain Extraction Tool
CBF	Cerebral Blood Flow
CBF	Cerebral Blood Volume
COX-2	Cycloxygenase-2
CT	Computed Tomography
CTP	Computed Tomography Perfusion
DWMRI	Diffusion-Weighted Magnetic Resonance Imaging
EEG	Electroencephalography
EZ	Epileptogenic Zone
FDG	[F^{18}]-Fluorodeoxyglucose
FLAIR	Fluid-Attenuation Inversion Recovery
FLIRT	FMRIB's Linear Image Registration Tool
FSL	Software: FMRIB Soft Library
FWHM	Full Width at Half Maximum
HU	Hounsfeld Units
IED	Interictal Epileptiform Discharge
ILAE	International League Against Epilepsy
IMF	Impulse Residue Function
Lt	Left
MEG	Magnetoencephalography
MRI	Magnetic Resonance Imaging
MTT	Mean Transit Time
NET	Neuroepithelial Tumor
PET	Positron Emission Tomography
PS-BBB	Permeability Surface Area Product of the Blood Brain Barrier
Pt.	Patient
rCBF	Relative Cerebral Blood Flow
rCBV	Relative Cerebral Blood Volume
ROI	Region-of-Interest
Rt	Right
sASL	Subtraction ASL
sCTP	Subtraction CTP
SOZ	Seizure Onset Zone
SPECT	Single Photon Emission Computed Tomography
TDC	Time Density Curve

TLE	Temporal Lobe Epilepsy
Tmax	Time to Maximum
TTP	Time to Peak
VEEG	Video-EEG Monitoring
VNS	Vagal Nerve Stimulation
VOF	Venous Output Function

CHAPTER 1: General Introduction

1.1 Epilepsy

1.1.1 The Epileptogenic Zone (EZ) and Identifying the Seizure Onset Zone (SOZ)

Epilepsy is a neurological disorder which is diagnosed in patients who experience two or more unprovoked seizures at least 24 hours apart. Epileptic seizures are a result of hyperexcitable and hypersynchronous neuronal activity. Epilepsy is among the most common and serious neurological disorders in the world and affects approximately 100,000 Canadians. (Hauser et al., 1990). Out of those affected, approximately 30% do not respond to anti-seizure medications and must live with drug-resistant (intractable) epilepsy (Sillanpaa, 2000). In these cases, the most effective intervention is surgical removal of the epileptogenic zone (EZ)

The EZ is clinically defined as the cortical regions responsible for generating seizures, but practically identified as the brain area which when removed, renders a patient seizure-free following epilepsy surgery. However, defining its precise location is a difficult task. The most important pre-surgical marker of the EZ is the seizure onset zone (SOZ), the brain area where seizures begin. Extensive surgical investigations have lead researchers to regard the SOZ and the EZ as two separate concepts (Luders, et al., 2006). The EZ can include an actual EZ, the cortical area generating seizures before surgery (it is equivalent or smaller than the actual SOZ); and a potential EZ, the area of cortex that may generate seizures after the pre-surgical SOZ has been resected. The dominant challenge in achieving post-operative seizure freedom is the removal of both (Fig. 1.1). Because the potential EZ only becomes clinically apparent postoperatively, there is no diagnostic modality currently available that can directly measure the entire EZ. Thus, the location of the EZ must be indirectly inferred by defining other cortical zones.

In addition to the SOZ and the delineation of the actual and potential EZ, there are other regions of importance when localizing the source of a person's seizures: the irritative zone, the region of cortex that generates interictal epileptiform discharges that can be recorded via electroencephalography (EEG) or magnetoencephalography (MEG), the symptomatogenic zone, the region of cortex that generates seizure symptoms, and epileptogenic lesion(s), which are structural lesion(s) that are causative of the epileptic seizures (Fig. 1.2) (Rosenow and Luders, 2001). Even with surgical intervention, many forms of epilepsy (e.g., extratemporal, parietal, occipital) have a success rate of less than 50% in achieving seizure freedom due to incomplete identification and removal of the SOZ and EZ (Tellez-Zenteno, et al., 2005). Indeed, the thorough and accurate localization of the SOZ remains an imperative component of diagnosing and surgically treating epilepsy.

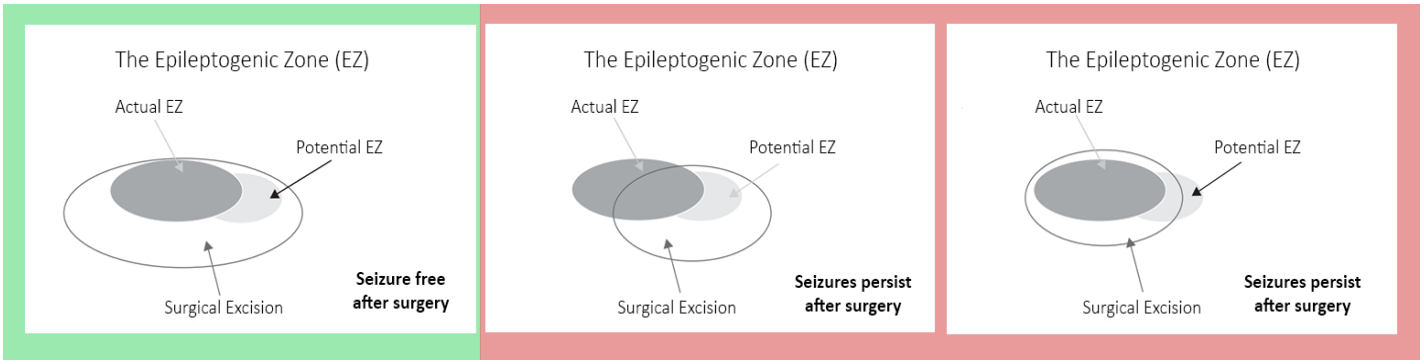

Figure 1.1: The epileptogenic zone (EZ) can be divided into the actual EZ and the potential EZ. Complete resection of both regions should result in seizure-freedom. Incomplete resection of the actual EZ, or the potential EZ will not result in seizure-freedom. (Luders, et al., 2006).

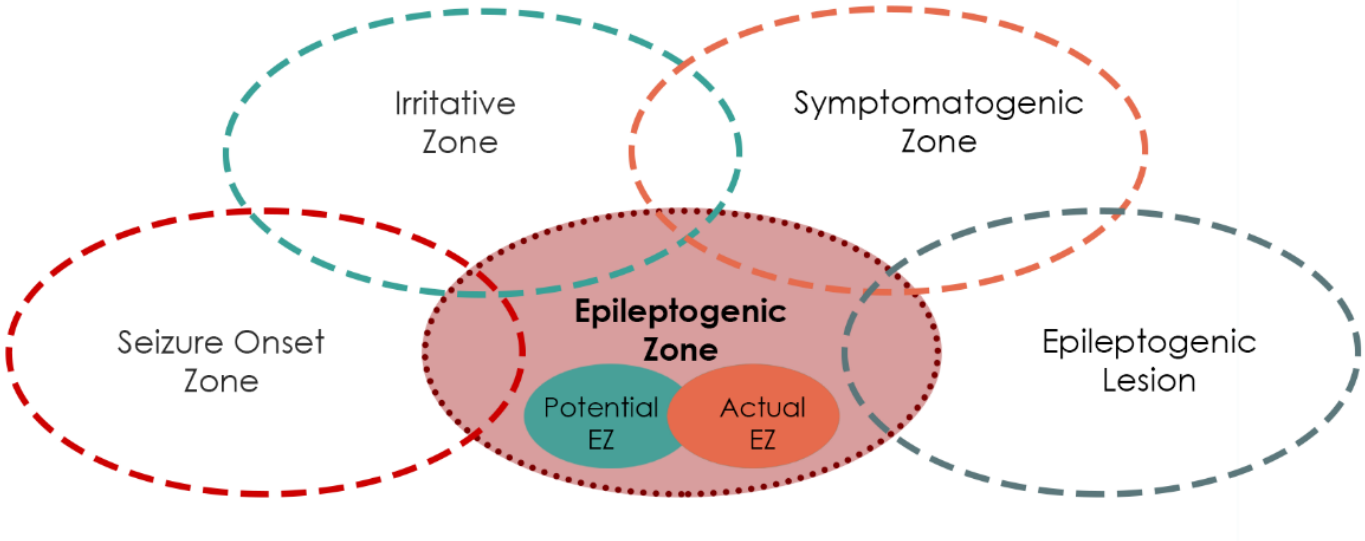

Figure 1.2: The epileptogenic zone is the area of cortex that is indispensable for the generation of epileptic seizures. Because the epileptogenic zone cannot be directly measured using currently available diagnostic modalities, the location of the EZ is indirectly inferred by defining the other cortical zones mentioned.

1.1.2 Pathophysiology of Epilepsy

Seizure initiation is characterized by high-frequency bursts of action potentials and hypersynchronization of a neuronal population (Bromfield, 2006). Epilepsy is associated with the presence of brief interictal spikes or electrographic activity lasting less than 250 milliseconds. It requires 20 cm^2 of synchronous cortical activation to generate a measurable sharp potential change seen using EEG (Tao, et al., 2007; Tao, et al., 2005). At the level of single neurons, epileptiform activity is characterized by 1) sustained neuronal depolarization resulting in a burst of action potentials, 2) a plateau-like depolarization with completion of the action potential burst, and 3) a rapid repolarization followed by hyperpolarization (Bromfield, 2006). This sequence is termed the paroxysmal depolarizing shift. The prolonged depolarization results in an influx of extracellular calcium current which leads to the opening of voltage-dependent sodium channels. This activation of voltage-dependent sodium channels leads to the influx of sodium ions and ultimately the generation of repetitive action potentials. The hyperpolarization that follows is mediated by GABA receptors and chlorine ion influx, or by potassium ions efflux depending on the cell type (Bromfield, 2006). It is the synchronized bursts from many neurons that result in a spike or sharp wave on EEG.

1.1.3 Classification of Epilepsy and Seizures

The etiology of epilepsy has been categorized by the International League Against Epilepsy (ILAE) into six general categories; genetic, structural, metabolic, immune, infectious, or unknown (Berg, et al., 2010). Epilepsies are classified as genetic when seizures are caused directly by a genetic abnormality, which could be inherited or attributed to environmental factors. A structural etiology is concluded when visible abnormalities, as seen through

neuroimaging (e.g., MRI), is concordant with EEG recordings of seizure events. Metabolic epilepsies are related to biochemical changes that increase the risk of seizures, such as uremia (build-up of urea in the blood). Epilepsy resulting from an immune disorder is concluded when evidence of autoimmune-mediated CNS inflammation is found. Particularly in developing nations, infections can be a common cause of epilepsy where infection of the CNS can lead to both acute and chronic seizures. Lastly, in cases where epilepsy does not fall into one of these categories, it is classified as an unknown etiology.

In addition to the classifications of epilepsy, most epileptic seizures can be further divided into generalized or focal seizures (Fisher, et al., 2017) (Fig. 1.3). Generalized seizures originate and rapidly spread within both cerebral hemispheres, and seizure onset localization and lateralization are inconsistent. In contrast, focal seizures are generated from a limited area of the brain and within one hemisphere; however, focal seizures may evolve to bilateral hemispheric involvement and secondarily generalize to encompass the entire brain. These seizures are referred to as focal to bilateral tonic-clonic and reflects the propagation pattern of seizure activity rather than a unique seizure type. Some seizures are of unknown origin or unclassifiable. The scope of this thesis will focus primarily on focal seizures.

Focal epilepsy is further classified based on the lobe in which the seizures are originating from such as frontal, temporal, parietal, or occipital lobe epilepsy. Depending on the seizure origin and area of spread, focal seizures may result in varying degrees of impairment. Thus, focal seizures can be further classified based on level of awareness. In the context of seizures, awareness is clinically defined as knowledge of self and environment during a seizure. If awareness of the event is impaired for any portion of the seizure, the seizure is classified as a

focal seizure with impaired awareness. In contrast, a focal aware seizure implies that awareness is retained during the seizure.

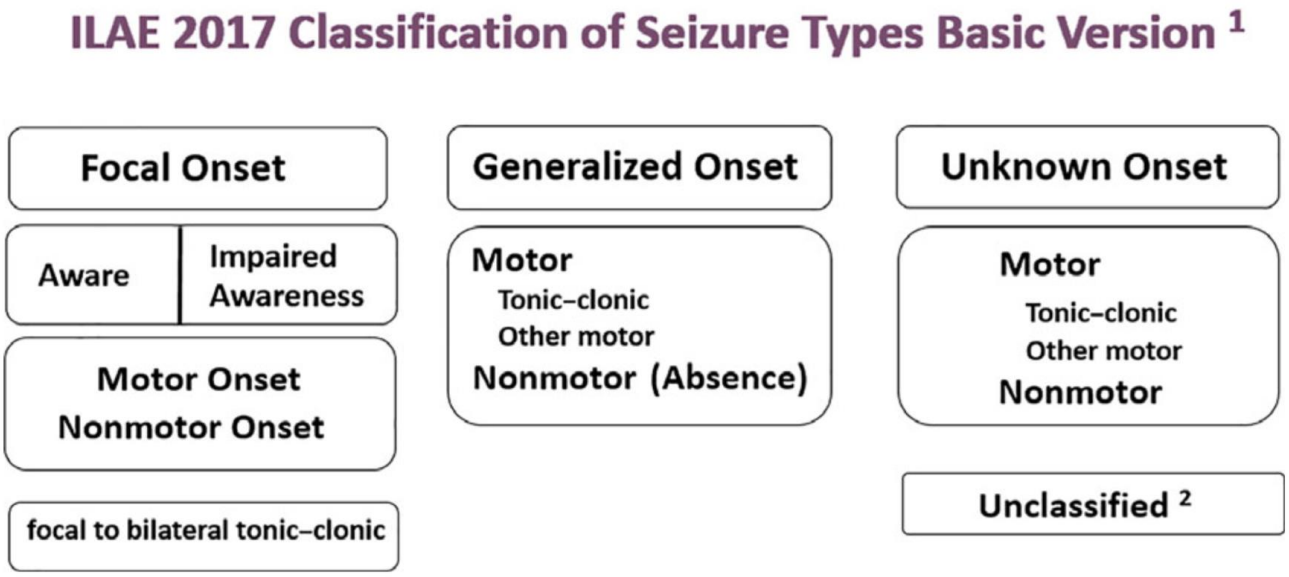

Figure 1.3: The basic ILAE 2017 operational classification of seizure types. Adapted from Fisher RS, et al., (2017).

1.1.4 Treatment of Epilepsy

1.1.4.1 Anti-Seizure Drug (ASDs)

The initial therapy for patients with epilepsy is treatment with one or more anti-seizure drugs (ASDs). The type or combination of ASDs used to control an individual's seizures primarily depends on the patient's seizure type, drug tolerance, and other factors including side effects, cost, and drug availability. ASDs primarily reduce seizure frequency by modulating excitatory and inhibitory neurotransmission to control the excessive and synchronous firing of neurons during epileptic events. Mechanisms of action include the enhancement of GABAergic inhibition, inhibition of sodium channels to decrease neuronal excitation, inhibition of neurotransmitter release by suppression of presynaptic calcium channels, and alteration of glutamate levels (Duncan, et al., 2006).

Unfortunately, ASDs do not reduce or eliminate seizures in approximately 20-30% of patients. Drug resistance can be due to numerous factors and remains a field of active investigation. It is estimated that approximately 60% of all drug resistance cases occur in patients with focal epilepsy (Regesta and Tanganelli, 1999). When two or more ASDs fail to control seizure activity, the patient is considered to have intractable epilepsy, and epilepsy surgery may be considered.

1.1.4.2 Epilepsy Surgery and Outcomes

For individuals with intractable epilepsy, surgery is a widely accepted and relatively effective therapeutic option. Surgical procedures for epilepsy commonly include resections (temporal resections, hemispherectomy), and disconnection procedures (corpus callosotomy, multiple subpial transections) (Noachtar and Borggraefe, 2009). For successful surgical treatment, it is critical to identify the full extent of the SOZ as precisely as possible. Being the area of cortex

that is indispensable for the generation of epileptic seizure, the total removal or disconnection of the EZ is necessary to obtain seizure-freedom (Rosenow and Luders, 2001).

Surgical resection of the SOZ remains the preferred procedure in individuals with intractable epilepsy, especially in cases where localization investigations are convergent. Although postoperative seizure freedom depends on complete removal of the SOZ (and ultimately the EZ), the planned extent of the resection may conflict with important cerebral structures. In these cases, the retention of neurological and cognitive functions post-operatively remains a primary goal and surgical plans may be altered in order to spare risk of damage to, or removal of, eloquent tissue.

Disconnection procedures are generally introduced as a surgical option for patients with symptomatic generalized epilepsy or cases where the EZ lies in functionally essential cortex that cannot be resected (Abou-Khalil, 2010; Noachtar and Borggraefe, 2009). These procedures function by disrupting horizontal connections, thus slowing, and in some cases fully preventing inter-hemispheric propagation and generalization of seizure activity. This can theoretically preserve neurological function during an ictal event (Spencer and Huh, 2008). For patients experiencing drop attacks, a sudden loss of posture and consciousness, a corpus callosotomy is a very effective treatment (Maehara and Shimizu, 2001). Although disconnection procedures have been shown to reduce seizure frequency, many studies continue to report disconnection procedures as predominantly being palliative therapy as patients rarely are completely free of seizures after long-term follow up (Asadi-Pooya, et al., 2008; Rosenow and Luders, 2001). Additionally, the variability in magnitude of disconnection, targeted seizure types, and criteria for seizure freedom produces variable statistics, making it difficult to systematically evaluate post-operative seizure freedom.

Systemic reviews suggest that 66-70% of patients are seizure free within the first 5 years; however, 15-20% of patients have relapses after initial seizure freedom at 5-10 years after surgery and require reoperation (Engel, et al., 2003). Even after a second surgery, only about 39-57% of patients remain seizure free in the long term (>5 years) (McIntosh, et al., 2004). Although these recurrences may be attributed to imprecise localization and incomplete removal of the SOZ, a growing theory is that postoperative seizure freedom is correlated to the duration of epilepsy; in a study done in 2005, authors found that 90% of patients who had epilepsy for less than 10 years became seizure free postoperatively, whereas only about 30% of those who had epilepsy for more than 30 years became seizure free after surgical intervention (Janszky, et al., 2005). The concern that recurrent seizures may have detrimental effects on the brain similar to kindling and secondary epileptogenesis has led to a global movement towards earlier surgical intervention (Noachtar and Borggraefe, 2009).

In summary, it is currently believed that surgical failures are attributed to incomplete resection of lesions, erroneous identification of epileptogenic regions, generation of new epileptogenic zones, and/or the resected areas having been limited to minimize risk of functional impairment.

1.1.4.3 Implanted Devices

When ASDs are ineffective at controlling seizure activity and patients are not candidates for surgical procedures, an approved treatment is vagal nerve stimulation (VNS), a process of applying electrical pulses via an implanted device. This cervical nerve has widespread connections throughout the brain, and its stimulation has been shown in clinical trials to reduce

seizures by at least 50% in 42.7% of patients, after three years of use (Morris and Mueller, 1999).

Recent investigations have explored deep brain stimulation of the anterior thalamic nucleus or hippocampus, as an alternative treatment method for intractable epilepsy. In an 11-year study period, researchers found 13.8% of participants were seizure-free for at least 12 months (Kim, et al., 2017).

1.1.5 Neuroimaging of Epilepsy

The results of epilepsy surgery depend on how well the EZ and SOZ can be identified and how completely it can be removed without resecting eloquent cortex. The pre-surgical evaluation is predominantly non-invasive and involves a combination of techniques such as EEG, video-EEG monitoring (VEEG), MRI, positron emission tomography (PET) and SPECT.

1.1.5.1 Electroencephalography (EEG) and Video-Electroencephalographic Monitoring (VEEG)

Despite the advances and development of other diagnostic techniques, EEG continues to be the gold standard for functional localization of the SOZ. EEG remains to be the most convenient and least expensive way to show the areas of excitability in the brain during ictal events (Pedley, Mendiratta, & Walczak, 2003). Interictal epileptiform discharges (IEDs) measured by EEG play a fundamental role in the understanding of the physiology of epilepsy, along with its diagnosis, classification, prognosis, and treatment. IEDs are defined as a unique pathological pattern of activity that occurs between seizures in patients with epilepsy; these patterns are clearly distinguished from the activity observed during the seizures itself. IEDs are highly correlated with epilepsy and are rare in EEGs of persons without a history of seizures.

Although the patterns of IEDs have been well characterized to date, when analyzed alone, EEG lacks the spatial resolution necessary for surgical planning. To remedy this, video-electroencephalographic monitoring (VEEG) is used, which greatly enhances the diagnostic power of EEG. Video is recorded concurrently with EEG, providing a record of the overt clinical manifestations of the epileptic events, in the same temporal resolution as the electrographic changes. VEEG is often used diagnostically in combination with additional clinical investigations such as ictal SPECT (described below), which can provide important clues towards the location of the SOZ.

In cases where non-invasive results are inconclusive, invasive implantation of intracranial electrodes may provide additional information regarding the localization and extent of the EZ. Intracranial electrodes have great sensitivity and can record signals from areas that do not generate a sufficiently strong signal for scalp electrode detection. Additionally, because the electrodes are directly placed on the cortex, the EEG signals are not attenuated nor refracted by the skull, scalp, or other neural tissue. Because these spatial averaging effects are eliminated, and due to their sensitivity, intracranial electrodes have advantages over scalp electrodes in their ability to detect seizures earlier, more often, and with improved localizing accuracy. However, intracranial electrodes are accompanied with some disadvantages, including surgical risk for the patient. The electrodes are also limited in the amount of cortical surface or volume from which they can detect signals, which stresses the importance of correct placement of the electrodes, as distant signals may not be detected.

1.1.5.2 Structural Imaging (MRI)

A high-resolution MR scan is conventionally used to investigate the presence of potential epileptogenic lesions such as hippocampal sclerosis and cortical dysplasia (Fig. 1.4). For patients with epilepsy being considered for surgery, the anatomical relationship of the EZ to a lesion is crucial information to physicians and surgeons. If a structural lesion is found, and its location is consistent with information pertaining to the SOZ from other investigations (EEG, SPECT), removal of the lesion may be sufficient to control seizures (Noachtar and Borggraefe, 2009). However, only approximately 25% of patients with epilepsy have some form of structural lesion or abnormality (Berkovic, et al., 2006); the majority of patients with epilepsy do not have a known epileptogenic lesion or genetic abnormality. The outcome of achieving post-surgical seizure freedom in patients with normal MRI is significantly worse (Immonen, et al., 2010). The lack of any MR findings makes localization especially challenging for patients with refractory temporal lobe epilepsy (TLE), and is often a predictor of surgical failure (Bien, et al., 2009). In a retrospective study investigating the long-term seizure outcomes following epilepsy surgery, 70-90% of TLE patients with abnormal MRI findings obtained post-surgical seizure freedom. In contrast, only 34-45% of TLE patients with non-lesional MRI scans obtained seizure freedom following surgery (Tellez-Zenteno, et al., 2005). Although non-lesional patients with epilepsy can still benefit from epilepsy surgery, more work is necessary in the pre-surgical investigations to identify the indications for surgery in patients with normal MRIs.

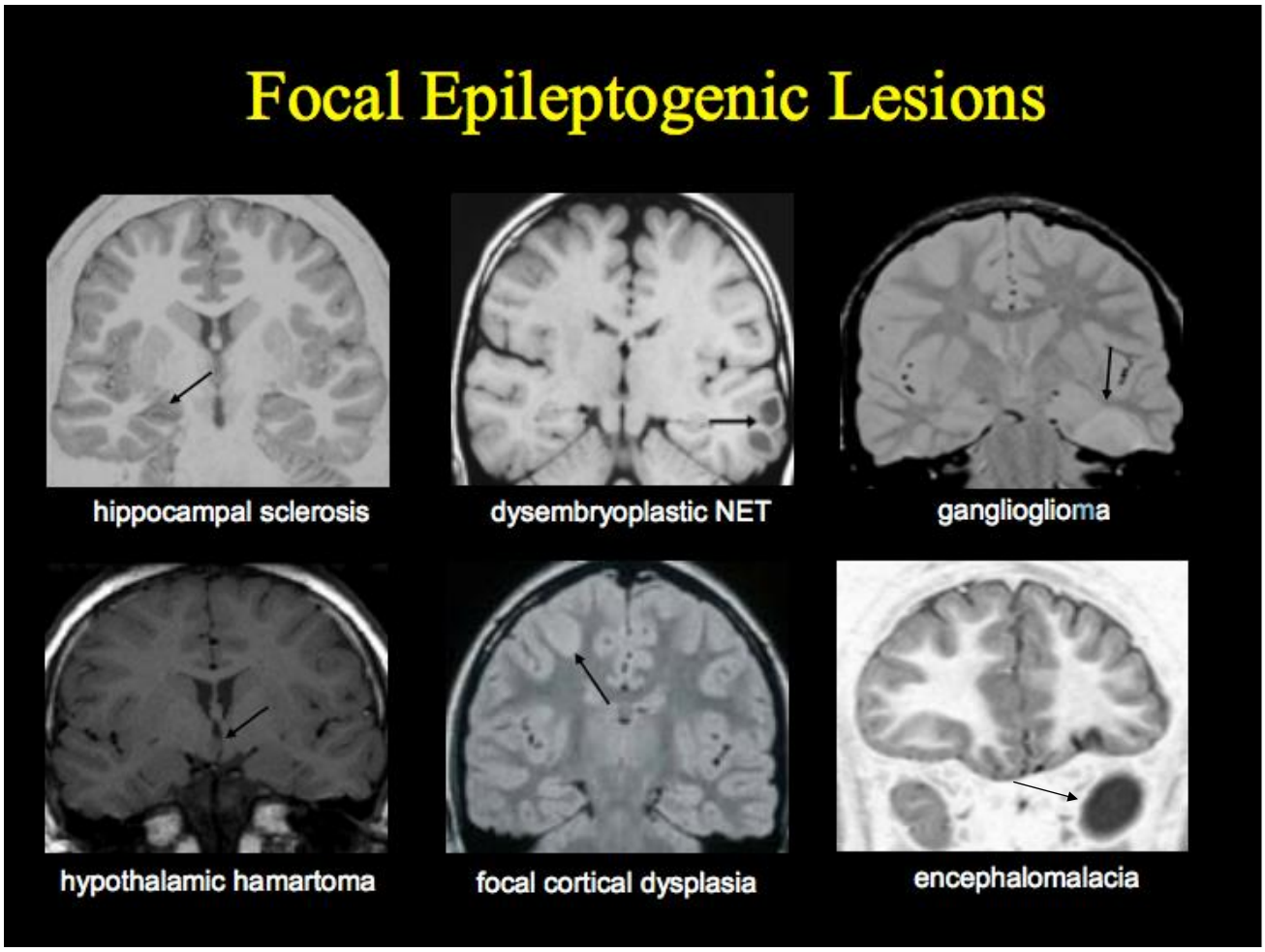

Figure 1.4: Examples of epileptogenic lesions as detected by MRI. Abbreviation: NET = Neuroepithelial Tumor

1.1.5.3 Single Photon Emission Computer Tomography (SPECT)

Changes in cerebral blood flow (CBF) corresponding to the suspected SOZ as detected by SPECT have been a widely observed and established phenomenon (Newton, et al., 1992; Stefan, et al., 1990). In 1939, researchers found that cortical stimulation was associated with temporary local increases in CBF (Penfield, 1939). Because increased neuronal activation during a seizure is accompanied by a relative increase in CBF, measuring cerebral perfusion has become a widely-accepted method for localizing the SOZ (Duncan, et al., 1992). States of cerebral hyperperfusion during the ictal periods and hypoperfusion during the interictal periods have been reported to correlate with the SOZ as identified by EEG (Otsubo, et al., 1995; Rowe, et al., 1991).

An ictal or interictal SPECT involves using a gamma-emitting radiotracer that crosses the blood brain barrier and emits gamma rays that can be seen through a gamma-camera. Ictal SPECT assumes that increased neuronal activity at the SOZ is associated with increased metabolism, and thus increased blood flow through cerebral auto-regulation and therefore increased tracer uptake (la Fougere, et al., 2009). Because of the transient nature between ictal and postictal perfusion patterns (Duncan, 2004), the injection of the radioactive tracer must be administrated as close (~30 s) to the start of a seizure as possible, when cerebral hyperperfusion most accurately reflects the area of seizure origin (Goffin, et al., 2008). Although there have been encouraging investigations into automatic and remote controlled ictal SPECT injections, this technology is not readily available to many medical institutions, and SPECT remains to be a labor-intensive and costly investigative procedure (Feichtinger, et al., 2007).

The role of interictal SPECT is to aid interpretation of ictal SPECT studies by providing a baseline for visual comparison or image subtraction. The SOZ may also exhibit hypoperfusion

between seizures (la Fougere, et al., 2009). A major benefit of SPECT is that once the tracer has been injected at seizure onset, it remains stable for many hours even after seizure termination. This allows image acquisition to take place after the patient has recovered and can easily submit for scanning. The acquired images will show the pattern of perfusion at the time of injection and consequently during the ictal event. The validity of ictal SPECT as a diagnostic tool in epilepsy has been long confirmed; the epileptic focus was correctly identified using ictal SPECT in over 500 patients with unilateral temporal lobe epilepsy as demonstrated by other clinical investigations (Rowe, Single-photon-emission Computer Tomography in Epilepsy, 2005).

1.1.5.4 Positron Emissions Tomography (PET)

Similar to SPECT, PET involves the injection of a radiotracer, [F^{18}]-fluorodeoxyglucose (FDG), a glucose analog, to measure brain metabolism instead of CBF. PET is most often clinically used interictally. Most studies have demonstrated interictal hypometabolism in 70-80% of patients with complex partial seizures corresponding with the epileptic focus (Abou-Khalil, et al., 1987; Engel, et al., 1982) (Theodore, 1992). Ictal PET studies show hypermetabolism however, these results are often viewed with more skepticism. A seizure is a short event compared to the total FDG uptake period of 30-45 minutes; thus, the "ictal" PET scans would include interictal, ictal, and postictal data. Thus, the metabolic activation captured from an ictal PET may represent regions beyond the ictal focus and presumably display propagation of the seizure.

1.1.6 Postictal Vascular Changes

Postictal dysfunction following epileptic seizures includes both transient and reversible manifestations that can last from minutes to days, these typically being motor, behavioral and

cognitive (Fisher and Schachter, 2000). Although the mechanisms that lead to these states are unclear, they can provide insight into the localization of the SOZ. There are multiple theories to explain the postictal state including alterations in local CBF, neurotransmitter depletion, neuronal desensitization, or other forms of inhibition not yet fully elucidated (Fisher and Schachter, 2000; Weinand, et al., 1997). Of these, altered local CBF postictally is currently the most widely accepted hypothesis.

The hemodynamic changes associated with postictal states have long been observed both clinically and experimentally (Meldrum and Nilsson, 1976) (Penfield, Santha, & Cipriani, 1939) (Meyer & Portnoy, 1959). In 1933, authors have hypothesized that the regions hypoperfused postictally might represent the seizure discharging area, or areas peripheral to it. These early studies used thermoelectric probes for absolute quantitative measurements of local blood flow and consistently found postictal decreases in blood flow surrounding the probe and established the basis of future postictal perfusion studies.

1.1.6.1 Cerebral Angiography

By the 1970s, cerebral angiography had been reliably established to describe flow abnormalities in a number of pathological processes; but it wasn't until 1974 that convulsive seizures were conclusively shown to be a disorder involving abnormal CBF (Farrell and Taveras, 1974). Researchers postulated that focal epileptic discharges lead to local vasomotor alterations and/or metabolic changes. These changes are associated with prolonged functional arterial venous shunting and cortical ischemia, that is manifested in forms of transient postictal disabilities. Subsequent studies revealed that in addition to flow abnormalities observed during

the ictal state, postictal neurological deficits such as Todd's paresis were also correlated with early veins and vascular staining (Yarnell, 1975) (Fig. 1.5).

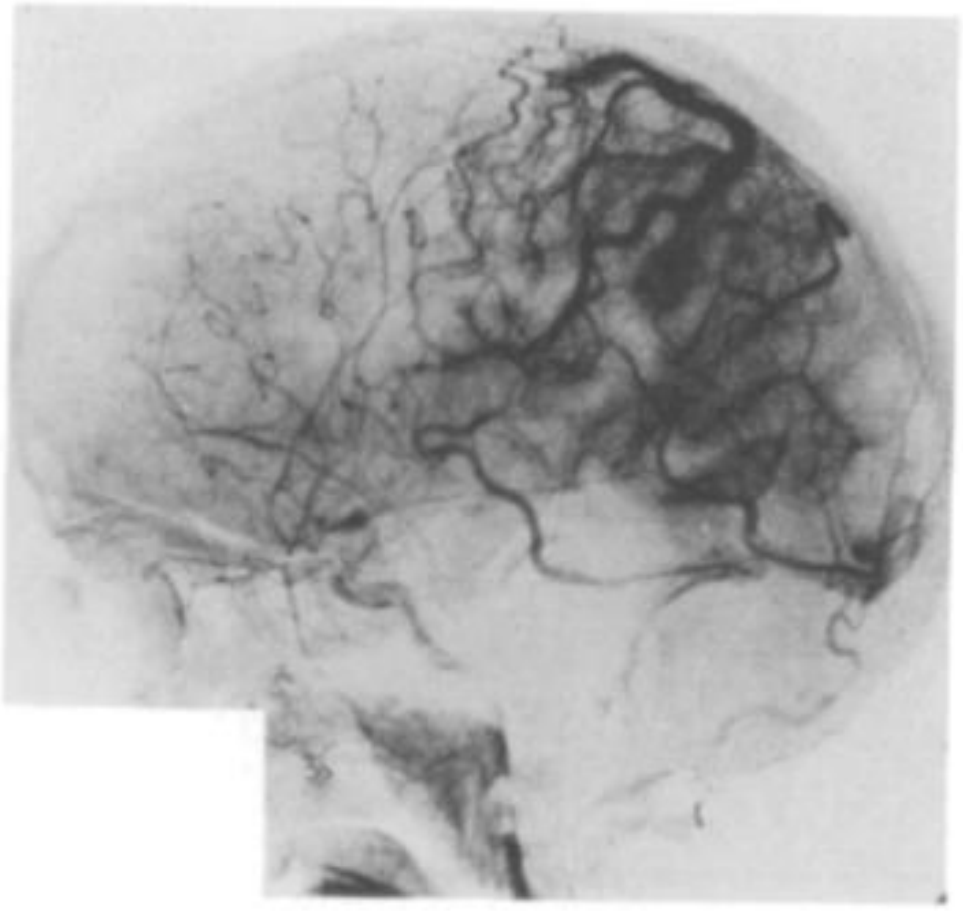

Figure 1.5: Left lateral carotid angiogram subtraction technique. Parietal area shows vascular staining with prominent early venous drainage for a 19-year old admitted because of several days' duration of right-sided focal and generalized seizures (Yarnel, 1975).

1.1.6.2 Postictal Single Photon Emission Computed Tomography (SPECT)

The investigation of postictal vascular changes continued with the development of advanced technologies, such as SPECT, to quantitatively measure CBF. Ictal studies using SPECT added legitimacy to the notion that CBF changes were present during a seizure, and soon postictal SPECT became more heavily investigated. During postictal SPECT, a tracer is injected as soon as practically possible after a seizure, and image acquisition generally follows within 2-3 hours. Unlike ictal SPECT, postictal SPECT studies reveals a significantly less extensive area of hyperperfusion. Early postictal SPECT studies produced conflicting results and revealed a combination of postictal hyperperfusion and hypoperfusion in patients with temporal lobe epilepsy (Duncan, et al., 1993; Rowe, et al., 1991). In a small group of patients, hyperperfusion was confined to the mesial regions and was largely unilateral (Rowe, et al., 1991). The majority of patients displayed patterns of lateral cortical hypoperfusion during the postictal stage. Unlike ictal SPECT investigations, little focal hypoperfusion was seen overall. The regions of hypoperfusion commonly extended beyond the temporal lobe, and often included the parietal and frontal regions (Rowe, et al., 1991).

Subsequently, investigators sought to explain the varying postictal perfusion results by studying the dynamic and transient nature of blood flow. In a follow-up study (Newton, et al., 1992), temporal lobe seizures were analyzed; researchers observed a constant pattern of unilateral global increases in temporal lobe perfusion during seizures, which quickly evolved to a pattern of relative mesial temporal hyperperfusion, and finally lateral temporal hypoperfusion in the immediate postictal period.

As the postictal switch in blood flow distribution was more closely evaluated, the importance of time as a critical factor when reviewing postictal hypoperfusion patterns became

apparent. Examining postictal perfusion on a finer temporal scale, hyperperfusion of the hippocampus with concurrent hypoperfusion of lateral temporal structures was seen up to two minutes postictally (Duncan, et al., 1993). Between 2-15 minutes postictally, only hypoperfusion was observed in the area of the suspected SOZ (Fig. 1.6). These findings helped explain the previously-conflicting results from Rowe et al. (1991) who did not observe mesial hyperperfusion after 5 to 8 minutes, which is consistent with the aforementioned timeline of perfusion changes proposed by Duncan et al. (1993).

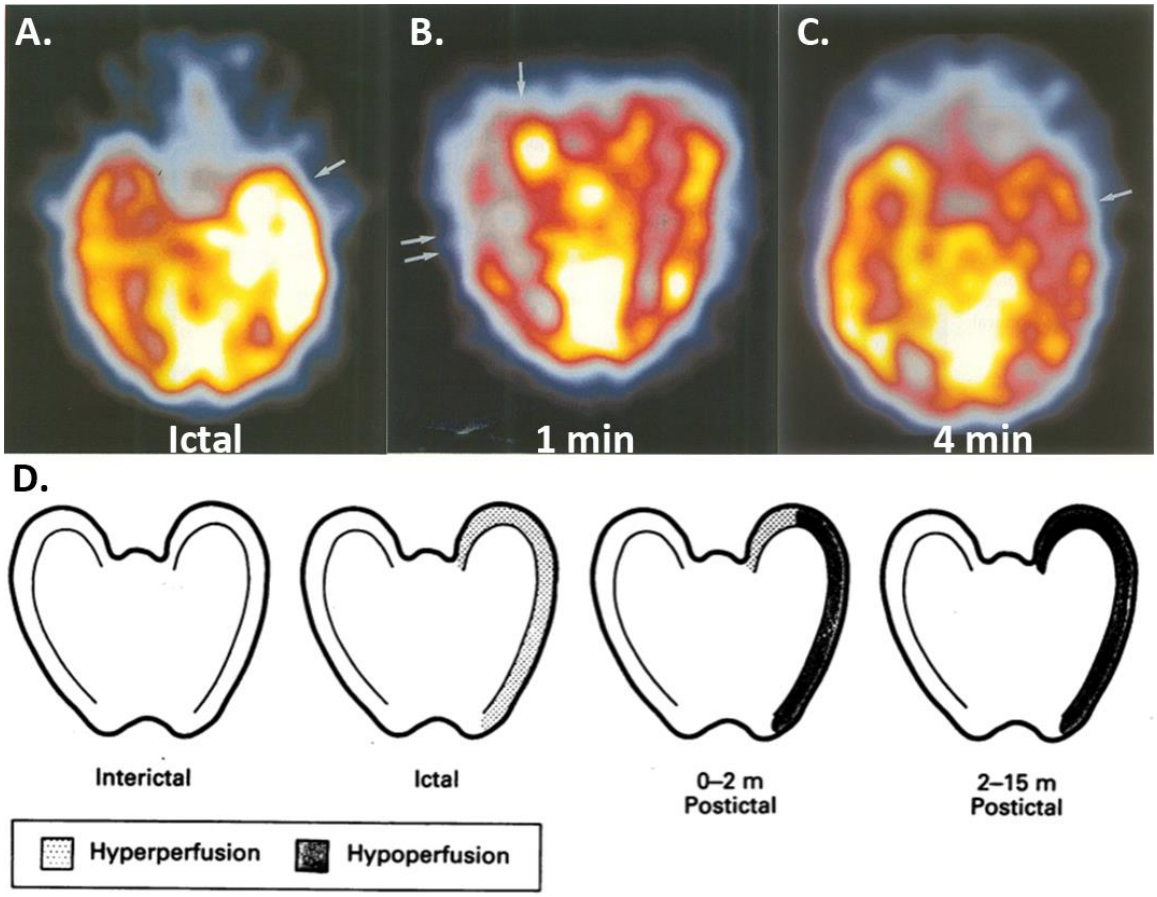

Figure 1.6: Ictal SPECT injections at various times for different seizures and the corresponding perfusion changes, demonstrating postictal switch. A. Scan following injection during a complex partial seizure showing hyperperfusion of the whole left temporal lobe (arrow). B. Scan following injection 1 minute after a complex seizure showing hyperperfusion of the right medial temporal cortex (arrow). C. Scan following injection 4 minutes after a complex partial seizure showing hypoperfusion of the medial and lateral temporal cortex (arrow). D. Possible sequence of changes in rCBF during and after seizures of temporal lobe origin. From left to right: normal rCBF, hyperperfusion of the whole temporal lobe, hyperperfusion of the medial temporal cortex with lateral hypoperfusion, and hypoperfusion of the whole temporal lobe. (Duncan, et al., 1993)

1.1.7 Postictal Hypoperfusion

The timeline for the prolonged period of postictal hypoperfusion has been investigated further in a variety of studies. Both animal and human studies have shown that vascular disturbances may be long-lasting and localized to the areas of the brain involved in seizure onset and propagation (Choy, et al., 2010; Weinand, et al., 1997). Earlier studies measured CBF invasively through implantation of various probes (Dymond and Crandall, 1976; Gibbs, 1934; Weinand, et al., 1997). In 1934, researchers used internal jugular vein thermocouple probes, or hippocampal depth electrodes, and found that the late postictal hypoperfusion was most pronounced on the side of ictal onset (Gibbs, 1934). These early findings were further confirmed in a study done in 1997, where patients underwent bilateral implantation of subdural CBF thermal diffusion sensors on the anterior inferior temporal cortical surface. The CBF sensors consisted of a heated and a neutral plate, and the temperature difference between the two plates were correlated with CBF (Weinand, et al., 1997). Weinand et al. expanded on the findings of Gibbs, Lennox, & Gibbs (1934) by further concluding that progressive hypoperfusion of the epileptic focus is correlated with increased epileptogenicity, further supporting the hypothesis that epileptic seizures are a function of progressive small ischemias.

Multiple animal studies have shown evidence of decreased apparent diffusion coefficient (ADC) following chemically induced status epilepticus in rats, as detected by diffusion-weighted magnetic resonance imaging (DWMRI) (Fabene, et al., 2003; Nakasu, et al., 1995; Wang, et al., 1996; Zhong, et al., 1995). These animal studies established that diffusion changes after focal or generalized status epilepticus may persist for hours to days.

In contrast to ADC changes seen after status epilepticus, dynamic ADC changes after single seizures have not been consistently observed in humans (Di Bonaventura, et al., 2009; Hufnagel,

et al., 2003). ADC alterations after single seizures were hypothesized to differ from those after status epilepticus because single seizure-induced cell membrane changes and ion imbalances are transient, leading to only minor morphologic damage undetectable using DWMRI.

1.1.7.1 Mechanisms of Postictal Hypoperfusion/Hypoxia

Recent animal work from the Teskey lab has comprehensively investigated local oxygen levels and blood flow following brief electrically elicited seizures in rats to characterize postictal hemodynamic changes. They found that seizures resulted in vasoconstriction that leads to reduced local blood flow and severely reduced oxygen levels that can last up to one hour in the hippocampus following seizure termination before returning to normal baseline values (Farrell, et al., 2016) (Fig. 1.7A). The relationship between the duration of the hippocampal seizures and the severity of postictal hypoxia was linear in both animal and human trials (Fig. 1.7B and C). Furthermore, agents such as acetaminophen, which inhibits cyclooxygenase-2 (COX-2) or nifedipine, which inhibits L-type calcium channels, reduced vasoconstriction and prevented the postictal hypoperfusion and hypoxia without affecting the seizure itself. The same agents reversed the memory and behavioral impairments seen during postictal hypoxia. These results indicated that it is the severe postictal hypoxia, and not the seizures themselves, that are the underlying cause for postictal motor weakness and behavioral impairments.

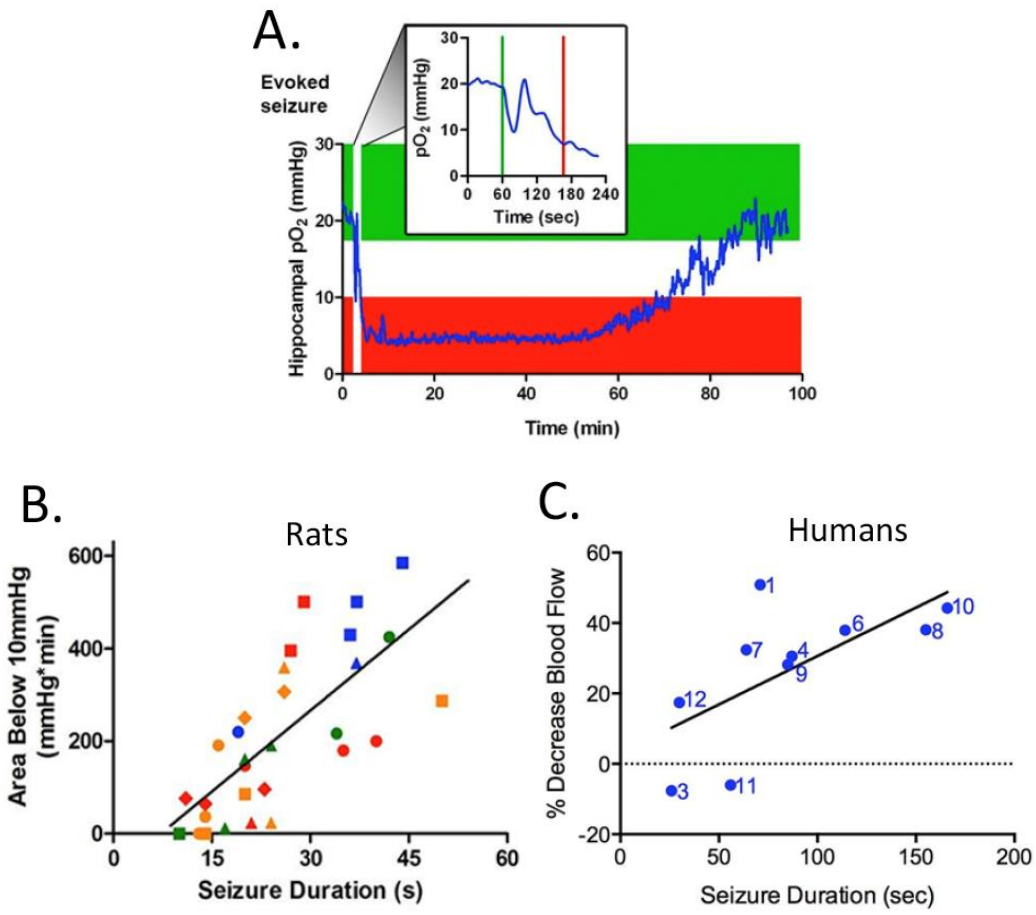

Figure 1.7: Prolonged postictal hypoxia/hypoperfusion is present in rats and humans. A. Representative oxygen profile before, during, and after a 106s electrically kindled seizure in a rat. The green and red lines denote the beginning and end of the seizure. B. Scatterplot of the relationship between the duration of kindled seizures in the dorsal hippocampus (primary after discharge) and the degree of severe hypoxia expressed as the total area below the severe hypoxic threshold (10mmHg) by time (min). Symbols of same colour and shape are from the same animal. C. Percent decrease in postictal blood flow as a function of seizure duration in human clinical trials. (Farrell, et al., 2016)

In a follow-up theoretical paper, Farrell et al. (2017) speculated that following sustained synaptic activity, neuronal COX-2 rapidly oxygenates its substrates to vasoactive products. These lipid-signaling molecules that are yet to be determined move from the neuron to act on receptors located on vascular smooth muscle. Activation of these receptors lead to L-type calcium channel conductance and an influx of calcium, which ultimately engages the molecular machinery that mediates vasoconstriction (Farrell, et al., 2017) (Fig. 1.8).

Although there is partial inhibition of L-type channels via ethosuximide, a commonly prescribed ASD, the majority of currently-prescribed ASDs do not affect calcium ion flow and thus does not act on the phenomenon of postictal severe hypoxia. Indeed, the findings of Farrell et al. (2016) clearly demonstrate that postictal impairments may be prevented by interfering with the pathways that lead to hypoxia, thus implying a potential re-evaluation of ASDs for treatment and seizure management.

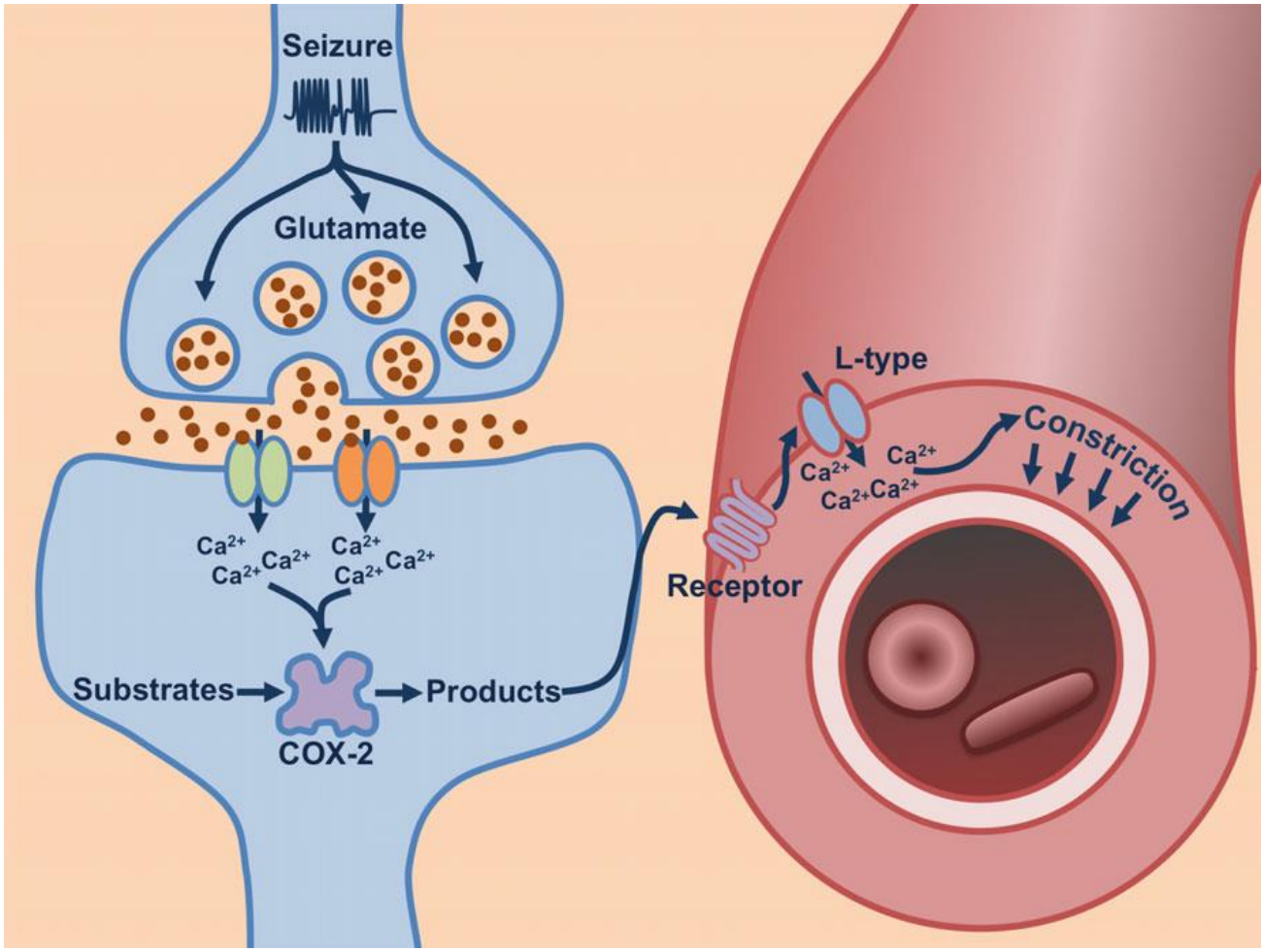

Figure 1.8: Proposed mechanism by Ferrell et al., (2017) of vasoconstriction following a seizure. Following a seizure and the resulting sustained synaptic activity, postsynaptic calcium accumulates and increases COX-2 activity. COX-2 enzymatically converts its substrates to several lipid-signaling molecules. These products act on receptor(s) located on vascular smooth muscle, leading to the opening of L-type calcium channels, and ultimately vasoconstriction.

1.1.7.2 Arterial Spin Labeling (ASL)

The findings of the postictal SPECT and prolonged hypoperfusion studies led to the application of arterial spin labeling (ASL) MRI as an imaging modality for measuring CBF changes in epilepsy. ASL has the potential to be a diagnostic tool for localizing the SOZ because it is a non-invasive, radiation-free technique for measuring CBF. It has been used to measure cerebral perfusion in other cerebrovascular diseases, but its applications in epilepsy are a recent development (Hendrikse, et al., 2012). In cases of focal epilepsy, ASL has been used to measure interictal and postictal cerebral blood perfusion (Boscolo Galazzo, et al., 2015; Guo, et al., 2015; Kim, et al., 2016).

Unlike SPECT where the perfusion analysis depends on the time of tracer injection, ASL assesses CBF at the time of image acquisition. Ictal SPECT assumes that the seizure focus is associated with increased metabolism and blood flow, and thus increased tracer uptake (la Fougere, et al., 2009). This characteristic makes it imperative that the tracer is injected as close to seizure onset as possible (<30s) otherwise the acquired images will be non-localizing and display areas beyond the epileptic focus. Instead of a time window of 30s to inject the tracer for an ictal SPECT, ASL benefits from the characterized prolonged period of hypoperfusion and has an hour-long time window for postictal image acquisition (Farrell, et al., 2016). To date, ASL has been used to detect interictal and postictal alterations in brain perfusion dynamics in patients with drug resistant focal epilepsy (Pizzini, et al., 2013; Storti, et al., 2014; Wolf, et al., 2001). These studies aimed to identify asymmetries in CBF using ASL to lateralize the abnormal side in patients with temporal lobe epilepsy (Guo, et al., 2015; Lim, et al., 2008; Wolf, et al., 2001). However, no ASL studies reported hypoperfusion in the immediate postictal state, focusing instead on the interictal period. These studies that performed interictal ASL showed alterations in

CBF in regions that were concordant with the presumed SOZ based on EEG, MRI, SPECT and PET. However, interictal CBF changes may not accurately reflect the SOZ (Sierra-Marcos, et al., 2016; Storti, et al., 2014). Pizzini et al. (2013) identified hyperperfusion in several patients that were imaged within an hour following seizure termination. Although the aforementioned ASL studies had generally revealed interictal hypoperfusion in brain regions corresponding to the SOZ as defined by other clinical investigations, many of these studies yielded inconsistent and conflicting results, including focal and hemispheric hypoperfusion, hyperperfusion or no significant perfusion changes (Pizzini, et al., 2013; Wolf, et al., 2001).

The inconsistencies in observed perfusion patterns may be explained by the findings of those initial postictal SPECT studies which demonstrated a distinct switch from postictal hyperperfusion to postictal hypoperfusion within the first 15 minutes after an ictal event. Notably, none of the aforementioned postictal ASL studies precisely defined the time period from seizure termination to ASL data acquisition because the timing was often not recorded or was based on patient recall: postictal scans were acquired as late as eight hours after presumed seizure termination. Thus, the variability of these ASL data may be related to the variability in timing when acquiring the postictal scans.

The Federico lab has circumvented these limitations by measuring postictal CBF in patients with drug resistant focal epilepsy using ASL within 90 minutes of an electrographically confirmed seizure (Gaxiola-Valdez, et al., 2017). Precise timing was obtained from review of the EEG data obtained while these patients were in hospital undergoing continuous video-EEG monitoring of their seizures, as part of their workup for epilepsy surgery. These ASL scans were compared to each patient's interictal ASL to identify the region(s) of most significant hypoperfusion following a seizure. Using this method, seizures were found to be associated with

postictal blood flow reductions of >20 ml/100g/min lasting up to 1 hr, localized to the SOZ as defined by EEG and ictal SPECT (Fig. 1.9).

While ASL is being established as a useful tool in localizing the SOZ by detecting areas of postictal hypoperfusion, the clinical use of ASL is hampered by the difficulty in obtaining MR scans within one hour of seizure termination. The clinical implementation of this type of investigation therefore requires the identification of a cost effective and readily available tool. To this end, CT Perfusion (CTP) imaging has the sensitivity and spatial resolution to detect postictal hypoperfusion at the SOZ, and CT scanners are also readily accessible on short notice in most hospitals.

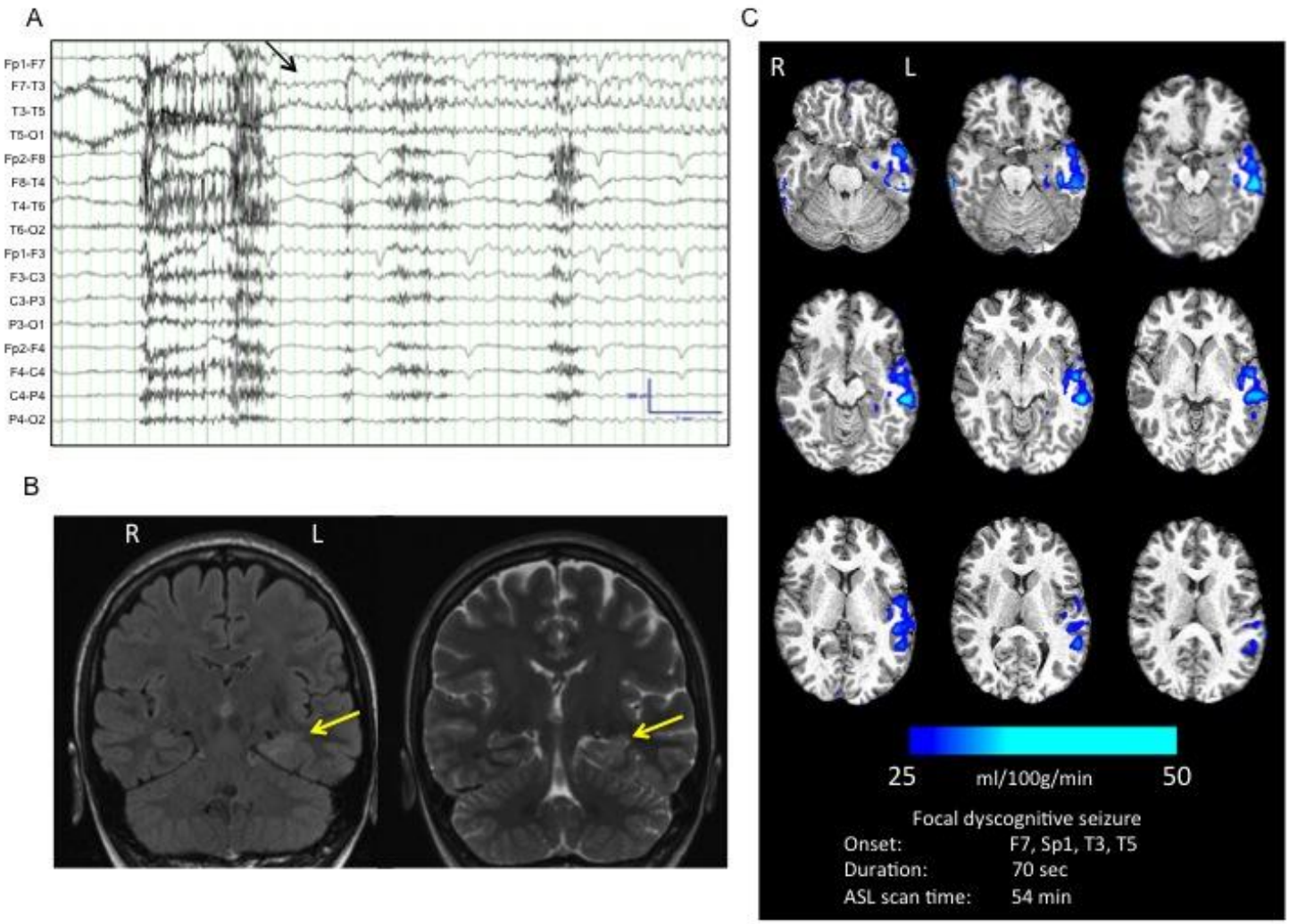

Figure 1.9: 33 year old right handed female with intractable epilepsy. A. Ictal EEG recording on a longitudinal bipolar montage with seizure onset over the left midtemporal region. B. Coronal MR images (FLAIR and T2-weighted) showing poor grey white matter differentiation and abnormal morphology of the left parahippocampal gyrus and hippocampus. C. Subtraction CBF map in blue (inter-ictal – postictal) superimposed onto the patient's T1-weighted anatomical image indicating areas of hypoperfusion > 20 CBF units (~ 33 % reduction compared normal gray matter CBF).

1.1.7.3 Computed Tomography Perfusion (CTP) Imaging

1.1.7.3.1 Collection and Processing of CTP

CT Perfusion (CTP) involves passing an intravascular contrast bolus through a mass of brain tissue and measuring the change of signal intensity of each voxel within a CT image over time. The intensity of the CT image as expressed in Hounsfield Units (HU), is linearly proportional to the efficiency of x-ray attenuation. Each pixel has a time-density (attenuation) curve (TDC) which is used to quantify perfusion measurements such as: cerebral blood flow (CBF), the rate at which a volume of blood moves through a mass of tissue [$ml \cdot min^{-1} \cdot (100g)^{-1}$]; cerebral blood volume (CBV), the total volume of blood moving through a mass of brain tissue [$ml \cdot min^{-1}$]; and several other parameters. The derived measurements of CBF and CBV can describe the hemodynamics within the entire vasculature of the brain including large arterioles, arterioles, capillary beds, venules, and veins.

Generation of hemodynamic functional maps is almost completely automated with current CTP software (GE Healthcare), requiring only the selection of an arterial input function (AIF). Following this, deconvolution and non-deconvolution based models are methods to calculate perfusion parameters based on the selected AIF.

The interpretation of studies using non-deconvolution techniques may be less reliable (Konstas, et al., 2009). One major assumption in the non-deconvolution method is assuming that there is no venous outflow; this is only valid if there is a very high rate of contrast agent injection rate – at least 10 mL/s – which cannot be routinely achieved in clinical practice (Konstas, et al., 2009). Thus, the no-venous-outflow assumption is an oversimplication and yields relative rather than absolution perfusion measurements. Despite non-deconvolution-based models being more

straightforward compared to deconvolution models, they depend on over-simplified assumptions regarding the underlying vascular architecture that may not be true.

Deconvolution techniques corrects for the inability to directly deliver a contrast bolus into the supplying artery of the tissue of interest. When introduced at a peripheral vein, the bolus undergoes delay and dispersion prior to arriving at the artery. Deconvolution corrects for this by calculating the fraction of contrast medium that remains in the tissue over time after a bolus injection into the arterial input: the impulse residue function (IRF). Although deconvolution techniques are technically more demanding and involve more complicated and time-consuming processing in order to account for the calculation of an IRF, they are more physiologically appropriate. Thus, the work contained in this thesis uses the deconvolution process.

1.1.7.3.2 CTP in Epilepsy

Dynamic perfusion CT is becoming a widely-accepted imaging modality for the clinical investigations of acute stroke patients, but to date, the use of CTP in epilepsy has been limited. Most studies using CTP in epilepsy have focused on differentiating between acute stroke, status epilepticus, or postictal states such as Todd's paresis. Investigations studying the extensive usage of CTP as a diagnostic tool in localizing the SOZ in patients with focal refractory epilepsy have not been performed.

With the development of faster continuous data acquisition from spiral CT, CTP has exceeded standard CT in depicting cerebral hypoperfusion, performing at a sensitivity of up to 90% for the detection of embolic and hemodynamic lesions within cerebral hemispheres (Konig, 2003; Mayer, et al., 2000). In comparison, non-contrast CT allows for the detection of early ischemic changes with an overall sensitivity of only 38-42% in patients in hyperacute phase, and

has often underestimated the severity of ischemia and the spatial extent of hypoperfusion (Piliszek, et al., 2016). These findings have led to the preferential use of a contrast agent during CTP scanning (Grond, et al., 2000).

Postictal paresis is associated with vascular changes that strongly lateralize to the SOZ in patients with focal epilepsy. For example, CTP was used to show left hemispheric hypoperfusion in a case report of a patient with a left hemispheric seizure with prolonged right-sided postictal paresis (Mathews, et al., 2008).

CTP has also been used to differentiate between status epilepticus and postictal states. Several studies focused on using CTP to observe patterns of hyperperfusion in patients with non-convulsive status epilepticus in comparison to patterns of postictal hypoperfusion (Hauf, et al., 2009; Wiest, et al., 2006). Overall, these studies successfully revealed detection of postictal focal hypoperfusion using CTP lateralizing to the SOZ as determined by EEG in the majority of patients (Fig. 1.10). In one of these studies, investigators explicitly imaged patients within 30-90 minutes of seizure termination (Hauf, et al., 2009). This is an important detail, as recent animal studies have shown that the most severe hypoxia occurs between 20-60 minutes post-seizure (Fig. 1.7).

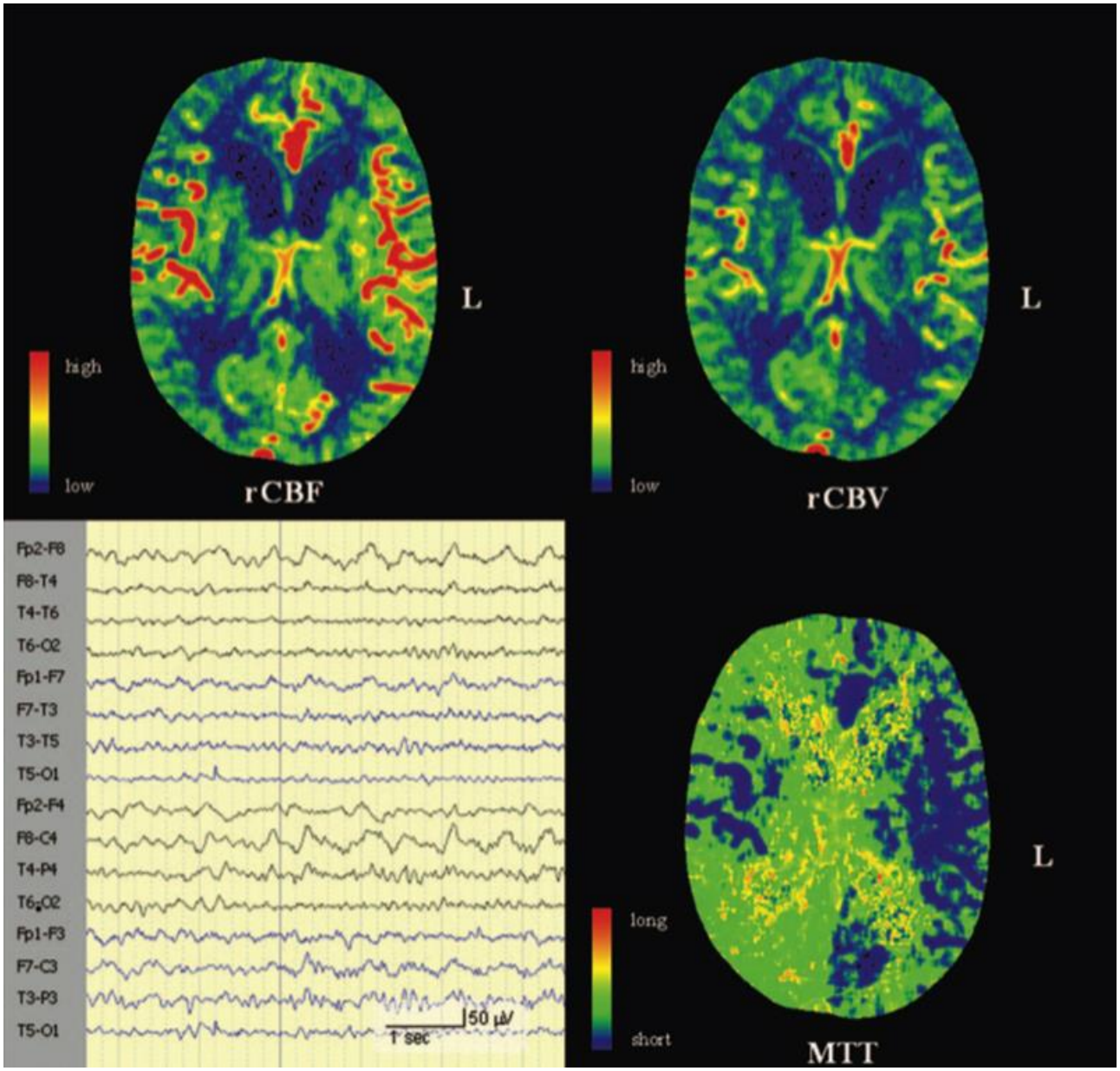

Figure 1.10: CTP maps obtained from a patient in a postictal state demonstrating widespread hypoperfusion over the right hemisphere. Bottom left: EEG shows a diffuse right hemispheric slowing (Hauf, et al., 2009).

In other work investigating postictal perfusion patterns using CTP, patients were imaged up to 72 hours after seizure termination (Gelfand, et al., 2010). The authors found that in a group of 27 patients who received CTP scans 1-9 hours after seizure termination, those who were scanned more than two hours postictally showed significantly fewer abnormal perfusion patterns than those scanned at less than two hours (Fig. 1.11). These findings further illustrate the transient and temporal sensitivity of the postictal hypoperfused state and suggest that the timing of postictal image acquisition is critical.

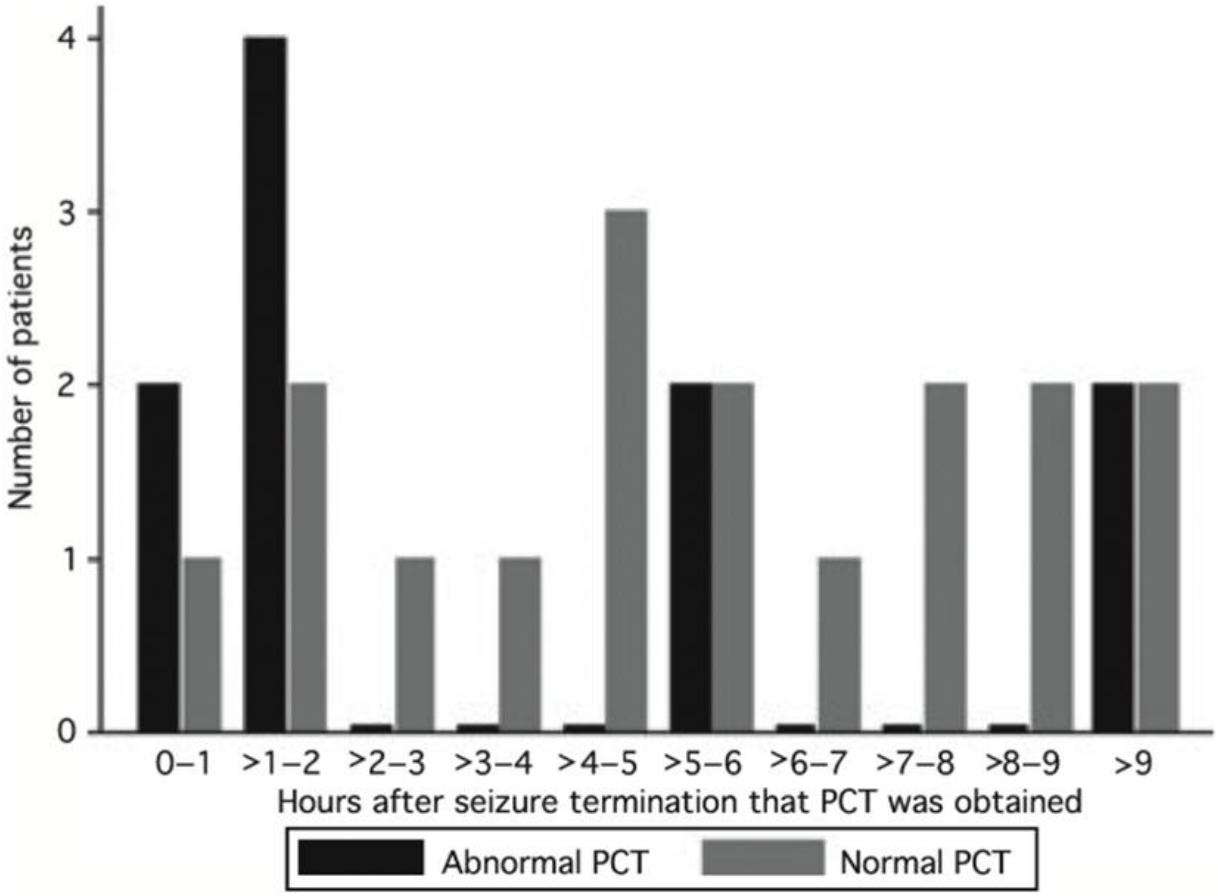

Figure 1.11: Distribution of time between seizure termination and CTP imaging in patients with abnormal and normal PCT. Imaging within 2 hours after seizure termination was associated with a greater likelihood of finding in abnormal postictal perfusion pattern on CTP (Gefland, Wintermark, & Josephson, 2010).

Despite these findings, each study faced methodological and analytical limitations. In each study, patients were coming from the emergency room after presenting with neurological defects. Thus, the time from seizure termination to image acquisition, if recorded, was based on patient or witness recall and was not electrographically confirmed (Gelfand, et al., 2010; Hauf, et al., 2009; Royter, et al., 2008; Wiest, et al., 2006). This issue is similarly present in the current ASL literature (Boscolo Galazzo, et al., 2015; Guo, et al., 2015; Hendrikse, et al., 2012; Kim, et al., 2016; Lim, et al., 2008; Pizzini, et al., 2013; Sierra-Marcos, et al., 2016; Sugita, et al., 2014; Wolf, et al., 2001).

To date, no CT studies have directly investigated patients with epilepsy that were under 24-hour video-EEG monitoring. This method allows for immediate clinical verification of an event, as well as accurate temporal quantification of seizure onset and termination. In order for results to be meaningful, it is critical that a systemic assessment at specific time-points is present because of the dynamic nature of CBF in relation to seizures. Ambiguity in the actual time of seizure termination and image acquisition may significantly limit the applicability of findings.

Measuring and comparing absolute reduction in CBF values relative to the baseline values of each patient may provide a more accurate representation of postictal blood flow. Most studies of CBF changes used a control group to statistically quantify baseline CBF changes instead of collecting a baseline scan for each individual patient (Gelfand, et al., 2010; Hauf, et al., 2009; Mathews, et al., 2008). Hauf et al. (2009) used clustering of asymmetry perfusion indices to compare CBF, cerebral blood volume (CBV) and mean transit time (MTT) between patients under different conditions (e.g., postictal vs. status epilepticus). Hypoperfusion was defined as an asymmetry perfusion index < -10 (Fig. 1.12). Although this statistical method has logistical

benefits in only needing to collect one scan, studies have shown significant variance between healthy subjects for average CBF values collected using CTP (Ziegelitz, et al., 2009). Furthermore, this approach may be an oversimplification and not fully representative of postictal CBF changes occurring in patients with epilepsy who may have baseline CBF abnormalities.

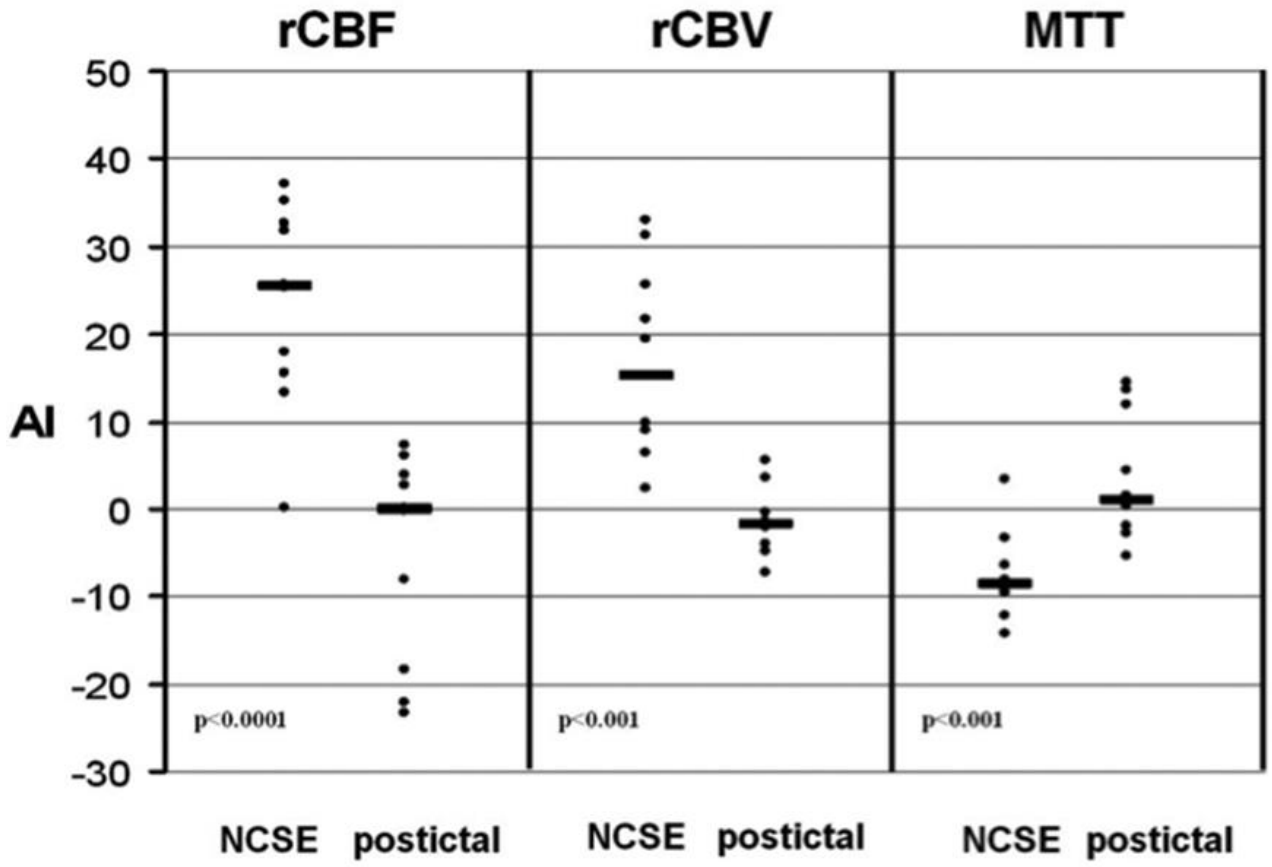

Figure 1.12: Group comparison between patients in non-convulsive status epilepticus (NCSE) and postictal state demonstrates significantly higher rCBF, rCBV, and shorter MTT in NCSE vs. postictal states. (Hauf, et al., 2009)

1.2 Rationale

The Federico lab has performed ASL in 25 patients and observed postictal hypoperfusion (decreases of >20 ml/100g/min) co-localizing with the SOZ for approximately 80% of patients. However, the widespread clinical translation of this exciting approach to pre-surgical SOZ localization is hampered by the difficulty in obtaining MR scans within one hour of seizure onset. The next step is to identify a cost effective and readily available tool to measure postictal hypoperfusion at the SOZ.

If CTP can be shown to accurately measure CBF during the postictal period, it may provide an additional localization tool for determining the SOZ via perfusion patterns. Compared to MRI scans, CT scans are more cost-effective, readily available, and have the necessary spatial resolution to detect postictal hypoperfusion corresponding to the SOZ. EEG is time consuming to analyze and has a spatial resolution of >10 cm^2 which is insufficient to direct surgical resection alone. While SPECT does offer better resolution of around 1 cm^2, it is labor intensive and costly: tracer injection must occur within 30s of seizure onset to be useful, making it necessary to have hospital personnel on standby for a seizure that can take up to weeks to occur. Ictal SPECT is also very costly since SPECT tracers can be used only for one day at a cost of $650 each and is also only available during regular working hours (0900-1530 on weekdays). In comparison, CTP offers a spatial resolution of 0.25 cm^2 and a substantially lower economic burden per scan (~$350/scan).

In 2015, the Calgary epilepsy center was able to attempt 56 ictal SPECT studies over 377 hospital days and obtained injections in 42 patients. In contrast, because CTP has 24/7 has 24-hour availability, it would only take 146 days to obtain CTP scans in the 51 patients who had

seizures in hospital (Fig. 1.13). Thus, more patients can be studied in less time. The shortened hospital admission time ad reduced CTP operating cost results in a predicted savings of $723,500/year for the Calgary center alone.

Since our ASL studies have shown that postictal hypoperfusion can last >1 hour, a major advantage that CTP has over ictal SPECT is that instead of a time window of 30s to inject the tracer for an ictal SPECT which requires constant staff surveillance and presence, CTP has a one-hour window for postictal image acquisition. The other major benefit of CTP is that most hospitals have 24-hour access to CT scanners, in comparison to the limited availability of working hours that SPECT and MRI scanning have.

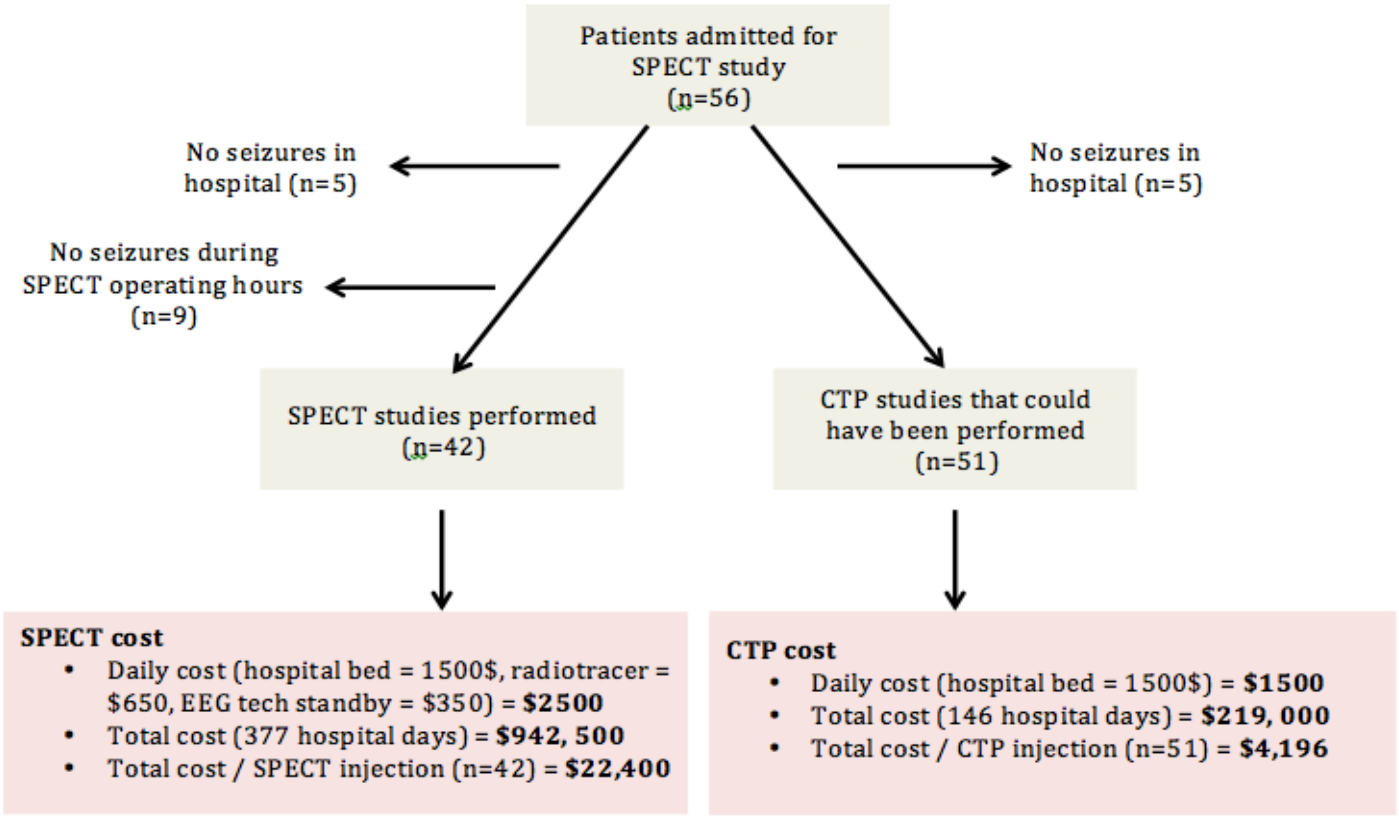

Figure 1.13: Summary for the 56 ictal SPECT studies performed in Calgary 2015. Note that it took 377 days to obtain 42 SPECT injections in 56 patients. In contrast, because CTP has 24/7 availability, it would have taken only 146 days to obtain CTP scans in 51-56 in-patients.

1.3 Significance

Identifying the SOZ is a crucial step in the pre-surgical assessments of patients with refractory focal epilepsy. As described in the previous section, measuring postictal hypoperfusion by CTP offers a reliable, easily accessible, cost-effective tool (estimated annual savings of $723,500) to identify the SOZ in patients with refractory epilepsy undergoing presurgical evaluations. In addition, the importance of this proposal is strengthened by the fact that CT scanners and CTP protocols are readily available 24/7 in most hospitals and they are cost-effective, thereby significantly improving health care delivery and reducing health care costs.

1.4 Summary

Pre-surgical clinical investigations such as EEG, SPECT, PET, and MRI, are currently the standard approach for identifying the SOZ. More recently, arterial spin-labeling (ASL) magnetic resonance imaging (MRI) has shown significant and long-lasting reductions in perfusion following a seizure, which may correspond with the SOZ (Boscolo Galazzo, et al., 2015; Storti, et al., 2014; Sugita, et al., 2014). Each of the aforementioned imaging modalities have their respective limitations: EEG has limited spatial resolution, SPECT is labor intensive and costly, and MR scans have narrow availability. In contrast, computed tomography perfusion (CTP) imaging is a cost-effective and readily available tool for measuring postictal blood flow changes that may help localize the SOZ. CTP has 24-hour accessibility in hospitals, is more economically viable compared to other imaging modalities such as SPECT and has the spatial sensitivity to detect the postictal hypoperfusion. Therefore, *I will investigate the degree to which*

CTP measures of postictal hypoperfusion can help identify the SOZ, which is determined by EEG and other investigations.

1.5 Hypothesis and Research Objectives

Overall Hypothesis: *The area of postictal hypoperfusion can be detected using CTP and it will define the seizure onset zone.*

Specific Hypothesis 1: *Postictal CTP CBF maps will qualitatively exhibit localized hypoperfusion corresponding to the seizure onset zone as defined by EEG or ictal SPECT.*

Objective 1: Collect two quantitative CTP scans; 1) within one hour of seizure termination and 2) when the patient has been seizure free for more than 24 hours. Two reviewers will blindly review the postictal and baseline CBF maps together for each patient and visually localize hypoperfusion based on hemisphere, and lobe. The location of postictal hypoperfusion detected by CTP will then be compared to the location of the presumed SOZ as defined by EEG or ictal SPECT.

Specific Hypothesis 2: *Postictal CTP CBF maps will quantitatively exhibit localized hypoperfusion corresponding to the seizure onset zone as defined by EEG or ictal SPECT.*

Objective 2: Develop a pipeline that can quantitatively detect the postictal hypoperfusion as seen between the baseline and postictal scans and determine if CTP can detect the full extent of the SOZ compared to current standards of EEG and ictal SPECT.

CHAPTER 2: Postictal Hypoperfusion Measured by CT Perfusion

2.1 Introduction

Epilepsy is one of the most common and serious neurological conditions in the world. Approximately 30% of patients with epilepsy cannot control their seizures using medication (Kwan and Sander, 2004). In these cases, the most effective treatment is removal of the seizure onset zone (SOZ). The SOZ is conventionally localized by electroencephalography (EEG) recordings of seizures or single photo emission computed tomography (SPECT) measures of blood flow during the ictal phase (Salmenpera and Duncan, 2005). However, EEG has limited localization accuracy and ictal SPECT is labor-intensive and costly. The surgical cure rate is less than 50% due to imprecise identification and removal of the seizure generating tissue (Spencer, et al., 2005).

Vascular changes have been increasingly investigated in its potential to localize the SOZ. Transient postictal vascular changes localizing to the SOZ have shown to be long-lasting in both animal (Choy, et al., 2010) and human studies (Weinand, et al., 1997). Through invasive implantation of CBF sensors, researchers concluded that progressive hypoperfusion of the epileptic focus is correlated with increased epileptogenicity, further supporting the hypothesis that epileptic seizures are a function of progressive small ischemias (Weinand, et al., 1997). More recently, arterial spin labeling (ASL) MRI has been used to non-invasively detect interictal and postictal alterations in cerebral blood flow (CBF) (Guo, et al., 2015; Lim, et al., 2008; Pizzini, et al., 2013; Storti, et al., 2014; Wolf, et al., 2001). These studies performed interictal or postictal ASL and showed CBF changes in regions concordant with the presumed SOZ based on EEG, MRI, SPECT and positron emission tomography (PET). Similarly, computed tomography

perfusion (CTP) has also detected postictal focal hypoperfusion and interictal hyperperfusion in patients in status epilepticus lateralizing to the SOZ (Gelfand, et al., 2010; Hauf, et al., 2009; Mathews, et al., 2008). Although these studies revealed interictal hypoperfusion in regions corresponding to the presumed SOZ, many of these studies yielded inconsistent results, including contralateral focal and hemispheric hypoperfusion, hyperperfusion, or no significant perfusion changes (Gelfand, et al., 2010; Hauf, et al., 2009; Mathews, et al., 2008; Pizzini, et al., 2013; Wolf, et al., 2001).

A recent study systematically demonstrated hypoperfusion and severe hypoxia (oxygen partial-pressure < 10mmHg) in the hippocampus lasting up to one hour after hippocampal kindled seizures in rats (Farrell, et al., 2016).

Recently, we measured postictal CBF in 21 patients with drug resistant focal epilepsy using ASL within 90 min of an electrographically confirmed seizure (Gaxiola-Valdez, et al., 2017). Localized postictal CBF reductions of approximately 30% of baseline CBF values were observed in 71% of patients, localizing to the presumed SOZ in 80% of cases.

While these ASL data support the possibility of using postictal ASL CBF measurements as a useful tool to localize the SOZ, clinical implementation of ASL is hampered by difficulty in obtaining MR scans within one hour of seizure termination. CTP imaging has the necessary spatial resolution to detect postictal hypoperfusion and is readily accessible on short notice in most hospitals. Therefore, the aim of the present study was to use CTP to measure the extent of the postictal hypoperfusion in patients with refractory focal epilepsy.

2.2 Methods

2.2.1 Participants and Study Protocol

Fifteen patients with drug-resistant focal epilepsy admitted to the Seizure Monitoring Unit at the Foothills Medical Center for continuous scalp video-electroencephalography (VEEG) monitoring between September 2016 and December 2017 were prospectively enrolled in the study. The study was approved by the Conjoint Health Research Ethics Board of the University of Calgary and all patients provided informed consent. Exclusion criteria for the study were multiple seizure onset zones, and contraindications to CT (e.g., pregnancy, allergy to IV contrast material) or MR imaging (e.g., claustrophobia, ferromagnetic intracranial devices).

When a habitual seizure was observed, a physician immediately reviewed the VEEG monitoring data. Once a qualifying seizure was confirmed patients underwent CTP imaging within 65 min of seizure termination. After collecting the postictal scan and while still in hospital, patients underwent a baseline interictal CTP scan following a seizure-free period of >24 hours. EEG electrodes were removed for both scans.

2.2.2 Clinical Data Collection

All patients underwent continuous scalp VEEG using 10-20 electrode placement in order to capture habitual seizures. Demographic data including age, sex, duration of epilepsy, seizure frequency and seizure types were recorded. As part of presurgical investigations, structural MRI using our center's standard epilepsy protocol was obtained for all patients. Ictal and interictal SPECT and PET investigations were obtained as clinically indicated.

2.2.3 Definition of the Seizure Onset Zone

The SOZ was determined by clinical history, interictal and scalp VEEG, structural MRI, PET, interictal and ictal SPECT, and expert consensus from our weekly multidisciplinary epilepsy surgery rounds. We referred to this area as the "presumed SOZ", as the true epileptogenic zone can only be identified post-operatively and not all cases underwent surgery.

2.2.4 CT Perfusion Data Collection and Functional Maps

Whole-brain CTP images were acquired with 5 mm thickness (2 x 2 mm in plane resolution) and reconstructed at 1.25 mm thickness (GE Healthcare Revolution, Waukesha, WI, USA). The CTP protocol consisted of 45 ml of an inert CT contrast agent (Omnipaque, GE Healthcare) that was power injected at 6 ml/s followed by a 40 ml saline chase. Scanning began after a delay of 5 sec from contrast injection, sampled at 2.8 sec for a total acquisition time of 75 sec. Foam padding was placed around patients' heads to minimize motion during scanning. Each study was analyzed using commercially available delay-insensitive deconvolution software (CT Perfusion 4D, GE Healthcare).

For each study, the arterial input function was manually selected from the internal carotid artery using a 2 x 2 voxel (in-slice) region-of-interest (ROI). Absolute maps of CBF ($ml/100g^{-1}/min^{-1}$) were calculated by deconvolution of time density curves and arterial input function using a delay-insensitive (deconvolution) algorithm (CT Perfusion 4D, GE Healthcare). In-plane patient motion was corrected using automated software. In cases of extreme motion, time points were manually removed as needed.

2.2.5 Visual Reviewers

CTP data were reviewed in two different manners. First, CT perfusion maps were reviewed qualitatively. Second, a more objective, quantitative subtraction analysis was performed (described later). For the qualitative review, images were anonymized and displayed using OsiriX medical image viewer. Two reviewers (TL, CE) with extensive experience in viewing CTP quantitative maps were recruited to visually assess absolute CTP CBF maps for perfusion abnormalities. Each reviewer was given an explanation of the data collection process as well as an explanation of the two different scans (immediate postictal and baseline). Reviewers were informed that all patients had suspected focal epilepsy but were otherwise blind to patient clinical information.

2.2.6 Visual Evaluation of Hypoperfusion Detected by CTP

In the first condition, reviewers were presented with a series of 27 CTP CBF maps (14 postictal, 13 baseline) from 14 patients alongside a higher contrast CTP average map for additional anatomical delineation and differentiation between areas of hypoperfusion and white matter in the CBF maps. Reviewers were blinded to whether a scan was postictal or baseline and assessed each case independently in a randomized order. Areas of hypoperfusion were visually assessed on perfusion symmetry.

In the second condition, reviewers were unblinded to the order of the images and viewed the baseline and postictal maps side-by-side for each patient for 13 image sets. In addition to intra-scan perfusion symmetry, symmetry between the postictal and baseline perfusion patterns were also compared. Scales were manually adjusted to visually match intensities between

images, or both images were assessed on the same intensity scale to visualize any global perfusion differences.

In both conditions, reviewers identified areas of hypoperfusion based on hemisphere (left, right, no localization) and lobe (frontal, temporal, parietal, occipital, no localization), and provided a confidence score (1 [least confident] - 5 [most confident]) for each assessment.

Both conditions were completed twice for each reviewer and in independent individual sessions; the first round assessed images of 5 mm thickness, the second round assessed images of 1.25 mm thickness. Each round was done approximately 2-3 months apart. CT image thicknesses of 1.25 mm and 5 mm were assessed in order to determine which image thickness to use for subsequent quantitative subtraction analysis.

2.2.6.1 Statistical Analysis of Visual Evaluation Data

Cohen's Kappa (κ) was calculated to statistically determine interrater reliability as it normalizes the observed agreement between reviewers due to chance and produces a coefficient between 0 (indicating chance agreement) and 1 (indicating perfect interrater agreement). For hemispheric assessments (left, right, or no localization), a Kappa coefficient was calculated to evaluate interrater agreement between the baseline, postictal, and baseline vs. postictal image sets. Assessments were evaluated as either complete agreement or complete disagreement.

As summarized in Table 1, a weighted Kappa allowed for additional assignments of different weightings of disagreement and was used when assessing interrater agreement in lobar assessments (frontal, temporal, parietal, occipital, and no localization). Complete disagreements were assigned a weighting of 1 and was applied in cases of frontal vs. occipital, and for no

localization vs. any localization. Partial disagreements were assigned a weighting of 0.5 in all other cases between lobar assessments (Table 1).

Table 2.1: Kappa weightings for lobar assessments in evaluation of interrater agreement.

		Reviewer 1				
Reviewer 2		FRONTAL	TEMPORAL	PARIETAL	OCCIPITAL	NOTHING
	FRONTAL	0	0.5	0.5	1	1
	TEMPORAL	0.5	0	0.5	0.5	1
	PARIETAL	0.5	0.5	0	0.5	1
	OCCIPITAL	1	0.5	0.5	0	1
	NOTHING	1	1	1	1	0

Unlike comparative statistics, there is no intrinsic significance associated with interrater reliability metrics. Instead, investigators rely on established benchmarks to report qualitative descriptions of the quantitative measures. The interpretation of the Kappa value was based on the guidelines from McHugh (McHugh, 2012), as summarized in Table 2.

Table 2.2: Kappa value thresholds for evaluating level of agreement between raters.

Kappa	**Agreement**
0 - 0.20	None
0.21 - 0.39	Minimal
0.40 - 0.59	Weak
0.60 - 0.79	Moderate
0.80 - 0.90	Strong
> 0.9	Almost perfect

2.2.7 CTP Subtraction Analysis for SOZ Localization

For the subtraction analysis, postictal CT average maps were registered to each patient's baseline CT average maps using an affine transformation (12 degrees of freedom) from FSL FLIRT toolbox (http://www.fmrib.ox.ac.uk/fsl/). Because the anatomical CT images and the CBF CT images share a collective space, the same transformations may be applied to the CBF data, thereby allowing the CBF images to inherit the same accuracy as the anatomical registration. After spatial normalization, the intensities of the postictal CBF maps were normalized to the baseline CBF maps based on global mean CBF value and standard deviation. This was done to account for potential global changes between the two scanning time points. After intensity normalization, the CTP quantification maps were smoothed by a 5-mm full-width-half-maximum Gaussian kernel to improve signal to noise and reduce small-scale registration errors. A global minimum of 0 CBF units and maximum of 100 CBF units was applied to baseline and postictal CBF maps to reduce artifactual hyperperfusion resulting from vessel artifacts. Using these co-registered CBF maps, a subtraction CBF map (baseline minus postictal) was generated for each patient. Additional cluster filtering (at 400 voxels in 3D) was applied to reduce noise from small registration errors and remaining vessel artifacts. The resulting subtraction map was superimposed onto the patient's CT anatomical average map to identify the anatomical brain areas with postictal CBF reductions of at least 15 CBF units relative to their own baseline. A threshold of 15 CBF units was used based on animal studies showing a 30% reduction of CBF (Farrell, et al., 2016).

2.2.7.1 Concordance of CTP Hypoperfusion and Presumed Seizure Onset Zone

The areas showing postictal hypoperfusion on subtraction CTP (sCTP) maps were identified by one reviewer (PF) and classified as follows:

1) Hemisphere and lobe
2) Unilateral vs bilateral
3) Distribution - focal (area within a lobe) or multifocal (involving two or more lobes in hemispheres)

A confidence score from 1 to 5 (1 - not confident, 5 - very confident) was also used to rate the confidence that the reviewer had that the observed areas of hypoperfusion were genuine as opposed to artifact.

An epileptologist (PF) and epilepsy fellow (JP) reviewed all clinical data for each patient and reviewed the expert consensus report from our weekly multidisciplinary epilepsy surgery rounds to confirm the location of the presumed SOZ. To assess concordance, the areas showing postictal hypoperfusion on subtraction CTP (sCTP) maps were compared to the location of the presumed SOZ. The most prominent area of hypoperfusion was considered. Concordance was classified as one of three groups:

1) Fully concordant – CTP hypoperfusion was observed in the same lobe as the presumed SOZ.
2) Partially concordant – CTP hypoperfusion was observed in a different lobe in the same hemisphere as the presumed SOZ.
3) Discordant – CTP hypoperfusion was observed in the hemisphere contralateral to the presumed SOZ.

2.2.7.2 Areas of Seizure Spread and Concordance with EEG Defined Areas of Seizure Propagation

An epileptologist (PF) and epilepsy fellow (JP) reviewed the VEEG of the captured seizure for each patient and identified areas of seizure propagation based on EEG. Areas of hypoperfusion in the sCTP maps seen outside to the area of maximal hypoperfusion were further

assessed as potential areas of seizure spread. Areas of hypoperfusion possibly reflecting seizure spread was classified as concordant with EEG spread if the clusters were in the same hemisphere and lobe(s), or discordant with EEG spread if they were in different lobe(s) in the same hemisphere or on the contralateral side.

2.2.7.3 Region of Interest Analysis of Maximal Postictal Hypoperfusion

The cluster(s) with the maximal hypoperfusion in the presumed SOZ in the subtraction CTP maps was selected and isolated as a 3D ROI. Cluster maps were viewed with a minimum threshold of 15 CBF units. No ROIs were generated in the patient that had no significant postictal hypoperfusion based on sCTP analysis (Pt. 11). In patients where multiple isolated clusters were seen within the presumed SOZ, the two largest clusters were considered for ROI analysis (Pts. 5 and 14). The average CBF value of the cluster, representing the average difference between the baseline and postictal scans, was calculated.

2.3 Results

2.3.1 Patient Selection and Demographics

Fifteen patients were enrolled in the study. One patient did not undergo a baseline CTP scan and one patient did not have the contrast agent fully administered during the postictal scan leading to unusable data. Additionally, two patients had their baseline scans collected using our hospital's clinical protocol (5 mm slice thickness) instead of the study protocol (1.25 mm slice thickness; these two patients were still analyzed and included in the study cohort. Thus, 14 postictal datasets and 13 baseline datasets were visually evaluated. Similarly, 13 patients were fully analyzed using the quantitative subtraction pipeline.

2.3.2 Patient Characteristics

Patient demographic data, clinical information and investigations are summarized in Table 3. The mean age of the patients at the time of the study was 36.6 years (range 22-60 years). Nine patients (60%) were female. The mean duration of epilepsy was 23.7 years (range 6-47 years). Patients had seizures ranging from multiple per day to monthly. Patients 3 and 9 had previous surgical resections (left temporal lobectomy, and right anterior insular resection). MRI was non-lesional in four patients, ictal SPECT was captured for eleven patients (seven of which were on the same event as the postictal CTP study), and PET was obtained for ten patients (Table 3).

Table 2.3: Summary of patient demographics, clinical features, investigations, final presumed seizure localization.

ID	Age/ Sex	Epilepsy Duration (years)	Seizure Frequency	Seizure Description	Interictal EEG	Ictal EEG	Structural MRI	Ictal SPECT	PET	Final Presumed SOZ
1	60 F	25	Monthly	Rt arm dystonia, oroalimentary automatisms, Rt head version, tonic-clonic convulsions	Lt temporal IEDs (Sp1, F7, T3)	Lt anterior temporal	Lt mesial temporal sclerosis	n/a	Lt mesial temporal lobe and hippocampus	Lt temporal
2	33 F	24	Weekly	Hyperkinetic from sleep	Rt hemispheric (max T3, T5) and Rt temporal IEDs (F7, Sp1)	Diffuse onset (max T4)	Malformed Rt middle frontal gyrus, Rt superior/middle temporal gyrus and posterior insula	Rt anterior insula and frontal operculum	Rt temporal, Rt frontal, Rt insula	Rt middle frontal gyrus
3	51 M	26	Monthly	Behavioral arrest, stare, Rt facial twitching, tonic-clonic convulsions	Lt temporal (T3, T5) IEDs and slowing	Lt temporal (max T3)	Lt temporal lobectomy and post-op gliosis.	Rt mid-posterior temporal lobe and insula. Lt temporal operculum and orbitofrontal	Lt orbitofrontal, Lt anterior insula, Rt anterior mesial temporal	Lt temporal
4	52 F	30	Weekly	Hyperkinetic, head version to Lt, and Lt fencing posture	Rt frontal (Fp2, F8, F4) and Rt temporal (F8, Sp2, T4) IEDs	Diffuse onset	Normal	Rt temporal lobe, insula, and frontal operculum	Rt anterior mesial temporal, insula, frontal operculum, inferior orbitofrontal	Rt temporo-frontal
5	32 F	26	Weekly	Dysphasia	Lt hemispheric (max T3, T5) IEDs	Lt posterior quadrant (max T5)	Normal	Lt temporo-occipital and parietal	Lt anterior temporal, Lt occipital	Lt posterior temporal occipital

6	29 F	11	Weekly	Lt sided turning, Rt hand fisting, oral and Rt hand automatisms	Lt temporal (Sp1, T3) IEDs	Lt frontopolar and temporal (SP1, F7, FP1, F3)	Enlarged Lt amygdala	Lt anterior mesial temporal, frontal operculum, & insula	n/a	Lt orbitofrontal - anterior temporal
7	49 F	16	Daily	Tingling in hands and mouth, epigastric rising sensation, profuse sweating	Rt temporal IEDs (Sp2, F8 > T4)	Rt mid-posterior temporal	Cortical encephalomalacia in Rt posterior inferior temporal gyrus and lateral margin of fusiform gyrus	Rt temporal lobe, Rt insula, Rt frontal operculum	n/a	Rt mid-temporal-insula
8	24 M	10	Monthly	Lt head version, tonic-clonic convulsions	Rt hemispheric IEDs, max frontotemporal	Generalized	Normal	Rt temporo-occipital, Rt superior perisylvian region, Rt putamen	Lt anterior mesial temporal, Lt orbitofrontal	Rt hemispheric
9	36 F	31	Weekly	Palpitations, fear, staring	Rt temporal IEDs (F8-Sp2-T4, T4-T6)	Rt frontal and Rt anterior temporal Sp2-T4)	Post-surgical changes in Rt anterior frontal operculum and insula	Lt mid-posterior frontal	Inferior frontal region	Rt fronto-temporal
10	22 M	20	Daily	Choking sensation, bimanual automatisms and confusion	Lt temporal IEDs (F7, T3)	Lt hemispheric maximum posterior quadrant	Longstanding bilateral occipital and parietal encephalomalacia	n/a	n/a	Bihemispheric
11	43 F	40	Weekly	Epigastric rising sensation, nausea, dysgeusia	Bilateral frontal central semi rhythmic theta	No EEG change	Lt hippocampal atrophy	Lt mid-temporal convexity	Rt orbitofrontal, Rt temporal	Lt temporal

12	26 M	20	Yearly	Rt head version, tonic-clonic convulsions	Generalized and bitemporal slowing	Lt hemispheric, max frontal (F7)	Normal	Rt orbitofrontal, periinsular, mesial temporal. Also, Rt frontal, temporal and parietal convexities	Rt mesial temporal, and mild Lt mesial temporal	Lt hemisphere, possibly frontal
13	22 F	6	Weekly	Profuse sweating, deja vu, palpitations, nausea	Rt hemispheric and Rt temporal IEDs (Sp2, T4)	Rt hemispheric, max temporal	Normal	Diffuse Rt temporal	Rt mesial temporal and operculum	Rt temporal
14	55 M	47	Monthly	Whole body tingling, grunting, Rt arm tonic posturing	Bitemporal slowing	Bilateral frontotemporal	Lt mesial temporal sclerosis	Lt orbitofrontal, Lt mesial temporal	Lt anterior mesial temporal, Lt orbitofrontal	Lt hemisphere, likely orbitofrontal

2.3.3 Localization of the Presumed Seizure Onset Zone

The presumed SOZ was identified in all 13 patients using all available information and was found to temporal in six patients, frontal in three, temporofrontal in two, hemispheric in one, and bihemispheric in one (Table 3). Patient 1 underwent surgery, and patients 2 and 5 underwent intracranial VEEG.

2.3.4 Recorded Seizures

Table 4 summarizes the details of the seizures that were used for the postictal CTP measurements. Eight patients experienced a focal seizure with impaired awareness, four had seizures evolving to bilateral convulsions, and two had a focal aware seizure. The seizures lasted an average of 102 sec (range 29-208 sec). Postictal CTP scans were obtained an average of 52.4 min following seizure termination (range 35 – 73 min).

Table 2.4: Summary of captured seizure information and timing of image collection.

ID	Seizure Type	EEG Onset	Seizure Duration (sec)	Time to CTP (min)	Interictal Baseline EEG
1	Focal to bilateral tonic clonic	Lt anterior and mid-temporal	153	62	Not very active
2	Focal impaired awareness	Diffuse Lt temporal. Post-ictal slowing Rt temporal and bifrontal.	67	35	Not very active
3	Focal to bilateral tonic clonic	Lt temporal (max T3), spread to Lt frontocentral (F3-C3)	110	43	Very active
4	Focal impaired awareness	Diffuse onset (marred by movement artefacts), Rt anterior temporal later	73	47	Very active
5	Focal impaired awareness	Lt hemispheric, later max frontotemporal (F7/T3/T5)	61	40	Very active
6	Focal impaired awareness	Frontotemporal (max SP1-F7-FP1-F3), spread to Lt temporal and later bifrontal	69	41	Not very active
7	Focal aware	Rt mid-temporal (max T4), spread to Rt parasagittal. Postictal Rt temporal delta.	29	80	Very active
8	Focal to bilateral tonic clonic	Generalized theta (max Rt hemisphere) for 3 secs, then persistent rhythmic delta/theta in Rt hemisphere	120	53	Not very active
9	Focal impaired awareness	Rt frontotemporal (max Fp2-F4-F8-Sp2)	94	36	Not very active
10	Focal impaired awareness	Lt fronto temporal, later posterior temporal	217	44	Very active
11	Focal aware	No EEG change	60	63	Not very active
12	Focal to bilateral tonic clonic	Lt frontotemporal (F7-Sp1), evolved to bifrontal (max Lt)	81	70	Not very active
13	Focal impaired awareness	Rt frontotemporal, evolving to Rt hemispheric (F8, Sp2)	97	46	Not very active
14	Focal impaired awareness	Rt frontal, later bifrontal.	208	73	Not very active

2.3.5 Localization of Postictal Hypoperfusion: Visual Assessment

Table 5 summarizes the visual evaluations of the two reviewers. For 5 mm thick slice evaluations, Reviewer 1 detected localized hypoperfusion in seven postictal scans (concordant with the presumed SOZ in four cases; Pts. 3,4,6,13), zero baseline scans, and 12 baseline vs postictal comparisons (concordant with the presumed SOZ in with ten cases; Pts. 1-10). Reviewer 2 detected localized hypoperfusion in nine postictal CTP scans (concordant with the presumed SOZ in seven cases; Pts. 2-4, 6-7, 10, 13), four baseline scans (concordant with the presumed SOZ in two cases; Pts. 7, 10), and eleven in baseline vs postictal comparisons (concordant with the presumed SOZ in eight cases; Pts. 2-8, 14).

For 1.25 mm thick slice evaluations, Reviewer 1 detected localized hypoperfusion in eight postictal CTP scans (concordant with the presumed SOZ in six cases; Pts 2-4, 8, 11, 13), two baseline scans (concordant with the presumed SOZ in zero cases), and eight baseline vs postictal comparisons (concordant with the presumed SOZ in five cases; Pts. 2-4, 8, 11). Reviewer 2 detected localized hypoperfusion in ten postictal scans (concordant with the presumed SOZ in nine cases; Pts. 1-5, 8, 10-11, 13), three baseline scans (concordant with the presumed SOZ in two cases; Pts. 9, 12), and eleven baseline vs postictal comparisons (concordant with the presumed SOZ in nine cases; Pts. 1-5, 8-11).

In 1.25 mm and 5 mm thick slices, global postictal hypoperfusion was detected by both reviewers in 4/13 patients and 5/13, respectively. Fig. 2.1A shows an example where the postictal scan was globally hypoperfused relative to the baseline in one patient. In addition, localized maximal hypoperfusion was also seen in the right mid-posterior temporal lobe, consistent with hyperperfusion seen during ictal SPECT for the same seizure. The remaining

patients had similar global CBF ranges postictally and interictally, but also displayed localized hypoperfusion. Fig. 2.1B shows an example where the postictal scan showed localized maximal hypoperfusion in right midtemporal region, consistent with hyperperfusion seen during ictal SPECT for the same seizure. Patient 11 did not have any EEG change with her seizure and visual review of the CTP data was non-localizing in all assessments between both reviewers.

Table 2.5: Summary of visual assessments from each reviewer for 5 mm and 1.25 mm thick slices and their concordance to the presumed SOZ. Abbreviation: Con. = concordance.

ID	Final Presumed SOZ	5mm slices											
		Postictal				Baseline				Postictal vs. Baseline			
		Reviewer 1	R1 Con.	Reviewer 2	R2 Con.	Reviewer 1	R1 Con.	Reviewer 2	R2 Con.	Reviewer 1	R1 Con.	Reviewer 2	R2 Con.
1	Lt temporal	No localization	n/a	Rt temporal	N	No localization	n/a	No localization	n/a	Lt parietal	Y	Rt parietal	N
2	Rt middle frontal gyrus	Lt frontal	N	Rt temporal	Y	No localization	n/a	No localization	n/a	Rt temporal	Y	Rt parietal	Y
3	Lt temporal	Lt parietal	Y	Lt parietal	Y	No localization	n/a	Rt temporal	N	Lt temporal	Y	Lt parietal	Y
4	Rt temporofrontal	Rt frontal	Y	Rt parietal	Y	No localization	n/a	No localization	n/a	Rt temporal	Y	Rt temporal	Y
5	Lt posterior temporal occipital	No localization	n/a	No localization	n/a	No localization	n/a	No localization	n/a	Lt frontal	Y	Lt frontal	Y
6	Lt orbitofrontal - anterior temporal	Lt temporal	Y	Lt parietal	Y	No localization	n/a	No localization	n/a	Lt hemisphere	Y	Lt parietal	Y
7	Rt mid-temporal- insula	No localization	n/a	Rt parietal	Y	No localization	n/a	Rt parietal	Y	Rt temporal	Y	Rt temporal	Y
8	Rt hemispheric	Lt parietal	N	No localization	n/a	No localization	n/a	No localization	n/a	Rt temporal	Y	Rt temporal	Y
9	Rt fronto-temporal	No localization	n/a	No localization	n/a	No localization	n/a	No localization	n/a	Rt temporal	Y	No localization	n/a
10	Bihemispheric	No localization	n/a	Lt temporal	Y	No localization	n/a	Lt parietal	Y	Lt temporal	Y	Rt frontal	N
11	Lt temporal lobe	No localization	n/a	No localization	n/a	No localization	n/a	No localization	n/a	No localization	n/a	No localization	n/a
12	Lt hemisphere, possibly frontal	Rt temporal	N	Rt parietal	N	No localization	n/a	No localization	n/a	Rt temporal	N	Rt hemisphere widespread - temporal	N
13	Rt temporal	Rt parietal	Y	Rt parietal	Y	n/a	n/a	n/a	n/a	n/a	n/a	n/a	n/a
14	Lt hemispheric, likely orbitofrontal	No localization	n/a	No localization	n/a	No localization	n/a	Rt parietal	N	Rt temporal	N	Lt temporal	Y

ID	Final Presumed SOZ	1.25 mm slices											
		Postictal				Baseline				Postictal vs. Baseline			
		Reviewer 1	R1 Con.	Reviewer 2	R2 Con.	Reviewer 1	R1 Con.	Reviewer 2	R2 Con.	Reviewer 1	R1 Con.	Reviewer 2	R2 Con.
1	Lt temporal	Rt temporal	N	Lt temporal	Y	Rt temporal	N	No localization	n/a	Rt temporal	N	Lt temporal	Y
2	Rt middle frontal gyrus	Rt temporal	Y	Rt temporal	Y	No localization	n/a	No localization	n/a	Rt parietal	Y	Rt parietal	Y
3	Lt temporal	Lt temporal	Y	Lt frontal	Y	No localization	n/a	No localization	n/a	Lt temporal	Y	Lt frontal	Y
4	Rt temporofrontal	Rt temporal	Y	Rt temporal	Y	No localization	n/a	No localization	n/a	Rt parietal + temporal	Y	Rt parietal	Y
5	Lt posterior temporal occipital	No localization	n/a	Lt temporal	Y	No localization	n/a	No localization	n/a	No localization	n/a	Rt occipital	Y
6	Lt orbitofrontal -anterior temporal	No localization	n/a	No localization	n/a	No localization	n/a	No localization	n/a	Rt hemisphere	N	No localization	n/a
7	Rt mid-temporal-insula	No localization	n/a	No localization	n/a	No localization	n/a	No localization	n/a	No localization	n/a	No localization	n/a
8	Rt hemispheric	Rt temporal	Y	Rt temporal	Y	No localization	n/a	No localization	n/a	Rt temporal	Y	Rt temporal	Y
9	Rt fronto-temporal	No localization	n/a	No localization	n/a	No localization	n/a	Rt temporal	Y	No localization	n/a	Rt temporal	Y
10	Bihemispheric	No localization	n/a	Lt occipital	Y	Rt parietal	N	Rt temporal	N	No localization	n/a	Lt temporal	Y
11	Lt temporal	No localization	Y	No localization	Y	No localization	n/a	No localization	n/a	No localization	Y	No localization	Y
12	Lt hemisphere, possibly frontal	Rt temporal	N	Rt temporal	N	No localization	n/a	Lt temporal	Y	Rt temporal	N	Rt temporal	N
13	Rt temporal	Rt hemisphere	Y	Rt temporal	Y	n/a	n/a	n/a	n/a	n/a	n/a	n/a	n/a
14	Lt hemispheric, likely orbitofrontal	No localization	n/a	No localization	n/a	No localization	n/a	Rt temporal	N	Rt temporal (baseline was hypoperfused vs postictal)	N	Rt temporal (baseline was hypoperfused vs postictal)	N

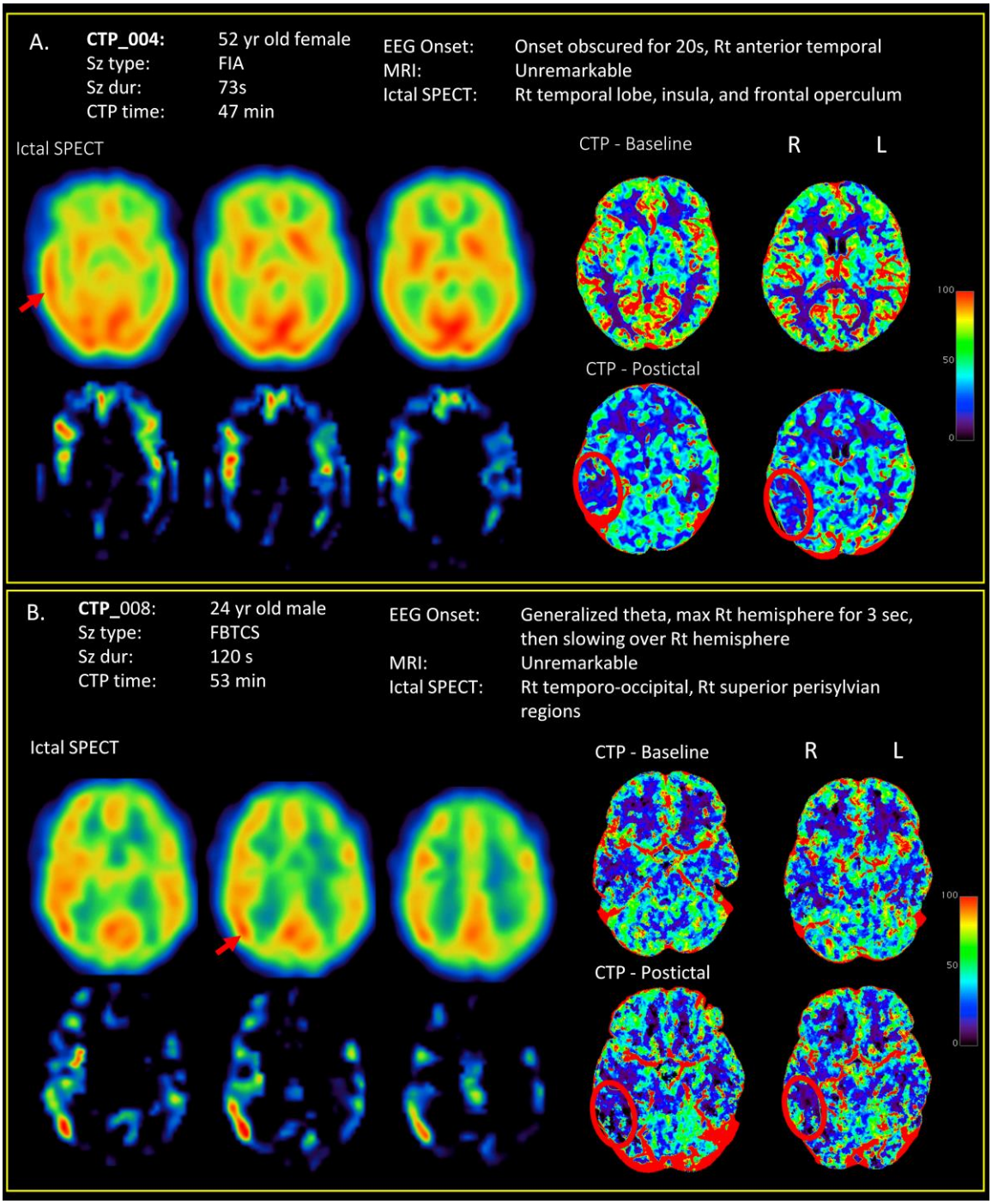

Figure 2.1: Examples of localizing visually detected post-ictal hypoperfusion. A. An example of global hypoperfusion relative to baseline, with more pronounced focal hypoperfusion in the right mid-posterior temporal region (5 mm). Ictal SPECT of the same seizure showed right temporal hyperperfusion (arrow). B. An example of focal post-ictal hypoperfusion with no global CBF differences (1.25 mm). Ictal SPECT of the same seizure showed right temporal hyperperfusion (arrow).

Table 6 summarizes the statistical sensitivity, positive predictive value, and Kappa coefficient for each reviewer in each condition. Kappa coefficients of interrater reliability were on average highest in the 1.25 mm thick slices compared to 5 mm thick slices. For both thicknesses, interrater agreement was on average highest in the side-by-side comparison, and lowest in viewing single baseline scans. Localization, PPV and sensitivity were highest in side-by-side comparisons and lowest in independent baseline scans. Indeed, visually reviewing one scan was minimally localizing, particularly interictal scans.

Table 2.6: Statistical summary of visual assessments.

			Baseline	**Post-ictal**	**Baseline vs Postictal**
5 mm slices	Kappa	*Hemisphere*	0	0.466	0.469
		Lobe	0.513	0.330	0.574
	Sensitivity	*Reviewer 1*	0	0.417	0.917
		Reviewer 2	0.167	0.666	0.900
	PPV	*Reviewer 1*	0	0.714	0.917
		Reviewer 2	0.5	0.889	0.818
1.25 mm slices	Kappa	*Hemisphere*	0.188	0.656	0.444
		Lobe	0.222	0.546	0.611
	Sensitivity	*Reviewer 1*	0	0.500	0.555
		Reviewer 2	0.167	0.692	0.818
	PPV	*Reviewer 1*	0	0.857	0.625
		Reviewer 2	0.167	1.00	0.900

2.3.5.1 Special Cases: Patients with Baseline Hypoperfusion (Pt. 14)

Reviewers 1 and 2 independently assessed Patient 14 as showing localized baseline hypoperfused relative to postictal in the 5 mm and 1.25 mm postictal vs baseline comparison. The postictal scan when viewed alone was non-localizing and globally uniform. Baseline hypoperfusion was subtle and was localized to the right temporal region. Interestingly, the localization of hypoperfusion in the baseline was the same for both reviewers and was partially concordant with the EEG onset location of the captured seizure and was in the same lobe to subtraction CTP results. Although partially concordant with the EEG of the captured seizure, the location of the baseline hypoperfusion was ultimately contralateral to the final presumed SOZ (left hemispheric, orbitofrontal). Both reviewers also gave a lower confidence score on their assessments.

2.3.6 Subtraction CTP (sCTP) Data

2.3.6.1 Localization of Postictal Hypoperfusion and Areas of Seizure Spread: Quantitative sCTP

Table 7 summarizes the results of sCTP localization of postictal hypoperfusion and additional areas of seizure spread. Localized postictal hypoperfusion was detected in 12/13 patients (92%; Pts. 1-10, 12, and 14). One patient (Pt. 11) who had a focal aware seizure without any EEG changes showed had no significant perfusion changes. Nine patients had unilateral postictal hypoperfusion, with a focal distribution in five (Pts. 1, 2, 6, 7, and 8) and multifocal distribution in four (Pts. 3, 4, 9, and 12). Three patients had bilateral and multifocal postictal hypoperfusion (Pts. 5, 10 and 14). Additional clusters of hypoperfusion identified as areas of seizure spread were seen in 12/13 patients. In addition, the degree of postictal hypoperfusion was

positively correlated with seizure duration (Fig. 2.2; Pearson r = 0.70, two-tailed significance; P = 0.006)

Table 2.7: Summary of sCTP results showing the location and distribution of postictal hypoperfusion and its concordance with the SOZ. Abbreviation: Con. = concordance.

ID	Final Presumed SOZ	Sz. Type	EEG Onset	sCTP Max. Location	Unilateral vs Bilateral	Distri-bution	Con. with SOZ	Confi-dence (1-5)	CTP superior to MRI?	CTP superior to SPECT?	CTP superior to PET?	EEG Spread	sCTP Seizure Spread Location	Con. with EEG Seizure Spread
1	Lt temporal	FBTC	Lt anterior and mid-temporal	Lt temporal	Unilateral	Focal	Fully concordant	5	Equal	n/a	Equal	Spread to Lt parasagittal region	Lt temporal and Rt temporal	Y
2	Rt middle frontal gyrus	FIA	Diffuse Lt temporal. Post-ictal slowing Rt temporal and bifrontal	Rt temporal	Unilateral	Focal	Partially concordant	3	Inferior	Inferior	Equal	Spread over bilateral frontal	Bifrontal (max Lt)	Y
3	Lt temporal	FBTC	Lt temporal (max T3), spread to Lt frontocentral (F3-C3)	Lt temporal	Unilateral	Multifocal	Fully concordant	3	Equal	Superior	Equal	Diffuse Lt hemisphere spread and spread to Rt temporal and frontal	Lt hemispheric	Y
4	Rt temporo-frontal	FIA	Diffuse onset (marred by movement artefacts), Rt anterior temporal later	Rt temporo-frontal	Unilateral	Multifocal	Fully concordant	3	Superior	Equal	Equal	Spread to Rt frontal and Lt temporal/frontal	Bilateral frontal and Lt frontal	Y
5	Lt posterior temporal occipital	FIA	Lt hemispheric, later max frontotemporal (F7/T3/T5)	Lt temporal	Bilateral	Multifocal	Partially concordant	2	Superior	Equal	Equal	Diffuse Rt occipitotemporal region	Rt occipitotemporal	Y
6	Lt orbito-frontal/ anterior temporal	FIA	Frontotemporal (max SP1-F7-FP1-F3)	Lt mesial temporal	Unilateral	Focal	Partially concordant	3	Equal	Equal	n/a	Spread to Lt temporal, Lt frontopolar, then Rt frontal	Lt frontopolar	Y

7	Rt mid-temporal-insula	FA	Rt mid-temporal (max T4), spread to Rt parasagittal. Postictal Rt temporal delta	Lt thalamus	unilateral	Focal	Discordant	3	Inferior	Inferior	n/a	Spread to Rt parasagittal regions	Rt posterior frontal	Y
8	Rt hemisphere	FBTC	Rt hemisphere	Rt temporal	Unilateral	Focal	Fully concordant	4	Superior	Equal	Superior	Spread to Rt temporal, then Lt temporal	Rt temporal and Lt temporal	Y
9	Rt fronto-temporal	FIA	Rt frontotemporal (max Fp2-F4-F8-Sp2)	Rt fronto-temporal	Unilateral	Multifocal	Fully concordant	4	Equal	Superior	Inferior	Spread to Lt frontotemporal	Lt temporal and Lt frontal	Y
10	Bi-hemispheric	FIA	Lt fronto temporal, later posterior temporal	Lt temporal	Bilateral	Multifocal	Partially concordant	4	Equal	n/a	n/a	Spread to Lt posterior temporal, and minimum spread to Rt	Lt frontotemporal and Rt temporal	Y
11	Lt temporal	FA	No EEG change	Not clear	n/a	n/a	n/a	n/a	Inferior	Inferior	Inferior	No EEG change	No spread observed	n/a
12	Lt hemisphere, possibly frontal	FBTC	Lt frontotemporal (F7-Sp1), evolved to bifrontal (max Lt)	Rt fronto-temporal	Unilateral	Multifocal	Discordant	5	Inferior	Equal	Inferior	Spread to Rt	Rt hemisphere including primary motor cortex	Y
14	Lt hemisphere, likely orbito-frontal	FIA	Rt frontal, later bifrontal	Rt temporal and Lt temporal	Bilateral	Multifocal	Partially concordant	5	Inferior	Inferior	Inferior	Bifrontal spread	Bifrontal	Y

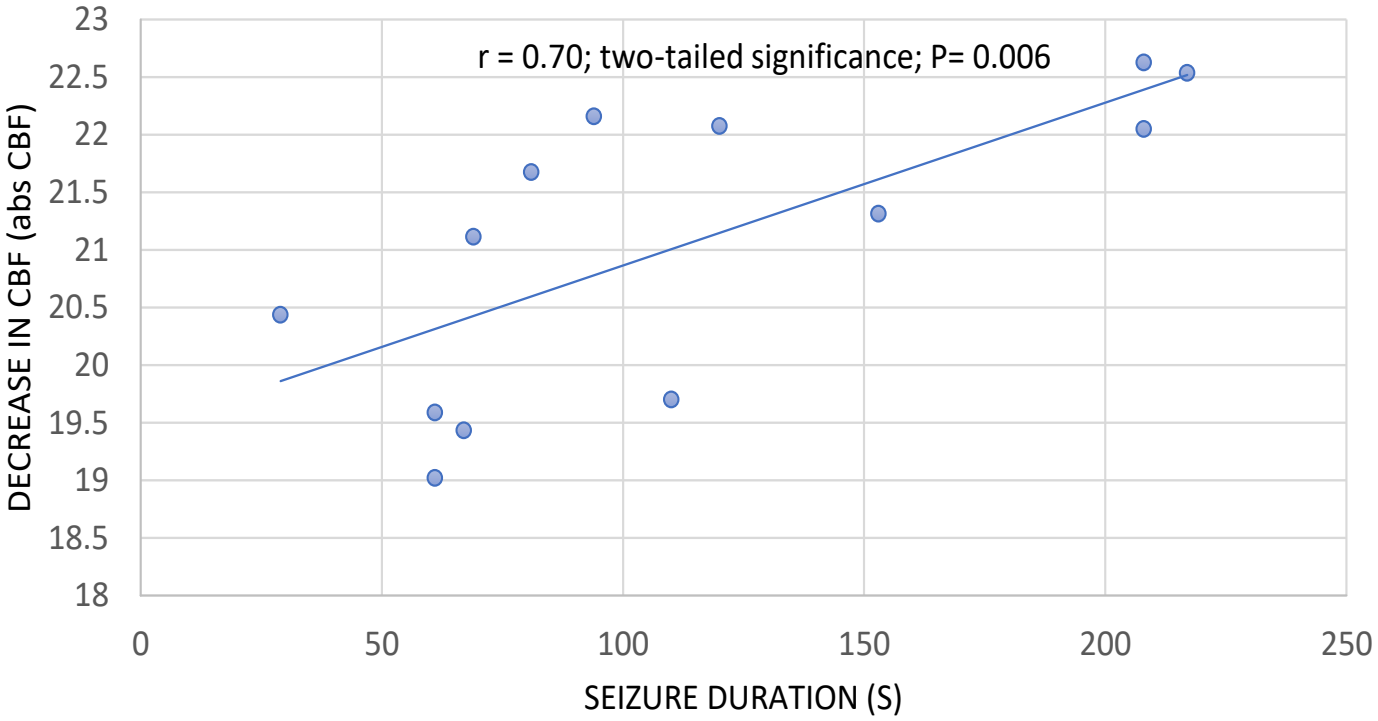

Figure 2.2: The degree of post-ictal hypoperfusion is directly related to seizure duration. Scatter plot of the relation between the absolute decrease of CBF (baseline minus postictal scans) in the suspected SOZ and seizure duration. A significant positive correlation was seen between these two measurements. (Pearson r = 0.70; two-tailed significance; P = 0.006).

2.3.6.2 Concordance with Seizure Onset Zone and Areas of Seizure Spread

Hypoperfusion was seen in 12/13 patients (92%) and the location of postictal hypoperfusion was fully concordant with the presumed SOZ in five patients (Pt. 1, 3-4, 8-9) partially concordant in five (Pt. 2, 5-6, 10, 14) (Table 7). An example of unilateral focal hypoperfusion concordant with the presumed SOZ is seen in Fig. 2.3. Specifically, sCTP correctly localized the ictal hemisphere in ten patients, and additionally the lobe in five.

Two patients (Pts. 7 and 12) were assessed as discordant. Interestingly, Patient 12 had a presumed SOZ in the left hemisphere, but he also experienced left hemiparesis for over 24 hours, suggesting a right-hemispheric involvement. Indeed, in this patient, localized postictal hypoperfusion was seen in the right postcentral gyrus (Fig. 2.4). The other discordant patient (Pt. 7) had a focal aware seizure with the shortest seizure duration (29 sec) of all patients.

The location of postictal hypoperfusion reflecting seizure spread was concordant with EEG patterns of seizure spread in all 12 patients that showed postictal hypoperfusion (Table 7). Fig. 2.5 shows an example where the presumed SOZ is highlighted as the most significant cluster with the additional areas of hypoperfusion reflecting seizure spread.

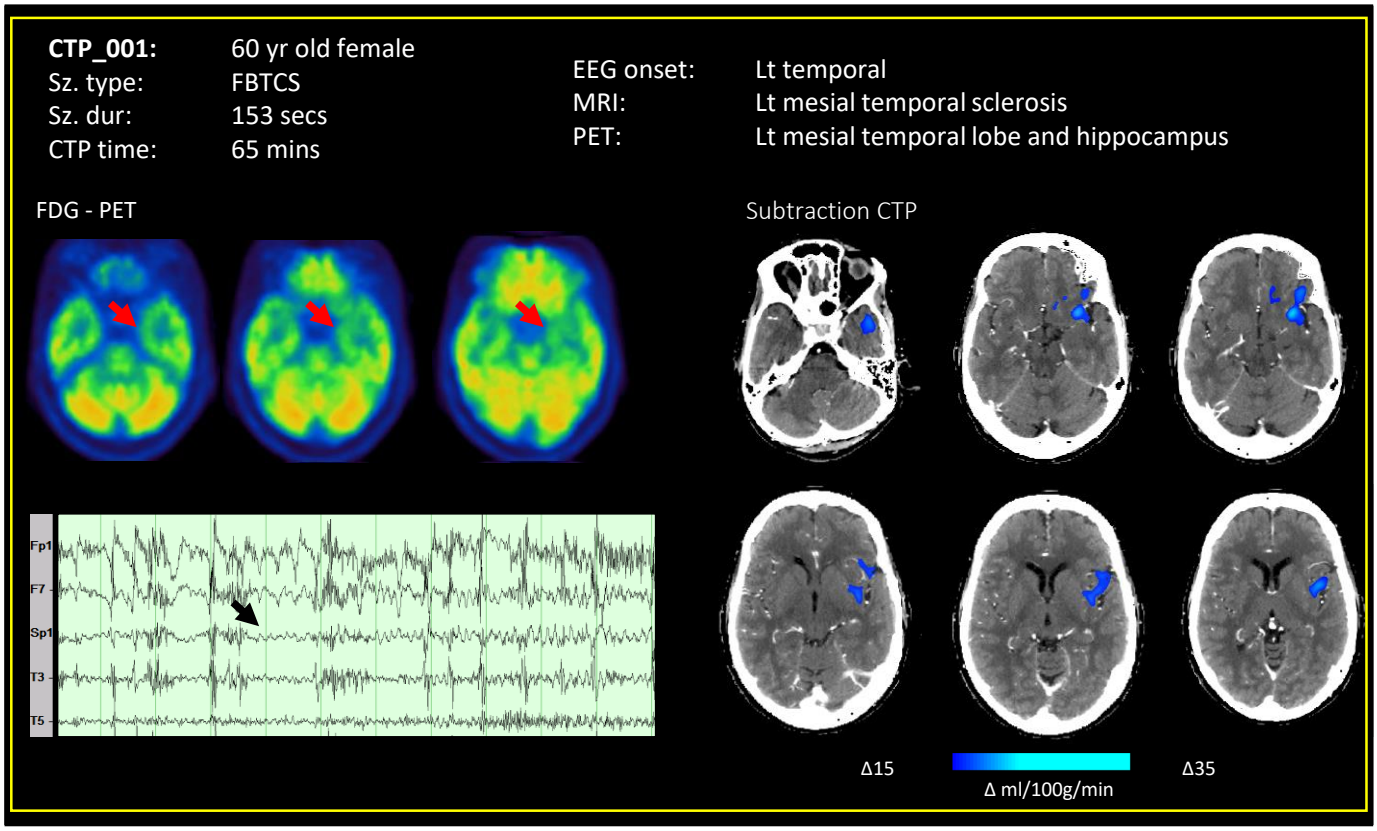

Figure 2.3: Example of unilateral focal hypoperfusion seen on sCTP in a 60 year old female with intractable epilepsy ipsilateral to the final presumed SOZ. FDG-PET (top left) localized to the left mesial temporal lobe and hippocampus (arrow). Ictal EEG recording (bottom left) showing seizure onset in the left temporal region (arrow).

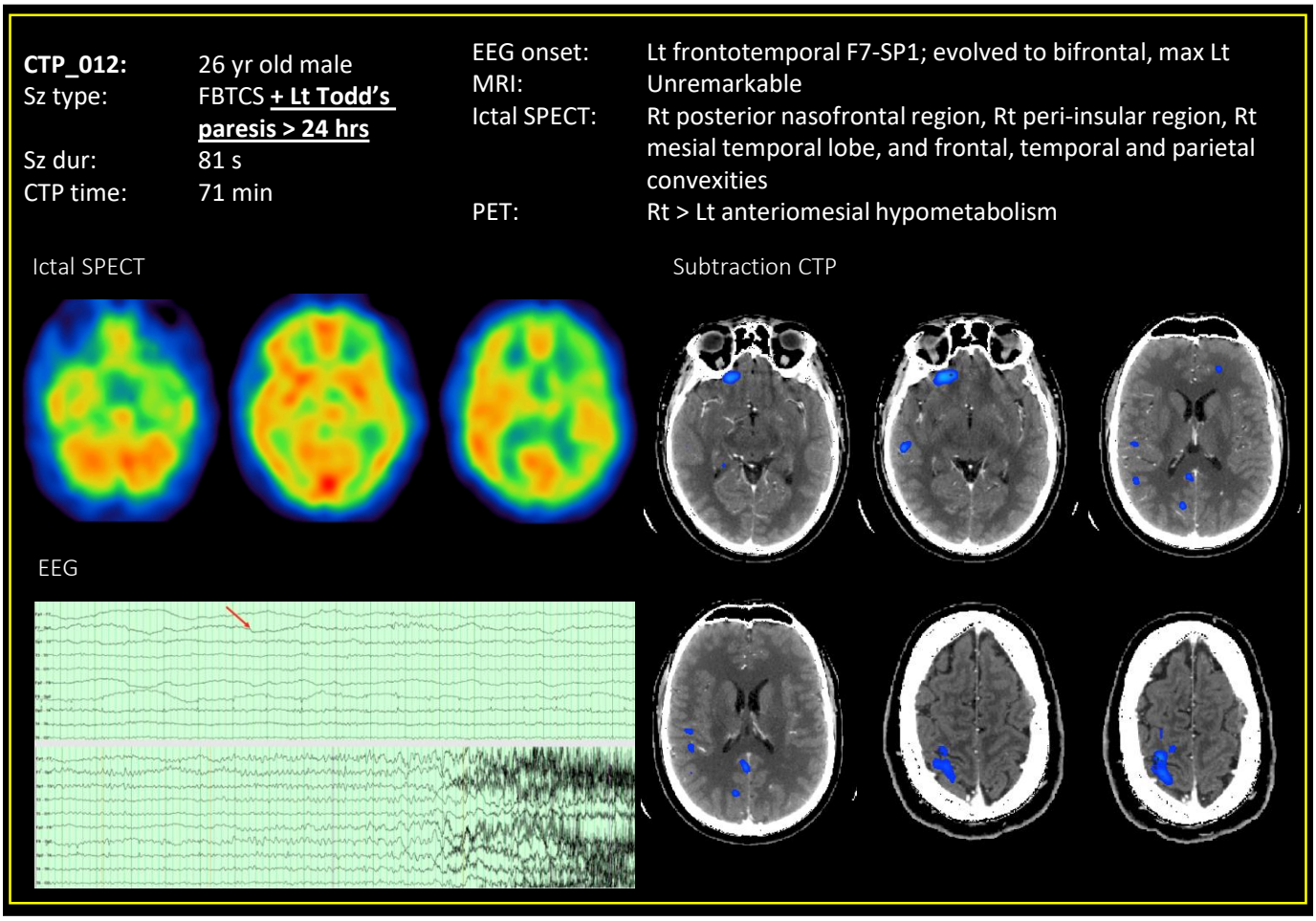

Figure 2.4: Example of unilateral multifocal hypoperfusion contralateral to the final presumed SOZ. Ictal SPECT (top left) of a different seizure showed right hemispheric hyperperfusion. Ictal EEG recording (bottom left) showing seizure onset in the left frontotemporal region (arrow). Case study where sCTP displayed hypoperfusion in the right hemisphere, contralateral to EEG onset, however the patient clinically exhibited left hemiparesis for over 24 hours following the same event.

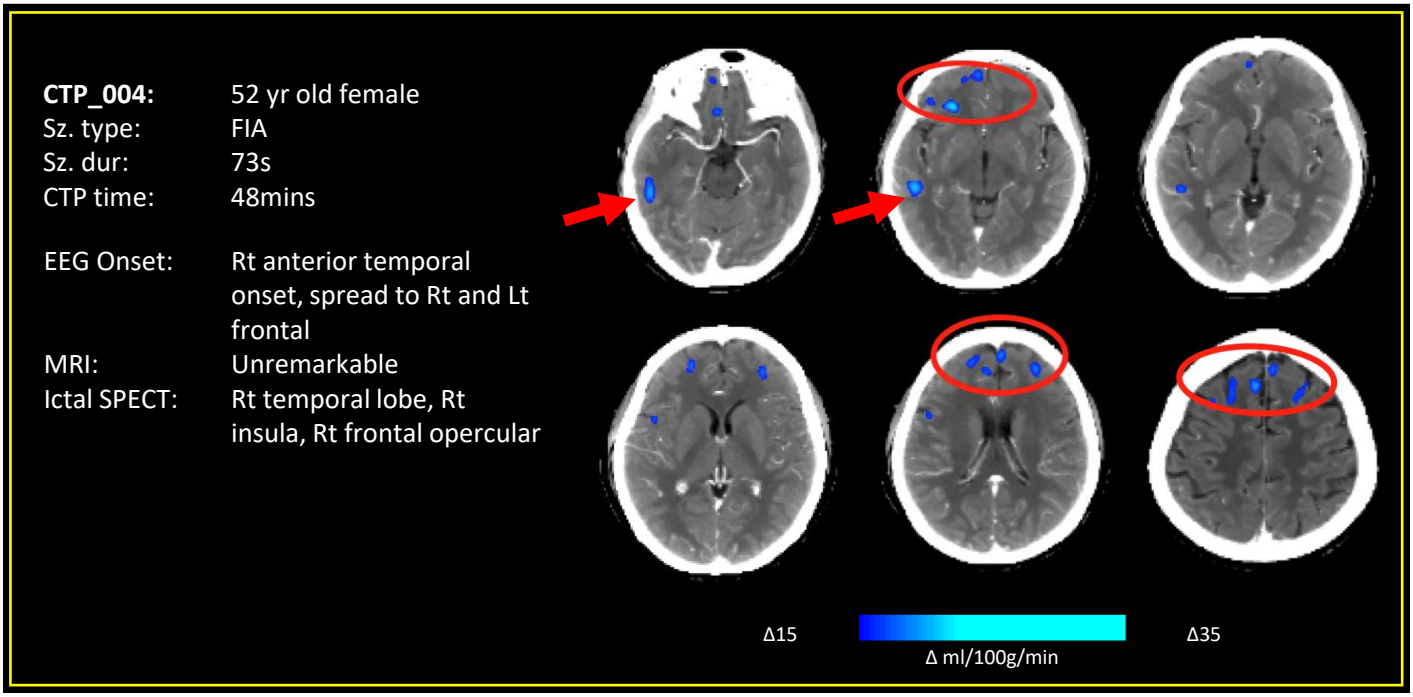

Figure 2.5: Example of sCTP detected unilateral focal hypoperfusion in area of seizure onset with additional hypoperfusion in areas of seizure spread as determined by ictal EEG. Arrow denotes cluster of presumed seizure onset, with circles representing additional areas of seizure spread.

2.3.6.3 Comparison with Clinical Imaging Data

Of the 12 patients where significant postictal hypoperfusion was seen, eight had lesional MRIs. sCTP was concordant with the MRI findings in six of these patients (Pt. 1-3, 6-7, 14) (Table 7). Of all 13 patients studied, sCTP provided similar localization to MRI in five patients (Pts. 1, 3, 6, 9-10), superior localization in three (Pts. 4, 5, 8), and inferior localization in five (Pts. 2, 7, 11-14).

PET was performed in 10/13 patients with significant postictal hypoperfusion and sCTP was concordant with PET in six patients (Table 7). Of all 13 patients in the study, sCTP provided similar localization to PET in five patients (Pts. 1-5), superior localization in one (Pt. 8), and inferior localization in four (Pts. 9, 11-12, 14).

Ictal SPECT was performed in 11/13 patients and sCTP was concordant with ictal SPECT findings in seven patients. Of all 13 patients studied, sCTP provided similar localization to ictal SPECT in five patients (Pts. 4-6, 8, 12), superior localization in two (Pts. 3, 9), and inferior localization in four (Pts. 2, 7, 11, 14). In seven patients (Pts. 2- 5, 7-8, 11), postictal CTP was performed on the same seizure as the ictal SPECT. This facilitated direct comparison of postictal CTP to ictal SPECT. sCTP localization in these cases was similar in three (Pts. 4-5, 8), superior in one (Pt. 3), and inferior in three (Pts. 2, 7, 11). Interestingly, 2/3 patients assessed as inferior had focal aware seizures and the remaining patient differed slightly in assessments with sCTP localizing to right temporal whereas SPECT localized to right frontal.

2.3.6.4 Special Cases: Patients with Previous Epilepsy Surgery

Two patients had previous epilepsy surgery. Patient 3 had a previous left temporal lobectomy and amygdalohippocampectomy and Patient 9 had a previous right anterior insular

resection. In both cases, sCTP displayed unilateral multifocal perfusion patterns that were fully concordant with the presumed SOZ and EEG of the captured seizure.

2.3.6.5 Special Cases: Patients Undergoing Intracranial EEG

Two patients subsequently underwent intracranial VEEG monitoring to further clarify the location of the SOZ (Pts. 2 and 5). Intracranial VEEG monitoring localized the SOZ to the right middle frontal gyrus in Patient 2 and the left posterior temporal occipital focus in Patient 5. Interestingly, the final localization of the SOZ for patient 5 was based on interictal discharges lateralizing to the left, whereas ictal onset was diffuse over the right occipitotemporal region. Although sCTP ultimately localized to the left temporal, there was a subtle bilateral distribution with clusters of hypoperfusion observed in the right occipitotemporal region concordant with ictal discharges seen through intracranial EEG monitoring.

2.3.6.6 Special Cases: Patient with Postictal Left Hemiparesis and Brainstem Hypoperfusion (Pt. 12)

The location of postictal hypoperfusion detected by sCTP for patient 12 was discordant with the presumed SOZ. Specifically, sCTP showed areas of hypoperfusion in the right pre- and postcentral gyrus, right orbitofrontal, and right temporal regions, contralateral to the presumed SOZ (left hemispheric, potentially frontal) and the EEG of the captured seizure (left frontotemporal onset) (Fig. 2.4). In addition, Patient 12 was the only patient that displayed clear clusters of hypoperfusion in the brainstem. Notably, the patient exhibited left hemiparesis for over 24 hours following the same event. Interestingly, ictal SPECT of a different seizure showed hyperperfusion in the right orbitofrontal, periinsular, mesial temporal as well as the right frontal, temporal and parietal convexities, which correlate with the clusters seen on sCTP.

2.3.7 Potential Confounders

Several cofounders were considered including late CTP data acquisition (> 65 min postictal), postictal scanning CTP scanning following focal aware seizures, seizure duration and duration of epilepsy. Of these potential confounders, late acquisition and seizure type may have been the greatest contributors to the absence of significant postictal hypo-perfusion. Postictal CTP studies were performed more than 65 min after seizure termination in three patients (Pts. 7, 12, 14). The location of postictal hypoperfusion for two of these patients were discordant with the presumed SOZ (Pts. 7,12). A focal aware seizure was captured for two patients; one patient did not have any EEG changes and showed no postictal hypoperfusion (Pt. 11) and the other had sparse regions of hypoperfusion in parasagittal regions contralateral to the presumed SOZ and was thus discordant (Pt. 7).

2.4 Discussion

This is the first systematic study observing immediate postictal hypoperfusion detected using CTP both qualitatively through visual assessments by expert reviewers, and quantitatively through subtraction of postictal and baseline images. We have shown that sCTP can be safely and rapidly performed in patients in the postictal state and is able to detect localized hypoperfusion corresponding to the presumed SOZ and areas of seizure propagation. When baseline and postictal CBF images were visually compared side-by-side, localized hypoperfusion was detected by at least one reviewer in 9/13 (69%) of patients, with an average concordance of 65% to the presumed SOZ. When quantitatively subtracted from the patient's baseline perfusion scan, CTP demonstrated postictal reductions of >15 CBF units in 12/15 patients (80%). The location of the hypoperfusion was partially or fully concordant with the presumed SOZ in 10/12 (83%) of these patients, and all patients localized additional clusters of hypoperfusion in areas of seizure propagation concordant with ictal VEEG.

2.4.1 Determining the Seizure Onset Zone

Our study was strengthened by comparing postictal CTP CBF images directly to ictal VEEG recordings, which are the gold standard for SOZ localization. Most previous CTP studies retrospectively investigated patients that presented to stroke centers and classified seizures and the presumed SOZ based on patient clinical history (Gelfand, et al., 2010; Hauf, et al., 2009; Mathews, et al., 2008; Shelly, et al., 2017). In these studies, most patients did not undergo EEG confirmation, and seizure descriptions were based on witness accounts. A few ASL studies used interictal scalp VEEG to determine the presumed SOZ (Sierra-Marcos, et al., 2016; Storti, et al., 2014), but none apart from a recent study from the Federico lab used concurrent ictal recordings (Gaxiola-Valdez, et al., 2017). Previous SPECT studies have shown that interictal SPECT may

lead to false localizations, had lower sensitivity (0.44) and was correctly localizing in 49% of patients, whereas ictal SPECT had higher sensitivity (0.97) and was correctly localizing in 81% of patients (Devous, et al., 1998; Spanaki, et al., 1999). Given the dynamic nature of CBF changes, interictal haemodynamic changes do not consistently correlate with the SOZ and may not be a dependable proxy of the SOZ, especially in patients with structural abnormalities (Sierra-Marcos, et al., 2016; Storti, et al., 2014). One study showed interictal hypoperfusion through ASL in 81% of patients up to 60 days after seizures (Kim, et al., 2016). However, none of these patients underwent continuous VEEG immediately prior to the ASL study, so any undetected seizures may have confounded these results. The Federico lab prospectively collected immediate postictal scans following an electrographically confirmed seizure and had accurate recordings between seizure termination and ASL scan collection (Gaxiola-Valdez, et al., 2017). Although immediate postictal hypoperfusion detected by ASL was reliably localizing in 80% of patients and does not involve radiation or administration of a contrast agent, it is logistically difficult to obtain immediate short notice access to the MR scanner. This study aimed to provide an alternative to ASL imaging, as CTP is more logistically feasible and clinically implementable for collecting immediate postictal CBF data. As our study was performed with accurate VEEG information about seizure onset, duration, type, and localization, we had the advantage of assessing concordance of the CTP data directly with the SOZ for the captured seizure.

2.4.2 Timing of Postictal CTP

Currently, there exists no clear definition of the duration of the postictal state. This has led studies to claim postictal status with image collection ranging from several min to several weeks after a seizure (Gelfand, et al., 2010; Guo, et al., 2015; Hauf, et al., 2009; Mathews, et al., 2008; Pizzini, et al., 2013; Shelly, et al., 2017; Wiest, et al., 2006; Wolf, et al., 2001). Additionally,

because many of these studies did not employ ictal VEEG, seizure onset was based on witness accounts leading to an inaccurate measure of the time passed between scan acquisition and seizure termination. A recent animal study systematically evaluated postictal hypoperfusion and hypoxia and found that these changes consistently lasted for approximately 60 min at the SOZ before returning to pre-seizure values (Farrell, et al., 2016). This temporal characterization of postictal hemodynamic changes may explain why previous postictal studies obtained conflicting or non-localizing results. Previous ASL studies that yielded both postictal hypoperfusion and hyperperfusion may also be a result of the different time points at which ASL scanning was performed. Previously, Hauf et al., (2009) performed CTP within approximately 30-90 min of seizure termination and found persisting localizing hyperperfusion in all patients presenting with status epilepticus, and lateralizing hypoperfusion in only 30% of patients in a postictal state. The authors did not report the time elapsed between seizure termination and CTP acquisition for each patient, thus it is possible that the three patients that exhibited postictal hypoperfusion were scanned closer to seizure termination. The time elapsed between seizure termination and image collection could also be longer than reported as seizures were witnessed instead of monitored via ictal VEEG. Gefland et al., (2010) found that patients who were scanned more than two hours after seizure termination showed significantly fewer abnormal perfusion patterns than those scanned at less than two hours. These findings further illustrate the transient and temporal sensitivity of the postictal hypoperfused state and suggest that the timing of postictal image acquisition is critical.

The dynamic nature of CBF changes in relation to seizures makes it crucial to accurately temporally quantify seizure onset and termination for postictal CBF measurements. The Federico lab recently completed a systematic study of postictal CBF in patients with drug resistant focal

epilepsy using ASL within 90 min of an electrographically confirmed seizure (Gaxiola-Valdez, et al., 2017). Postictal hypoperfusion was seen in 71% of patients in areas corresponding to the SOZ. Patients who had late postictal scans (> 60 mins) showed no significant hypoperfusion. Similarly, our study obtained postictal CTP within 80 min of seizure termination and postictal hypoperfusion corresponding to the SOZ was seen in 83% of patients. Thus, both studies emphasize the need to perform postictal studies prospectively, within an accurately measured and predetermined time window, and under continuous VEEG monitoring.

2.4.3 Statistical Analysis of Visual Assessments

No previous CTP study has collected both interictal and acute postictal scans for comparison. All previous studies retrospectively identified patients who presented at stroke centers with neurological deficits and underwent CTP imaging. Single scans were collected, typically outside the acute postictal period (<60 min of seizure onset). Neuroradiologists visually reviewed the scans for CBF abnormalities relative to the contralateral hemisphere (Gelfand, et al., 2010; Shelly, et al., 2017; Wiest, et al., 2006). In comparison, our study prospectively recruited patients and collected two CTP scans (acute postictal and interictal baseline) and directly compared the two scans. Our study, also justifies the need for two scans for optimal visual localization of postictal hypoperfusion.

Localization, PPV, and sensitivity were highest in side-by-side comparisons (1.25 mm: 70%, 0.76, 0.684; 5 mm: 92%, 0.868, 0.909) and lowest in the independent assessment of baseline scans (1.25 mm: 23%, 0.085, 0.085; 5 mm: 15%, 0.085, 0.25); values shown are the average between both reviewers. Indeed, visually assessment of a single scan is minimally localizing, especially if it is obtained interictally. Thus, the lack of two scans along with the single scans being obtained during the interictal period (rather than the acute postictal period)

likely explains why the previous CTP studies failed to identify localizing hypoperfusion. In contrast, in the current study, when baseline and acute post-ictal images are collected, focal hypoperfusion can be visually detected in 70% of patients (for 1.25 mm thickness) in the side-by-side comparisons.

Kappa values between reviewers were highest in the 1.25 mm thick slices compared to 5 mm thick slices. We believe that reviewers were generally more confident in their assessments of the 1.25 mm slices because suspected CBF changes would persist for multiple slices. Reviewers also noted that the 5 mm thick slices may have been subject to partial volume artifacts. For these reasons, the quantitative analysis was performed on 1.25 mm thick slices.

2.4.4 Subtraction CTP Technique

Previous CTP studies performed one acquisition, oftentimes in the interictal period, and were visually assessed by radiologists or statistically compared to the contralateral hemisphere (Gelfand, et al., 2010; Mathews, et al., 2008; Shelly, et al., 2017; Wiest, et al., 2006). From our study, visual assessments of CBF images were minimally localizing with only one scan, especially if collected in the interictal period. Statistical contralateral comparison also assumes that the contralateral hemisphere is normally perfused. We saw that this is not always the case as sCTP not only highlighted SOZ, but also hypoperfusion in areas of presumed seizure propagation, often in the contralateral hemisphere (Fig. 2.5). Similarly, most previous ASL studies collected interictal CBF data and used statistical comparisons with healthy controls to quantify CBF changes. However, minor differences in interictal CBF maps between patients and controls may provide inaccurate localization of the SOZ. One ASL study from our lab, circumvented these limitations by collecting postictal scans within 90 min of seizure termination

and performed a subtraction analysis to a second, interictal ASL scan (Gaxiola-Valdez, et al., 2017).

CBF is dynamic and differences in diet, caffeine consumption, medication changes, and circadian rhythms may influence global CBF. Thus, the challenge of collecting two CBF scans lies in how to quantitatively compare two CBF images collected at different times points in addition to different states of health. During visual assessments, the postictal scans were consistently found to be globally hypoperfused relative to baseline, with further hypoperfusion within the SOZ. With this global change, a voxel-by-voxel subtraction analysis would prove to be non-localizing when viewed on an absolute threshold. To account for potential global shifts in CBF range, we performed an intensity normalization to globally shift postictal scans and baseline scans to be in the same range. This allowed for a direct subtraction that highlighted focal areas of difference.

2.4.4.1 Subcortical Perfusion Changes

Four patients displayed clusters of hypoperfusion in deep subcortical structures including the thalamus and the putamen (Pts. 2, 3, 5, 7). Of these patients, the clusters were ipsilateral to the presumed SOZ in three (Pts. 2, 3, and 7) and patient 11 displayed bilateral hypoperfusion in the caudate. All four patients experienced a temporal seizure. These perfusion patterns are consistent with previous interictal SPECT studies which also found ipsilateral thalamic hypoperfusion (Takano, et al., 2001; Yune, et al., 1998). Tae et al. (2005) also noted additional ipsilateral hypoperfusion subcortical areas such as the putamen, insula and bilateral thalamus. Authors hypothesized that interictal hypoperfusion in these subcortical structures were due to repetitive ictal discharges propagating through the thalamo-hippocampal-insular network. The results of these studies suggest that hypoperfusion in subcortical structures, particularly the

thalamus, may have a complementary role in lateralizing the epileptic foci in patients with both temporal lobe epilepsy and frontal lobe epilepsy. The results of the present study also support this hypothesis.

2.4.4.2 Special Case: Patient 12 – A Case of Prolonged Postictal Hemiparesis Ipsilateral to Seizure Onset and Hypoperfusion in the Brainstem

sCTP and ictal SPECT measure perfusion changes and both lateralized to the right hemisphere in patient 12. These results are discordant with the EEG onset of the captured seizure as well as the presumed SOZ which localized to the left frontotemporal region. However, patient 12 experienced postictal left hemiparesis for over 24 hours suggesting significant right hemisphere involvement, either for ictal onset or seizure propagation. Interestingly, sCTP showed clear clusters of hypoperfusion in the right primary motor cortex consistent with the patient's postictal left hemiparesis (Fig. 2.4). Furthermore, ictal SPECT showed scattered hyperperfusion in the right hemisphere, including the frontal and parietal convexities. Thus, the sCTP results of patient 12, supported by the ictal SPECT, may be an example where conventional pre-surgical evaluation may provide inaccurate localization of the true epileptogenic zone. Notably, this patient has not undergone surgical resection, so final confirmation of the true epileptogenic zone is not available. This case highlights the fact that conventional pre-surgical evaluations may not always correctly localize the true SOZ and that confirmation of the true epileptogenic zone can only be determined post-surgically.

Interestingly, patient 12 was also the only patient that displayed clear sCTP clusters of hypoperfusion in the brainstem region, a major center respiratory center. Seizure-induced hypoxia in the brainstem has recently been suggested as a possible mechanism for Sudden Unexplained Death in Epilepsy (SUDEP). One study found that the pre-Botzinger complex

becomes severely hypoxic 20-45 seconds prior to breathing cessation in 50% of mice after a pharmaceutically induced seizure (Wall, 2017). Mice with brainstem hypoxia experienced seizures earlier in life, had significantly longer seizures, and were limp during the post-ictal period as compared to other mice. This coincides with the clinical background of patient 12 who has had epilepsy for over 20 years starting from early childhood, experiences long seizures of over 80 seconds, and experiences paresis following seizures. The animal study postulates that if epileptiform discharges were to originate in, or propagate to, breathing nuclei in the brainstem, local vasoconstriction and hypoxia could result. If hypoxia were severe enough to cause cellular dysfunction, the vital cardiorespiratory functions that these areas regulate, such as respiratory rhythm, may deteriorate to the point of hypoventilation and death. sCTP may be reliable tool to detect brainstem hypoperfusion and further elucidate patients who are in danger of SUDEP.

2.4.5 Hypoperfusion on CTP – Visual analysis versus Subtraction CTP

Visual evaluation from reviewers was performed to characterize if localizing hypoperfusion can be identified in postictal CBF data relative to baseline CBF data. Subtraction analysis was performed in effort to remove the subjectivity involved in visual assessments and to provide an objective quantitative measure of localized postictal hypoperfusion. Although visual assessments were able to lateralize to the correct hemisphere in most cases, it lacked precise spatial resolution in that only general lobar localization could be achieved. Ultimately, sCTP lateralized and localized to the presumed SOZ with higher spatial precision compared to visual assessments. Although sCTP may be more susceptible to artifacts and noise, if viewed with other conventional investigations such as PET and SPECT, sCTP can localize areas of seizure onset and seizure propagation with finer spatial precision and accuracy.

2.4.6 sCTP versus Neuroimaging Data

In our study, CTP offered similar or better localization than MRI, PET and SPECT in 60% of patients that underwent additional imaging. sCTP was inferior to ictal SPECT and PET, possibly for the following reasons: a focal aware seizure was captured which may be associated with less postictal hypoperfusion (Pts. 7 and 11), late postictal scan (Pt. 14), or diffuse EEG onset (Pt. 2). In previous studies, ictal SPECT has yielded variable success in localizing the SOZ, ranging 66-97%, depending on temporal or extratemporal localization (Lee, et al., 2008; Weil, et al., 2001; Zaknun, et al., 2008). In comparison, previous interictal PET studies have identified the SOZ varied in 30-60% cases (Ryvlin, et al., 1998).

Similar to sCTP, subtraction ASL (sASL) was superior or equal to MRI in 52% of cases, to ictal SPECT in 60% of cases, and to PET in 71% of cases. Amongst patients who demonstrated perfusion changes, both sCTP and sASL lateralized to the same hemisphere as the final presumed SOZ in approximately 70% of cases (sCTP: 10/14 patients, sASL: 10/15).

Thus, CTP offers similar SOZ localizing information to subtraction ASL, ictal SPECT, and interictal PET and is more cost effective. CTP also has a greater spatial resolution and greater accessibility.

2.4.7 Confounding Factors

2.4.7.1 Previous Surgery

Because we did not exclude patients with previous surgery, reviewers may have been biased in their lateralization and localization of hypoperfusion when they observed previous resections during visual assessment. The anatomical changes may have also influenced registration of CBF maps during quantitative analysis. If the areas of resection are mis-

registered, then there is a higher chance that other areas of hypoperfusion may be observed. Both patients that had previous surgeries had unilateral multifocal sCTP localization (Pts. 3 and 9).

2.4.7.2 Focal Aware Seizures

Two of the studied patients experienced focal aware seizures with short durations (Pts. 7 and 11), and one had no EEG change (Pt. 11). These factors may have influenced why patient 7 displayed very small clusters of hypoperfusion, but was ultimately discordant with the presumed SOZ, and why patient 11 was non-localizing and displayed no clusters of hypoperfusion. Non-localizing sCTP results on captured focal aware seizures is consistent with previous ictal SPECT literature similarly displaying little, if any, localized hyperperfusion for focal aware seizures (Ho, et al., 1996).

2.4.7.3 Timing of CTP

Previous animal work suggested that the period of most severe hypoxia following a seizure occurs between 20-60 min (Farrell, et al., 2016), highlighting the importance of the timing of postictal scans for investigating hypoperfusion. Our cohort involved three patients that had postictal CTP scans longer than 65 min after seizure termination (Pts. 7, 12, and 14). Indeed, Patients 7 and 14 experienced a focal aware seizure and focal impaired awareness seizure, respectively, and both showed minimal hypoperfusion. In contracts, Patient 12 had a focal to bilateral tonic clonic seizure and multifocal hypoperfusion, likely reflective of the more significant seizure that was experienced compared to the other two patients.

2.4.7.4 Interictal Baseline

Five patients had frequent interictal discharges. Although this was not a factor in all multifocal cases, 4/5 patients with an active interictal baseline EEG displayed multifocal postictal hypoperfusion, and the remaining patient experienced a focal aware seizure and showed

mild hypoperfusion in the subcortical structure that was ultimately discordant with the presumed SOZ. We suspect that frequent interictal epileptiform discharges could possibly lead to widespread mild CBF reductions as documented in recent studies (Boscolo Galazzo, et al., 2015; Storti, et al., 2014). Thus, comparing such a patient's baseline CBF to postictal CBF may not yield significant CBF differences, or areas that would normally be cancelled out might consequently be highlighted leading to widespread CBF changes.

2.4.8 Limitations

Despite showing good concordance of postictal hypoperfusion to the presumed SOZ, our results could not be validated by post-surgical outcome, as only one patient underwent surgery to date. The use of a clinical consensus as the gold standard for the presumed SOZ in statistical analysis and comparisons for concordance is limiting as the true epileptogenic zone can only be determined post-surgically. Thus, there is a possibility that the presumed SOZ may not be concordant with the epileptogenic zone. Indeed, two of the patients underwent further intracranial monitoring after this study highlighting that the pre-surgical consensus of the SOZ using scalp VEEG data can sometimes be unclear. In addition, EEG electrodes were removed ~ 20 min prior to each CTP scan, leading to the possibility of missing electrographic seizures during transport and image acquisition. Although we have justified the use of 15 CBF units as an absolute threshold to view sCTP hypoperfusion based on previous animal work and successful results of a prior ASL study, we recognize that other methods of analyzing postictal CBF changes exist. Using a different threshold or smoothing parameters may yield different results. Finally, the small study size could have influenced our results. Larger patient numbers and studying specific subgroups of epilepsy may lead to more consistent and statistically significant results.

2.5 Conclusions

Subtraction CTP is a safe, feasible, cost-effective, and readily available imaging modality that can be used in the postictal period to provide additional localization of the SOZ. Although ASL does not involve radiation and has been shown to be an effective modality in detecting postictal hypoperfusion, rapid access to MRI scanners pose a challenge for obtaining immediate postictal ASL scans. The use of CTP may circumvent these challenges as it often has 24-hour availability at most medical centers, and scans are short. With more studies replicating our findings, sCTP may be considered a potential candidate in replacing ictal SPECT given the logistical benefits of a one-hour time frame for collection over a 30 sec injection time window. sCTP can consistently detect not only seizure onset but also areas of seizure propagation. In addition, sCTP detected brainstem hypoperfusion which may further elucidate patients who are in danger of SUDEP. When the study is performed within 70 min of seizure termination and the seizure is not focal aware, hypoperfusion is seen in up to 80% of patients. The greatest degree of concordance was seen in patients experiencing focal temporal or temporal-plus seizures. sCTP was also successful in detecting focal hypoperfusion in patients with previous surgery. Given the favorable comparisons with subtraction ASL, ictal SPECT and PET, sCTP may be an additional tool for identifying the SOZ.

CHAPTER 3: General Discussion

3.1 Introduction

Although most patients will achieve lasting remission of seizures with antiseizure medications, about 20-30% of people with epilepsy will become refractory to medication (Schmidt and Schachter, 2014). The use of surgical intervention is increasing and with it, the need for precise localization of the origin of the epileptic activity. Unfortunately, post-operative seizure freedom is achieved in less than 50% of patients with epilepsy within five years of surgery on average, often due to inaccurate localization of the SOZ (de Tisi, et al., 2011). There is a continuous need for new localization methods to help thoroughly identify the SOZ as confidently as possible prior to surgery.

This thesis project sought to use CTP to measure immediate postictal perfusion changes to help localize the SOZ. CTP is readily available with 24-hour access in most medical centers and can be easily obtained in emergency situations. These advantages overcome the logistical difficulties observed when obtaining immediate postictal ASL scans (< 60 minutes) such as limited hours of scanner availability. The research conducted in Chapter 2 of this thesis suggests that CTP can reliably detect postictal hypoperfusion and provide information regarding the areas of seizure onset and seizure propagation.

3.2 Project Overview

The two major distinctions of this project from previous studies investigating the phenomenon of postictal hypoperfusion are the collection of both an immediate postictal scan and an interictal baseline scan and the accuracy of recorded time between an EEG verified seizure and image collection. Having two scans is necessary for not only performing the subtraction analysis, but also for visual assessments as we saw significantly impaired localization

when only one scan was provided, especially if the scan was interictal. The lack of an interictal baseline scan to serve as a point of reference to postictal values may explain why previous studies found minimal localizing hypoperfusion in their results when performing visual assessments (Gelfand, et al., 2010; Guo, et al., 2015; Hauf, et al., 2009; Masterson, et al., 2009; Mathews, et al., 2008; Wiest, et al., 2006). Given the temporal sensitivity of the hypoxic phenomenon, it is also critical to know the exact time between seizure termination and image collection. Previous studies reported confounding results including focal and hemispheric hypoperfusion, hyperperfusion, or no significant perfusion changes (Altrichter, et al., 2009; Lim, et al., 2008; Miyaji, et al., 2014; Nguyen, et al., 2010; Pendse, et al., 2010; Pizzini, et al., 2013; Sugita, et al., 2014; Wolf, et al., 2001) which may be the result of the variable time points at which images were collected. Only one other study collected two scans for each patient and accurately recorded the time between an electrographically confirmed seizure and the ASL scan collection (Gaxiola-Valdez, et al., 2017). Although ASL does not involve radiation or administration of a contrast agent, it is logistically difficult to obtain immediate short notice access to the MR scanner. This thesis project aimed to provide an alternative to ASL imaging, as CTP is more logistically feasible and clinically implementable for collecting immediate postictal CBF data.

3.3 Discovery of Postictal Global Hypoperfusion

This is the first study that visually compared between immediate postictal CBF images and interictal images for each patient. By performing such an assessment, we discovered that global hypoperfusion is observed in approximately 57% of patients, with localization of the SOZ being particularly hypoperfused relative to the widespread decrease. This phenomenon was not previously noted before in either animal or clinical studies. It is unclear why only a portion of the

cohort displayed global differences as no clear pattern exists between the patients who displayed global hypoperfusion versus those who did not in terms of seizure duration, EEG onset, seizure type, or interictal activity.

The concept of postictal hypoxia/hypoperfusion suggests that seizures may be a stroke-like event. Hypoxia/ischemia is an integral part of stroke and is associated with disruption of neuronal metabolism leading to depolarization of membrane potential which induces hyperexcitability and seizure genesis. There is now a question of whether it is the electrical event itself or the downstream resulting hypoperfusion that is responsible for anatomical alterations in some persons with epilepsy. Widespread anatomical changes may include enhanced blood-brain barrier permeability and formation of new capillaries (Farrell, et al., 2017). Unpublished experiments from Teskey and colleagues have identified other confounding factors such as the acute consumption of caffeine prior to a seizure which results in the extension of the degree and length of hypoperfusion following a seizure. These chronic anatomical changes resulting from repetitive instances of postictal hypoxia/hypoperfusion or confounding effects of certain drugs may explain why global hypoperfusion was observed in over half of the cases.

3.4 Necessity of Performing Intensity Normalization

The discovery of global postictal perfusion changes led to the implementation of an important step in the pipeline development for sCTP that was not included in the ASL subtraction pipeline: intensity normalization. The CBF data are collected from two different states of health (interictal vs postictal) as well as at two different time points. Studies have shown that CBF measurements can dramatically fluctuate over the course of 24 hours in healthy controls and are influenced by factors such as breath-holding, hyperventilation, or ingestion of caffeine (Kastrup, et al., 1999; Pollock, et al., 2009). Using ASL, Kastrup et al. (1999) found that

repeated challenges of breath-holding induced an overall rise in relative CBF values, particularly in grey matter of up to 87%. Similarly, Pollock et al. (2009) found that patients with hypercapnia showed global hyperperfusion on ASL. Both studies showed a positive linear relationship between cerebral perfusion and the partial pressure of carbon dioxide, with Pollock et al. (2009) further suggesting that rates of cerebral perfusion changed by 4.0 ml/100g/min for each 1 mmHg change in partial pressure of carbon dioxide.

To further confirm the results of the aforementioned studies, I also investigated the perfusion changes at different time points for a healthy individual using ASL and observed global CBF differences. ASL images were collected from a healthy control at several months, days, and hours apart with the collaboration of Dr. Gavin Winston at the University of College London. Visual assessment from one reviewer (CE) commented that there were global differences of approximately 5-10 CBF units between the scans that were several months and several days apart (Fig. 3.1). This range of baseline fluctuations in CBF is consistent with observed oxygen levels in animal studies (Figure 3.2) (Farrell, et al., 2016). Given that oxygen levels and CBF are closely related, these trends suggest that the global differences observed in our patients are physiological and not from the margin of error from scanning.

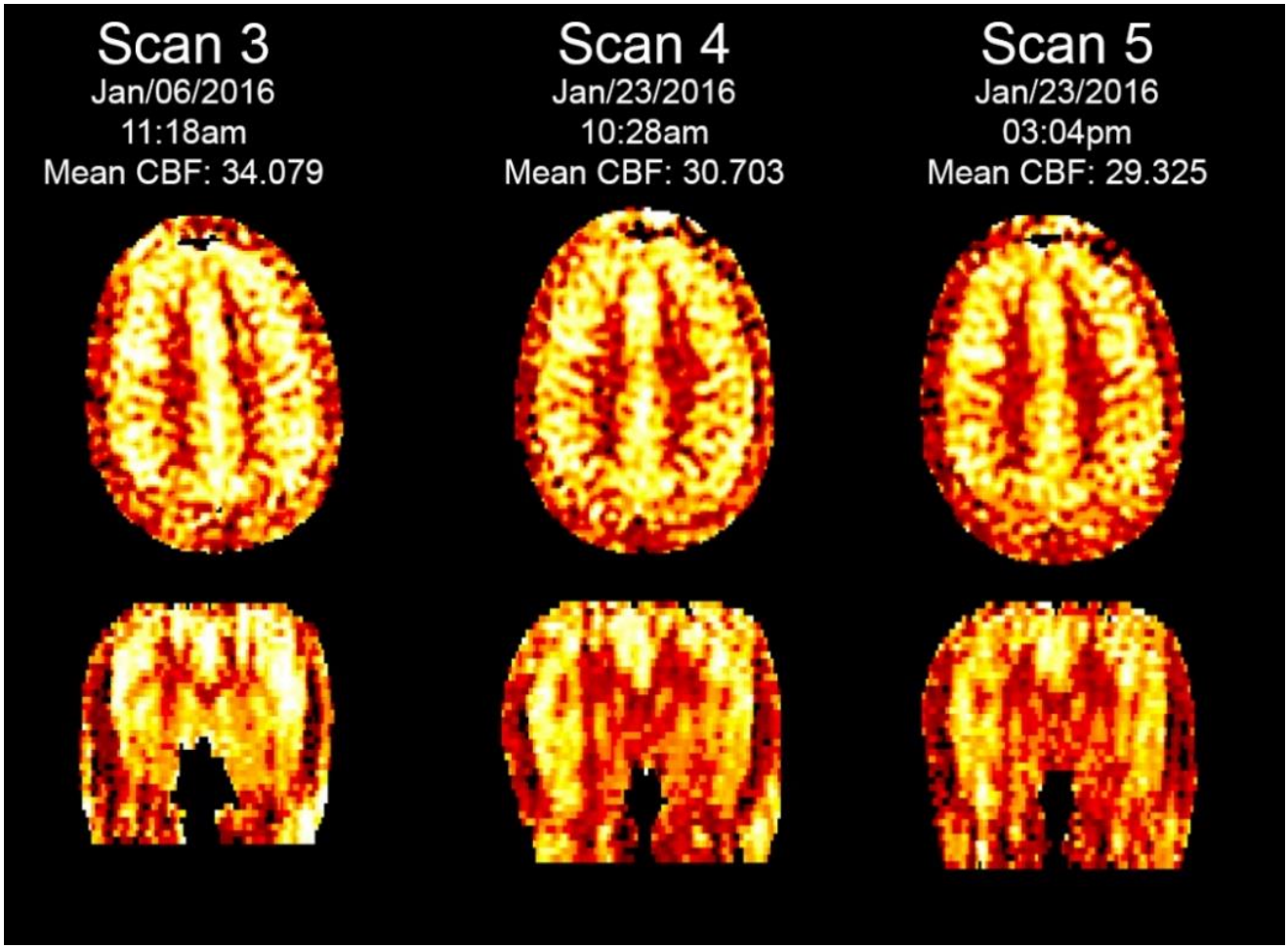

Figure 3.1: Example of visually comparing between ASL scans of a healthy control demonstrating global differences between scans taken several days apart (Scan 3 vs. Scan 4 & 5) and minimal global differences between scans taken several hours apart (Scan 4 vs. Scan 5). The mean global CBF is reported for each scan; notably, scan 3 is several CBF units different than scans 4 and 5.

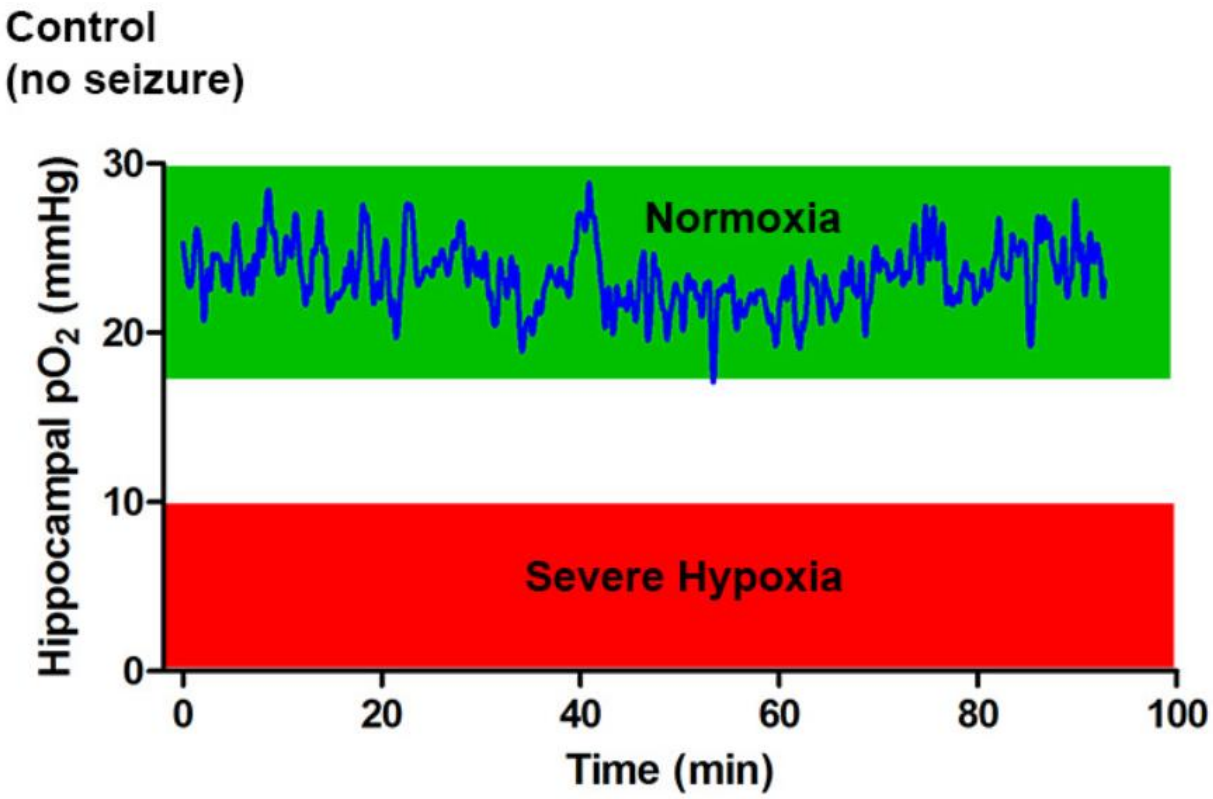

Figure 3.2: Local oxygenation measured in the hippocampus of an awake and free-moving rat (blue). Green denotes normoxia while red denotes severe hypoxia. Normoxic ranges are seen fluctuating within a 10mmHg range. (Figure from Farrell, et al., 2016).

The differences in global CBF values were smaller in scans acquired several hours apart compared to several days apart. In the context of a quantitative subtraction analysis, subtracting between the images should theoretically provide a predominantly null result given that these scans all represent a baseline state for a healthy control. In line with visual assessments, performing a subtraction between scans several days apart without intensity normalization provided a subtraction map that was globally different (Fig. 3.3A). In contrast, when the images were subtracted from one another after performing intensity normalization, the resulting image had significantly less hypoperfused voxels, with only minor clusters along the edges of the image, presumably from imperfect co-registration (Fig. 3.3B). Because remaining clusters were smaller than clusters when no intensity normalization was performed in both size and intensity, applying a filter to exclude clusters of low intensity and size would easily eliminate these from the final analysis. These results suggest that it is necessary to perform some form of intensity normalization when comparing between two CBF images collected at different time points to account for physiological perfusion changes.

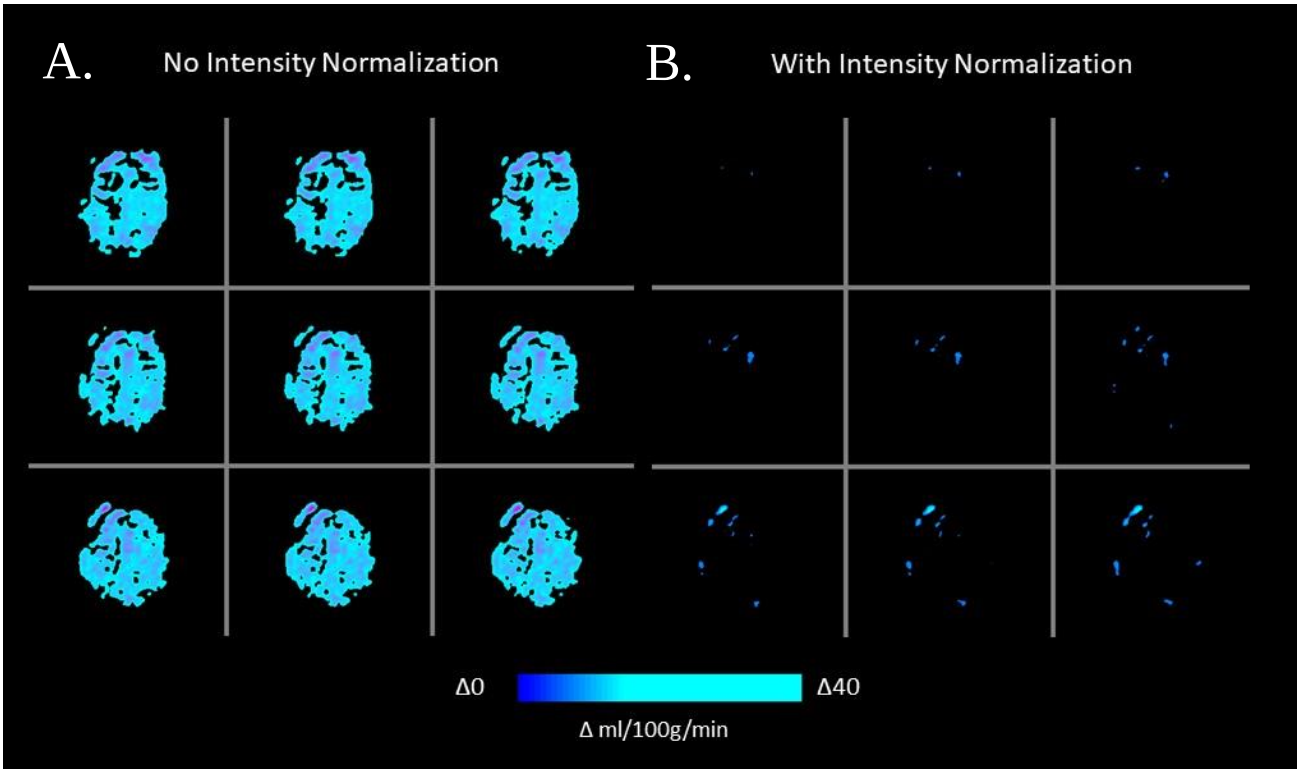

Figure 3.3: Example of performing subtraction analysis of Scan 3 minus Scan 4. A) Example of subtraction analysis without performing intensity normalization and demonstrating widespread CBF differences. B) Example of subtraction analysis after performing intensity normalization and demonstrating little to no CBF differences.

CBF values can be globally different at different time points even within healthy individuals, which poses an issue when performing a subtraction analysis between two sets of CBF data for epilepsy cases. The effects of hyper- or hypo- ventilation during a seizure, or drug/caffeine consumption acutely prior to seizure onset may also be present during the postictal or baseline scans and significantly affect CBF measurements. In an effort to circumvent these global changes, an intensity normalization step was performed whereby the postictal images were globally shifted to have the same average and standard deviation as the baseline images. By normalizing the intensities between the two images, it ensures that the differences between the two image sets are due to pathological reasons from the ictal event and not due to physiological differences between different time points. It must be acknowledged that there are multiple ways that one can approach normalizing the intensity between two images (see Appendix C), and this step can be further optimized by pursuing more complex methodologies (Brahim, et al., 2015).

3.5 Combining Visual analysis and Subtraction CTP (sCTP) for Clinical Use

Although the post-processing steps necessary to generate the sCTP results have been semi-automated, it is still a fairly manual process. Our results suggest that if both baseline and postictal scans are provided, visual assessments can lateralize to the same hemisphere and localize to the same lobe as the presumed SOZ in the majority of cases. Although accurate when compared to conventional measures, the visual assessments lacked finer spatial delineations in that reviewers were able to localize a general region but not a specific structure. In contrast, sCTP provides very fine spatial resolution in identifying specific areas of hypoperfusion, but it is also more susceptible to artifacts that may make it difficult to differentiate between clusters of true hypoperfusion over noise. The clinical implementation of postictal CTP may ultimately involve performing both forms of analyses to provide the most comprehensive set of

information. Visual assessment is fast and may provide a general localization to the suspected SOZ. Quantitative subtraction analysis may then be performed to provide finer spatial detail. Until the pipeline for quantitatively analyzing the data is fully optimized and becomes more automated, the combination of these two techniques may provide the most accurate and precise localization of SOZ in a timely manner.

3.6 Effects of Seizure Duration to Degree of Hypoperfusion

The severity of hypoperfusion as detected by sCTP positively correlated with seizure duration (see Ch.2, Fig. 2). Linear correlation was also seen in subtraction ASL (Gaxiola-Valdez, et al., 2017) . Similarly, Farrell et al. (2016), also observed that the severity of hypoxia was correlated positively with seizure duration, similar to blood flow.

Farrell, et al. (2017) proposed a mechanism model for postictal hypoperfusion that describes the roles of intracellular calcium, COX-2 and L-type calcium channels. COX-2 is a postsynaptic enzyme that catalyzes arachidonic acid into vasoactive prostanoids. Following sustained synaptic activity during a seizure, postsynaptic calcium accumulates and increases the activity of COX-2, which subsequently converts arachidonic acid into vasoactive prostanoids. Although the specific prostanoid and receptor mediating vasoconstriction is still unknown, it is proposed that prostanoid binding to GPCRs on vascular smooth muscle leads to downstream opening of L-type calcium channels, which subsequently increases intracellular calcium concentration in the vessels, ultimately resulting in vasoconstriction (see Fig. 1.8).

Following this model, a longer seizure would proportionally lead to increased synaptic activity and postsynaptic calcium accumulation, and ultimately result in more severe vasoconstriction and hypoperfusion. With three studies separately observing a proportional

correlation between seizure duration and degree of hypoperfusion, these data support the model mechanism proposed by Farrell, et al., (2017).

3.7 sCTP Perfusion Patterns of Different Seizure Types

It is not uncommon for patients with epilepsy to present with multiple seizure types. Because CTP involves radiation, this limited our ability to collect postictal CTP images for multiple seizure types from the same patient. A few studies have investigated whether localizing perfusion patterns change depending on seizure type using ictal SPECT (Shin, et al., 2002; Van Paesschen, et al., 2000). Investigators found that ictal SPECT injections for focal aware seizures gave no information in approximately 40% of cases, focal to bilateral tonic clonic seizures gave multiple regions of hyperperfusion, and focal impaired aware seizures gave the best localizing results. Very similarly, sCTP provided little to no localizing information when performed on focal aware seizures (two patients), resulted in unilateral widespread hypoperfusion in 2/4 (50%) patients that experienced focal to bilateral tonic clonic seizures, and was fully or partially concordant to the presumed SOZ in all patients that experienced a focal impaired aware seizure. Thus, ictal SPECT and postictal CTP share the same limitation of obtaining different perfusion patterns depending on the seizure type.

Interestingly, the duration of seizures seen in frontal lobe epilepsy tends to be shorter compared to seizures seen with temporal lobe epilepsy, and the postictal periods are shorter as well (Van Paesschen, 2004). In this project's cohort, five patients had a presumed SOZ in the frontal lobe or frontal-temporal region (Pts. 2, 4, 6, 9, 14). Although all five patients displayed clusters of hypoperfusion that were concordant in location to the clinical consensus of the SOZ, it should be noted that these clusters were less hypoperfused (lower voxel intensity) compared to

temporal lobe cases. These cases suggest that in addition to seizure type, onset location may also influence the postictal perfusion patterns observable on CTP.

3.8 Clinical Utility of Postictal CTP

The conventional modalities for localizing the SOZ in pre-surgical investigations include VEEG, PET, SPECT, and MRI. The preliminary data of this project supports that CTP was concordant with conventional modalities in at least 60% of cases and can be used to reliably detect postictal hypoperfusion which localizes to the SOZ. Given that ictal SPECT and postictal CTP both measure perfusion changes but at different time points, the clinical utility of these modalities was compared. Comparing the logistical details between the two modalities, ictal SPECT requires an EEG tech to be on standby to administer the radioactive tracer within 30 seconds of seizure onset and late injection may result in unusable data. Considering the tracer half-life and the working hours of EEG techs, ictal SPECT studies can only take place at the Foothills Medical Center from Monday to Friday, 9:00-4:00pm. This makes capturing nocturnal seizures and/or infrequent seizures particularly challenging. In contrast, postictal CTP has been collected up to 80 minutes following seizure termination and reliably showed postictal hypoperfusion localizing to the SOZ. CTP has 24-hour available access, no EEG tech is required to be on continuous standby, and no radioactive tracer is involved. For this project, electrodes needed to be removed to avoid causing image artifacts; this process often added up to 25 minutes to the time between seizure termination and image collection. Although 9/14 patients were able to be scanned within the ideal 60-minute timepoint despite the additional time needed to remove electrodes, the commute time can be easily decreased by using plastic electrodes, thus eliminating the need for electrode removal. For the majority of this project's duration, we were not able to take full advantage of the 24-hour CTP availability because a clinical fellow was not

available to confirm the seizure and accompany patients after hours. Additionally, the EEG technicians are unavailable after 10:00 pm to re-hook the electrodes following the CT scan. These limitations can be easily circumvented if postictal CTP was clinically implemented as nurses are capable of accompanying patients for evening/night events, and plastic EEG electrodes may be used to avoid the necessity of electrode removal. Indeed, postictal CTP has the capability of being a potential replacement to ictal SPECT: it is less costly, more logistically feasible, has similar reliability in SOZ localization and is a readily available modality in most medical centers. As a minimum, the two modalities are found to be complementary, and postictal CTP has the potential to be performed first given the greater logistical ease, followed by ictal SPECT if additional confidence is necessary.

3.9 Limitations

3.9.1 Use of Patients 4 and 6 – 5mm slices

As mentioned in Chapter 2, patients 4 and 6 had incorrectly collected baseline scans in that the clinical CTP protocol was used over the custom research protocol. The clinical protocol only collected 5mm thick slices. Although other differences between the research-designed protocol and the clinical protocol are slim, this error eliminated the ability to process 1.25mm thick slices, and the collected 5mm thick slices were not identical in terms of spatial coverage. Because of limited patient numbers, we chose to include these two patients into the overall cohort as sCTP and visual analysis was still possible to perform. However, this inclusion would have influenced the kappa statistics, sensitivity, and positive predictive values when comparing between 1.25mm and 5mm thick slices. With a larger patient cohort, these two patient data sets would not have been considered in order to maintain consistency in slice thickness, especially when performing sCTP analysis.

3.9.2 Production of CBF maps

Following CTP data collection, source images were transferred to a freestanding workstation for processing the CBF maps, arguably the most important step for any further analysis. There are multiple software packages capable of such processing. For this project, CBF maps were calculated by deconvolution of time density curves and arterial input function using a delay-insensitive (deconvolution) algorithm (CT Perfusion 4D, GE Healthcare). Inputs required for CTP map calculation included the manual selection of the arterial input function (AIF). Inappropriate selection of AIF could lead to inaccurate CTP parameter values. Although these functions were consistently selected to be within the internal carotid artery for each patient, the resulting CBF maps can vary dramatically depending on operator selection. In addition, the implications of laterality of AIF relative to the affected hemisphere remains controversial. No general consensus has been reached regarding whether the AIF should be chosen ipsi- or contralateral to the affected hemisphere, or in this project, the ictal onset (Konstas, et al., 2009). Although multiple studies have suggested that AIF region of interest does not significantly influence the CBV, CBF, and MTT values of the infarct core in the context of stroke (Konstas, et al., 2009; Sanelli, et al., 2004), there have been no studies regarding AIF laterality influences on more subtle perfusion changes as in the case of epilepsy.

3.9.3 Kappa Statistics Thresholds

The visual identification of postictal hypoperfusion in CTP is subject to variability between reviewers. The variability observed between the two reviewers suggests that more reviewers may be needed to determine if postictal hypoperfusion can be reliably detected through visual identification. Although Cohen's Kappa is the preeminent statistic for characterizing interrater reliability, it has three major shortcomings. First, the ratings compared using Cohen's Kappa are

limited to categorical data; we therefore had to limit the categories of localization to four lobes (frontal, temporal, occipital, and parietal). However, this limits the reviewer's ability to comment on combinations of lobes for finer spatial localization such as temporo-occipital, or fronto-temporal. In addition, adding all possible combinations of lobes could deter from potential complete agreements. By increasing the number of categories, agreement between reviewers would be lower, as review of frontal versus frontal-temporal would be considered disconcordant. Although a weighted Kappa test may circumvent small categorical differences such as a fronto-temporal versus temporal assessment by allowing partial agreements, the kappa test is ultimately not optimized for a wide range of categorical data (Tang, et al., 2015). Second, Cohen's Kappa was designed to evaluate the agreement between exactly two reviewers. Extending the Kappa test beyond two reviewers has been proposed but it would be subject to computational complexity and poor statistical distribution (Cao, et al., 2016; Nelson and Edwards, 2015). Finally, Cohen's Kappa reflects the agreement between the sensitivity and specificity of raters and is therefore dependent upon the trait prevalence. In this project, the statistic would vary based on whether hypoperfusion is expected to be present or not. In the case of reviewing interictal scans, hypoperfusion was theoretically not expected to be prevalent and raters assessed accordingly with most reviews being non-localizing; however, this resulted in kappa coefficients being low despite overall agreement between reviewers being high.

3.10 Future Directions

3.10.1 Assessing Intra-Rater Reliability for Visual Assessments

Given the small patient cohort and uniqueness of some cases (e.g. surgical resections), it was not possible to perform multiple trials of qualitative reviews for each thickness. Reviewers would start to recognize and remember the patient cases after multiple reviews of the same set of

images and provide biased evaluations. With a larger patient cohort, this portion of the study can be revisited, and reviewers can undergo multiple review trials for each scan. This would allow us to calculate intra-rater reliability and observe if reviewers can consistently localize to the same area for each patient. When comparing between the assessments of 1.25 mm and 5 mm thick slices, reviewers made contralateral evaluations in some cases (ex. 5 mm localized to left temporal, 1.25 mm localized to right temporal). Perfusion changes as detected in epilepsy patients were considerably more subtle than most stroke cases. Indeed, the visual evaluations were reasonably subjective and investigating consistency amongst reviewer assessments would further elucidate the reliability of localizing postictal hypoperfusion visually.

3.10.2 Pipeline Optimization

The development of the quantitative analysis pipeline involved multiple steps that can be further optimized. There are various methods to perform each post-processing step, with some methods being better optimized to perform a subtraction analysis compared to others (see Appendix C for previous attempts on pipeline development). Amongst the involved processes, there are two major steps that can be further investigated and optimized to best highlight clusters of postictal hypoperfusion on CTP.

First, spatial registration between the two scans is one of the most important steps. If registration is inaccurate, then all subsequent processes will be erroneous. Because anatomical and CBF data share an image space, the transformations used to co-register baseline and postictal anatomical images could be applied the baseline and postictal CBF data. This transformation allowed the CBF images to inherit the same accuracy as the anatomical registration. This method is more robust than registering low resolution CBF images directly onto a higher resolution anatomical image. However, default parameters were used and adjusting additional parameters in

linear registration were not fully explored, nor were non-linear registration methods. To ensure that clusters of hypoperfusion were from the pathological phenomenon and not from registration errors, this thesis focused on using images from one modality; however, T1-MRI images provide higher quality anatomical images compared to the CT anatomical average maps and it may be of future interest to find ways to perform reliable and accurate inter-modality spatial co-registration between the CTP images and MRI anatomical scans.

Second, intensity normalization (as previously discussed) was an important and necessary step in order to perform a subtraction between CBF data of two different time points (see section 3.4). The method of intensity normalization used in this thesis involves globally shifting the postictal CBF data to have the same average and standard deviation as the baseline CBF data. This was similar in concept to what some researchers used in their additive intensity correction model for ASL CBF measurements whereby global CBF values were uniformly shifted yet still reflected the expected physiological distribution (Stewart, et al., 2015). Although this was seen to be the best methodology amongst those that were tried (see Appendix C), I acknowledge that intensity normalization is common in pre- and post-processing image studies and there exists more complex models to perform a similar function. Further investigation and optimization of intensity normalization models may better circumvent the observed global CBF changes that dynamically occur physiologically.

3.10.3 Investigating Other Perfusion Parameters

A significant advantage that CTP has over ASL is that it can quantify several perfusion parameters beyond CBF, such as: cerebral blood volume (CBV), the total volume of moving blood in the mass of tissue [(ml·(100g)-1]; mean transit time (MTT), the length of time a certain volume of blood spends in the cerebral capillary circulation; the time-to-peak (TTP), an index of

time between the beginning of blood perfusion and maximum enhancement in the given region; the time-to-maximum of the tissue residue function (Tmax); and a new parameter used in the acute stroke setting, the permeability surface area product of the blood brain barrier (PS-BBB), the rate of contrast extravasation from intra- to extravascular compartments through a damaged barrier [ml·min-1·(100g)-1] (d'Esterre, 2013). Gefland et al. (2009) observed MTT, CBF, and CBV maps following a seizure and found focal areas of prolonged MTT with corresponding decreased CBF and CBV, consistent with hypoperfusion patterns. Although CBF, CBV, and MTT are all related through the central volume principle ($CBF = \frac{CBV}{MTT}$), the parameters are not always proportional to each other. For example, in stroke, the two major zones of injury are the core ischemic zone and the ischemic penumbra. In the first few hours of vascular insult, the penumbral pattern may exhibit low CBF and high CBV due to maximally functioning autoregulation mechanisms and collateral circulation, whereas the central volume principle would argue that CBF is always directly proportional to CBV. Thus, in the context of observing more subtle perfusion changes in the context of epilepsy, it may be worthwhile to further investigate these other parameters.

Further investigation of the permeability of the blood brain barrier (BBB) in the immediate postictal state through PS-BBB quantification maps may also be of particular interest. The BBB is a physical and metabolic barrier between the brain and the circulatory system and consists of tightly connected endothelial cells to restrict the passage of solutes. Seizures have been shown to result in increased BBB permeability (Michalak, et al., 2012; Michalak, et al., 2017; Rigau, et al., 2007; van Vliet, et al., 2007). However, it remains unclear whether BBB dysfunction leads to seizures, or if seizures lead to BBB breakdown. Blood circulation is re-established to limit cerebral injury in the context of ischemic strokes. However, during reperfusion, the return of

oxygenated blood to the ischemic area challenges the BBB with oxidative stress (Obermeier, et al., 2013). In viewing epileptic seizures as micro strokes from the phenomenon of postictal hypoperfusion, the concept that oxidative stress resulting from chronic reperfusion because of the repetitive instances of postictal hypoxia resulting from seizures being the primary cause of BBB damage and breakdown can be similarly applied. Increased BBB permeability may lead to leakage and passive accumulation of immunoglobulins in the brain. Rigau et al. (2007) proposed that persistent leaking of immunoglobulins into the interstitial space and uptake into neurons may result in neuronal dysfunction and hypoperfusion in cases of temporal lobe epilepsy, however the latter remains to be fully investigated mechanistically. Specifically, chronic disruption of the BBB may cause accumulation of albumin in the cytoplasm of neurons as well as increased albumin uptake by astrocytes which in turn increases extracellular potassium concentrations (Obermeier, et al., 2013). Thus, the combination of increased extracellular potassium, increased glutamate concentration, and severe hypoxia may lead to enhanced neuronal excitability and consequently spreading depolarization and increased seizures. Comparing between the postictal and baseline PS-BBB and obtaining a third PS-BBB several months or years from the initial baseline for the same patient may visually confirm if the BBB integrity changes postictally and over time from chronic hypoxia resulting from seizures. This investigation would further elucidate how BBB disruption and seizure events may correlate temporally.

3.10.4 Using Plastic EEG Electrodes

Despite the CT scanner having 24-hour access, data collection was limited to the schedule of the EEG technicians and scanning stopped after 10:00pm. Although conventional EEG electrodes do not pose any safety threats to patients if left on during scanning, the electrodes

produced significant streaking artifacts that diminishes the quality of the blood flow maps (see Appendix B). Thus, EEG electrodes had to be removed prior to each scan, and consequently placed back on by an EEG technician. Removal of electrodes consistently added approximately 20 minutes to the commute time from the hospital unit to the scanner. In addition, replacing the electrodes back onto the patient is a timely process and requires requesting an EEG technician to come into the hospital, oftentimes after hours. A future methodological improvement may be to employ non-metal EEG electrodes in the clinic. One study described 23 critically ill adults who underwent CTP scans with conductive plastic electrodes (Das RR, 2009). All scans were assessed to have had excellent image quality without significant CTP artifacts. In contrast, another study investigated 13 children who underwent CTP scanning with conductive plastic electrodes and observed artifacts that were not attributable to the leads, but rather the wires that inadvertently remained connected (Abend NS, 2015). The artifacts observed when wires were removed were significantly better compared to using metal electrodes. Thus, researchers concluded that plastic electrodes do not produce problematic CT artifacts if the wires are properly disconnected. Overall, using non-metal electrodes in the clinic would allow for faster collection of postictal scans and extension of scannable hours.

3.10.5 Post-surgical follow-up

Although good concordance of postictal hypoperfusion to the presumed SOZ and areas of seizure spread were shown, the results could not be validated by post-surgical outcomes as only one patient underwent surgery to date. Future studies should aim to correlate post-operative seizure freedom with the extent of surgical removal of the SOZ as defined by CTP. Patients who undergo surgery will usually have a post-operative structural MRI within three months of operation which will help provide an ROI for the area of surgical resection. The surgical

resection ROI can then be co-registered with the sCTP results on the same patient. This can be used to confirm the extent to which the areas of hypoperfusion as detected by CTP were removed during surgery. Further follow-ups to investigate the degree of post-operative seizure freedom as well as the correlation of the extent of surgical removal of the SOZ determined by CTP should be completed in order to further delineate in the accuracy of postictal hypoperfusion as a measure for the SOZ.

3.11 Overall Conclusions

Epilepsy is a serious neurological disorder affecting approximately 200,000 Canadians. For people who have medically refractory epilepsy, their prognosis is oftentimes poor for obtaining post-operative seizure freedom due to the risk of incomplete identification and removal of the SOZ. There is an urgent need to better the detect to SOZ to guide epilepsy surgery and ultimately improve post-surgical seizure freedom.

This thesis project explored if Computerized Tomography Perfusion (CTP) imaging can better show the SOZ compared to conventional methods by detecting areas of postictal hypoperfusion. The hospital stay for a patient with epilepsy is intensive: patients are under 24/7 surveillance, have over 20 scalp electrodes to record brain activity, and are often sleep deprived to provoke seizures during day-time working hours. Additionally, many patients must travel across cities to reach a hospital with the adequate resources to help treat epilepsy. The conventional methods such as EEG and nuclear imaging have limitations: EEG provides limited spatial information, and nuclear imaging is labor intensive, costly (~$22,400/patient) and has limited availability. In contrast, CTP is standard in hospitals, has 24/7 availability, costs ~$4,000/scan, involves less radiation than SPECT imaging, and may provide more accurate information. In addition to the financial benefits, patients will be relieved of an unnecessarily

long hospital admission and will have increased accessibility to the healthcare they require. These preliminary results indicate that the postictal CBF changes are localized to the SOZ as well as areas of seizure spread and can be reliably detected using CTP. With additional patients and further improvements in the optimization of the subtraction pipeline, CTP has the potential to be a cost-effective and readily available modality that can be included as an additional imaging modality in conventional pre-surgical investigations to further help localize the SOZ in patients with medically refractory epilepsy. The results of this study could be immediately translated and applied to raise health care quality in epilepsy diagnosis and allow clinicians to better direct surgery to improve post-surgical outcomes.

APPENDIX A: Determining Feasibility of Cross Modality Comparison

A.1 Introduction

Arterial Spin Labeling (ASL) is a sensitive MRI perfusion technique for measuring cerebral perfusion without the need for an intravenous administration of contrast. Instead, ASL magnetically labels arterial blood water and images using the patient's own blood as an endogenous tracer (Petcharunpaisan S, 2010). Using ASL, Gaxiola-Valdez et al. (2017) observed postictal hypoperfusion localized to the seizure onset zone in 12 of 15 patients. Indeed, ASL provided a non-invasive and no-radiation technique for quantitatively investigating the phenomenon of prolonged and localized postictal hypoperfusion in patients with epilepsy.

A restriction of ASL is limited scanner availability and logistical difficulties in collecting a scan <60 minutes after seizure termination. In the Seaman MR Center, there is one dedicated research MRI scanner and it is often fully scheduled for other research studies. Occasionally, a postictal ASL scan can be collected in between other scheduled studies. However, if the previously scheduled study involves a longer sequence (e.g., fMRI protocols that often take >45 minutes), then it would be too late to obtain a postictal ASL. Baseline ASL scans were easier to collect as they could be scheduled ahead of time, but this was not feasible for the postictal scans.

A benefit of CTP is that it provides 24/7 availability, and other CT protocols are short (20 minutes was the longest CT scan in comparison to a 45 minute fMRI protocol). Indeed, collecting a postictal CTP scan is logistically much easier than ASL. However, CTP has the disadvantage of being invasive, due to the necessity for the intravenous administration of a contrast agent (iodine), as well as the use of radiation.

Given that both modalities measure CBF, I attempted a cross-modality combination of baseline ASL and postictal CTP in effort to minimize radiation from CTP. The logistically

difficult scan (postictal) was collected using CTP, while the easily-schedulable scan (baseline) was collected using ASL, so that only one scan required contrast administration and exposure to radiation. I hypothesized that this would not be problematic as both ASL and CTP measure CBF in the same units (ml/100g/min), thus allowing for a quantitative comparison of postictal CTP and baseline ASL datasets. As discussed below, my results lead to the conclusion that a cross-modality collection of CBF measurements does not allow for further quantitative processing and was not feasible for my thesis work.

A.2 Materials & Methods

A.2.1 *Participants and Study Protocol*

Patients were recruited from those that had been admitted to the SMU at the Foothills for pre-surgical evaluation and/or focal epilepsy, and written consent from patients was obtained. Exclusion criteria for the study were multiple seizure onset zones, contraindications to CT (e.g., pregnancy, allergy to IV contrast material) or MR imaging (e.g., claustrophobia, ferromagnetic intracranial devices), and prior brain surgery. Four patients participated in the study. One patient had a vagal nerve stimulator (contraindicated in MRI) and could not have an ASL baseline; a comparison to an ASL scan averaged from 100 healthy controls was done instead. Another patient consented to having a baseline scan collected using ASL MRI and CTP.

When a patient had a habitual seizure, a physician immediately reviewed the video-EEG monitoring data and confirmed the qualification of the seizure. Once confirmed, patients underwent CTP imaging within 65 min of seizure termination. After collecting the postictal scan and while still in hospital, patients underwent a baseline interictal ASL scan following a seizure-free period of >24 hours. EEG electrodes were removed for both scans.

A.2.2 *Imaging Protocols*

A.2.2.1 Postictal CTP Acquisition

CTP images were collected with 120mm coverage, with 5 X 5 mm thick slices acquired at 80 kVp and 150 mA, 1 sec rotation time (GE Healthcare Revolution, Waukesha, WI, USA). After the scan, a retro recon for slice thickness of 1.25 mm at 1.25 mm intervals was performed, allowing the collection of both 5 mm thick and 1.25 mm thick slices. The CTP protocol consisted of 45 ml of an iodinated CT contrast agent (Omnipaque, GE Healthcare) that was power injected at 6 ml/s followed by a 40 ml saline chase. Scanning began after a delay of 5 s from contrast injection every

2.8 sec for 75 sec. Each study was analyzed using commercially available delay-insensitive deconvolution software (CT Perfusion 4D, GE Healthcare).

A.2.2.2 CTP Functional Maps

For each study, the arterial input function was manually selected from the internal carotid artery using a 2 x 2 voxel (in-slice) region-of-interest (ROI). Absolute maps of cerebral blood flow (CBF; ml/100g/min) was calculated by deconvolution of time density curves and arterial input function using a delay-insensitive (deconvolution) algorithm (CT Perfusion 4D, GE Healthcare). In-plane patient motion was corrected using automated software, and in cases with extreme motion, time points were manually removed as needed.

A.2.2.3 Baseline ASL and T1-Weighted MR Image Acquisition

All MR images were collected using a 3T scanner with an 8-channel phase-array head coil (GE Discovery MR750, GE Healthcare). ASL images were collected using a pseudo-continuous ASL sequence (1.9 x 1.9 x 5 mm; 28 slices; TE = 14.7 ms; TR = 5513 ms; post-label delay = 2525 ms; labelling duration 2025 ms; spiral acquisition with 1024 points and 8 arms). Subsequently, quantitative CBF calculations were made and displayed in units of ml/100g/min. The structural imaging protocol includes an axial-3D volumetric T1-weighted series, coronal fast spin-echo, T2-weighted imaging, and fluid attenuated inversion recovery imaging performed in an oblique axial and oblique coronal plane using the long axis of the hippocampus as a reference. These images formed the basis for image co-registration with CTP, and ASL data.

A.2.3 *CTP and MR Image Co-registration*

The baseline ASL and postictal CTP quantification maps were co-registered (spatially normalized) to the T1-weighted images acquired from each patient's clinical structural MRI protocol using a free available software package (FSL: FMRIB Software Library, Release 5.0

University of Oxford). A normalized mutual information metric was selected. Normalized mutual information is one of five metrics available in FSL and allows images with different contrasts to be registered. The process used a 12-parameter affine transform that accommodates scaling and shearing in addition to translation and rotation for better alignment between subjects. Registration was verified through visual inspection of the images.

A.2.4 *Comparison of Postictal CTP and Baseline ASL Perfusion Data – Preliminary Pipeline Analysis*

Patients were scanned under two different conditions: postictal CTP (<60 min after a seizure) and baseline interictal ASL (>24 hr seizure-free). One patient volunteered to have an additional baseline interictal CTP (>24 hr seizure-free) to allow for an intra-modality comparison.

The CTP and ASL quantitative CBF maps were spatially normalized to each patient's T1-weighted images (described in A.2.3). If a patient's structural MRI was unavailable, then the Montreal Neurological Institute (MNI) template was used as a reference image. After co-registering, a threshold of minimum 0 ml/100g/min and maximum 100 ml/100g/min was applied; values outside of these ranges were beyond the physiological range of CBF measurements and were deemed to be artifactual. CTP and ASL maps were then smoothed by a 6 mm full-width-half-maximum Gaussian kernel, to improve signal-to-noise and reduce the impact of small-scale registration errors.

A subtraction CBF map (baseline minus postictal) was generated for each patient and superimposed onto the patient's T1-weighted images. This process allowed for the identification of anatomical areas with postictal CBF reductions of at least 15 ml/100g/min. Three subtraction combinations were attempted: 1) baseline ASL averaged from 100 health controls minus

postictal CTP, 2) each patient's baseline interictal ASL minus the same patient's postictal CTP, and for one patient, 3) patient's baseline interictal CTP minus patient's postictal CTP.

A.2.4.1 *Baseline ASL Averaged from 100 Healthy Controls Minus Postictal CTP*

In the interest of minimizing radiation and evaluate whether the baseline ASL scan could eliminated completely, each patient's postictal CTP scan was compared to a baseline ASL scan collected from 100 healthy controls from the MR centers normal imaging database. Baseline ASL scans of 100 healthy controls were spatially normalized onto MNI template and consequently averaged to create an average baseline ASL CBF map. The postictal CTP map and the 100 control averaged ASL baseline maps were co-registered onto each patient's T1-weighted image using parameters described in A.2.3. Patient 3 had an implanted vagal nerve stimulator making him MR-incompatible and he therefore had no T1-weighted image available. The MNI template was instead used as a reference image for co-registering CBF maps.

After each map was spatially normalized to a common stereotactic space, postictal CTP CBF maps were compared to the 100 control averaged ASL CBF baseline maps by performing a subtraction (baseline – postictal).

A.2.4.2 *Patient Baseline ASL Minus Patient Postictal CTP*

In an effort to establish spatial localization of postictal hypoperfusion, while also minimizing radiation, each patient's postictal CTP CBF maps were compared to their own baseline ASL CBF maps. First, postictal CTP and baseline ASL maps were spatially normalized to the patient's T1-weighted images. Next, the postictal CTP maps were quantitatively subtracted from the ASL maps to detect differences in perfusion.

A.2.4.3 *Patient Baseline CTP Minus Patient Postictal CTP*

To delineate whether the observed widespread hypoperfusion was artefactual from a cross-modality comparison, or physiological, one patient agreed to the collection of two baseline scans: ASL and CTP. Previous efforts were all cross-modality, thus, collecting a CTP baseline allowed an intra-modality comparison of postictal and baseline CBF maps. Both postictal and baseline CTP CBF maps were spatially normalized onto the patient's T1-weighted images and a subtraction of the two CBF maps (baseline CTP – postictal CTP) was performed; images were also normalized using the CT anatomical average map that was collected concurrently with CBF measurements as a reference image.

A.3 Results

A.2.1 Patient Demographics

Four patients (2 males, 2 females) were included in this study. Their demographics are summarized in Table A.1. Table A.2 summaries details of additional clinical investigations including EEG onset, ictal SPECT, and structural imaging data. Patient 3 had an implanted vagal nerve stimulator and did not undergo an ASL baseline scan; thus, his postictal CTP data were compared to the averaged ASL data of 100 healthy controls. Patient 4 consented to having both a CTP and ASL baseline collected for comparing between a cross-modality vs. intra-modality CBF map subtraction.

Table A.1: Demographics for patients that obtained a postictal CTP scan and a baseline ASL scan.

ID	Age	Sex	Seizure Duration (s)	Seizure Type	Time to Postictal CTP (min)
1	48	M	167	Focal impaired awareness	56
2	21	F	117	Focal impaired awareness	62
3*	22	M	79	Focal to bilateral tonic-clonic	57
4**	60	F	153	Focal to bilateral tonic-clonic	65

* Patient 3 had an implanted vagal nerve stimulator. Thus, ASL data were not collected.

**Patient 4 had a baseline ASL scan and a baseline CTP scan

Table A.2: Summary of clinical investigations of participating patients.

ID	EEG Onset	Ictal SPECT	MRI
1	Lt anterior and mid-temporal	Hyperperfusion in mesial and anterior Lt temporal lobe	Lt temporal lobe encephalomalacia
2	Lt frontotemporal / hemispheric	Hyperperfusion in mesial and lateral aspect of Rt temporal lobe	Rt hippocampal atrophy
3	No ictal EEG change	Hyperperfusion in Lt temporal lobe	Normal
4	Lt anterior and mid-temporal	n/a	Lt mesial temporal lobe atrophy and mesial temporal sclerosis

A.3.1 Comparing Postictal CTP to Averaged Baseline ASL from 100 Healthy Controls

All four patients displayed apparent global hypoperfusion when comparing postictal CTP CBF maps to an averaged ASL CBF map (Figure A.1 and Figure A.2). Despite increasing the minimum threshold to represent a 50% decrease, no localization could be detected using this comparison method.

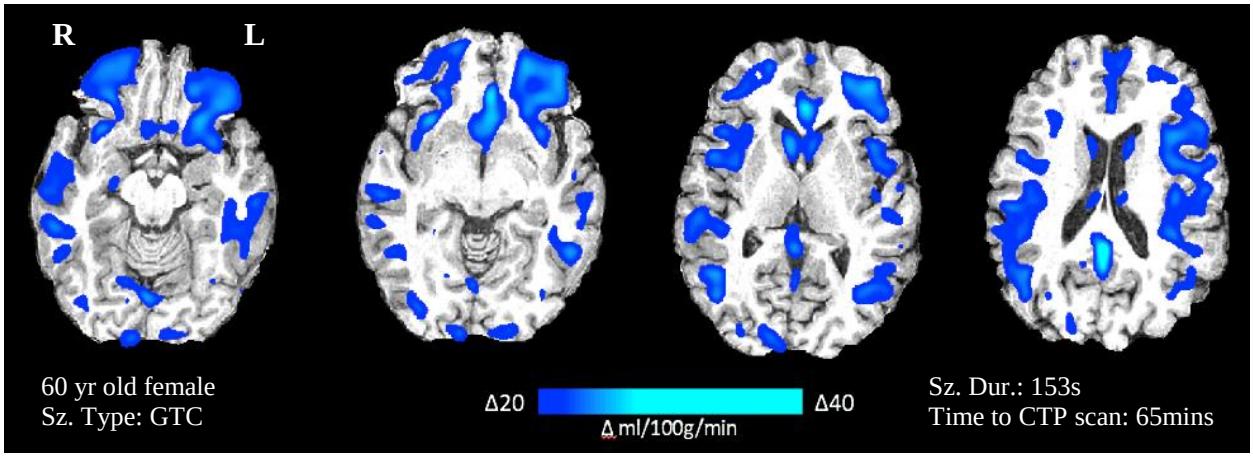

Figure A.1: Example of global hypoperfusion seen on sCTP through comparing a patient's postictal CTP CBF maps to baseline ASL maps obtained from 100 healthy controls. Data are shown for Patient 4 and are superimposed on T1-weighted images.

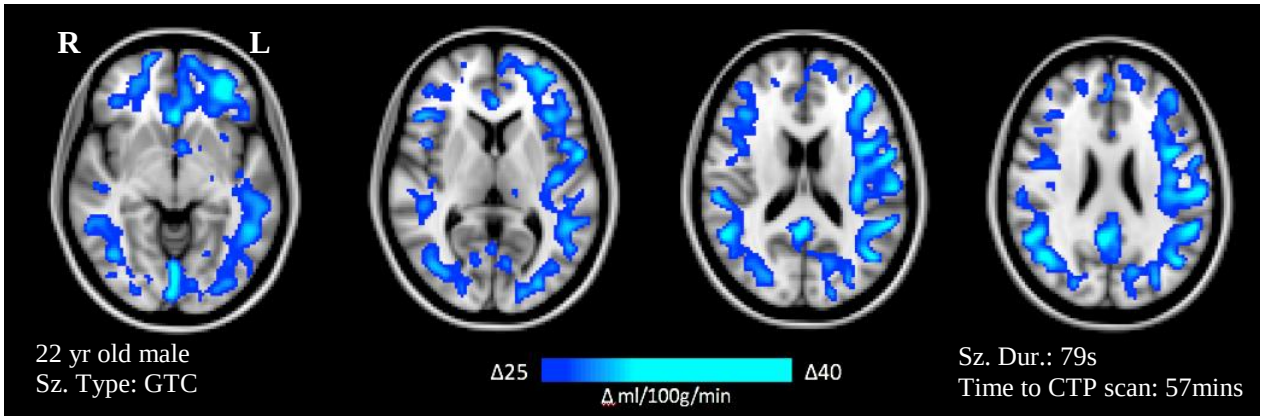

Figure A.2: Example of global hypoperfusion seen on sCTP through comparing a patient's postictal CTP CBF maps to baseline ASL maps obtained from 100 healthy controls. Data are shown for Patient 3 and are superimposed on MNI T1-weighted images.

A.3.2 *Comparing Postictal CTP to Patient Baseline ASL*

Subtracting a patient's own baseline ASL data from the postictal CTP data also produced apparent global hypoperfusion in all three subjects. However, the hypoperfusion was less widespread than in the previous comparison that used 100 normal controls as a baseline. Again, no clear site of maximal hypoperfusion was visualized. (Figure A.3). Improvements included less widespread clusters of hypoperfusion; however, the clusters were still non-lateralizing.

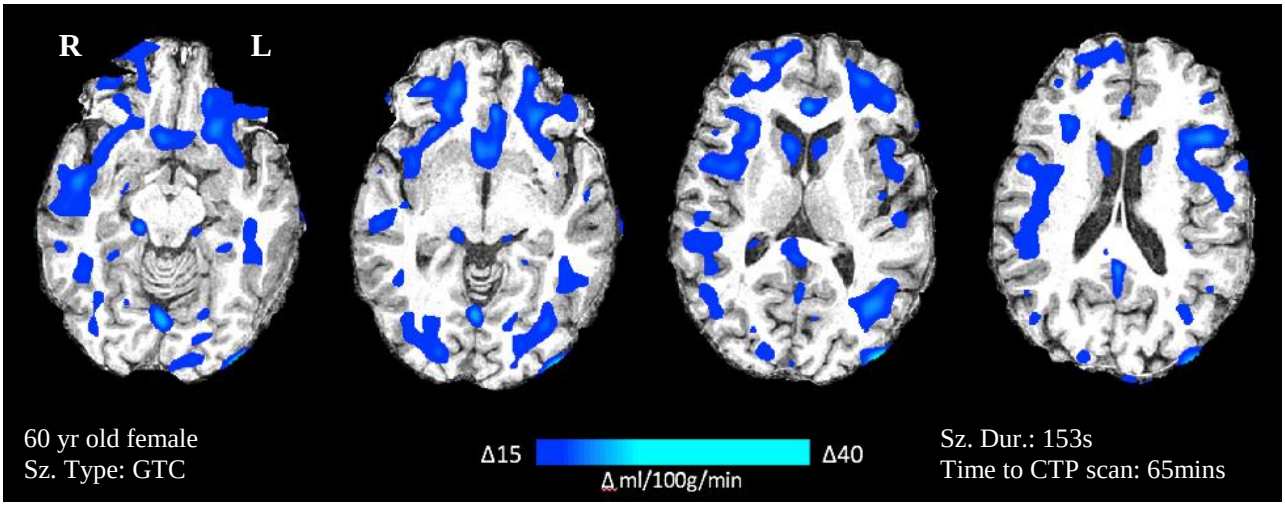

Figure A.3: Example of global hypoperfusion seen on sCTP through comparing a patient's postictal CTP CBF maps to the patient's baseline ASL maps. Data are shown for Patient 4 and are superimposed on T1-weighted images.

A.3.2 Comparing Postictal CTP to Patient Baseline CTP

Collecting both baseline and postictal CBF maps using the same modality (CTP) provided significantly cleaner results compared to subtraction between two different modalities (Figure A.4). For Patient 4, hypoperfusion was maximal in the left temporal-insular region.

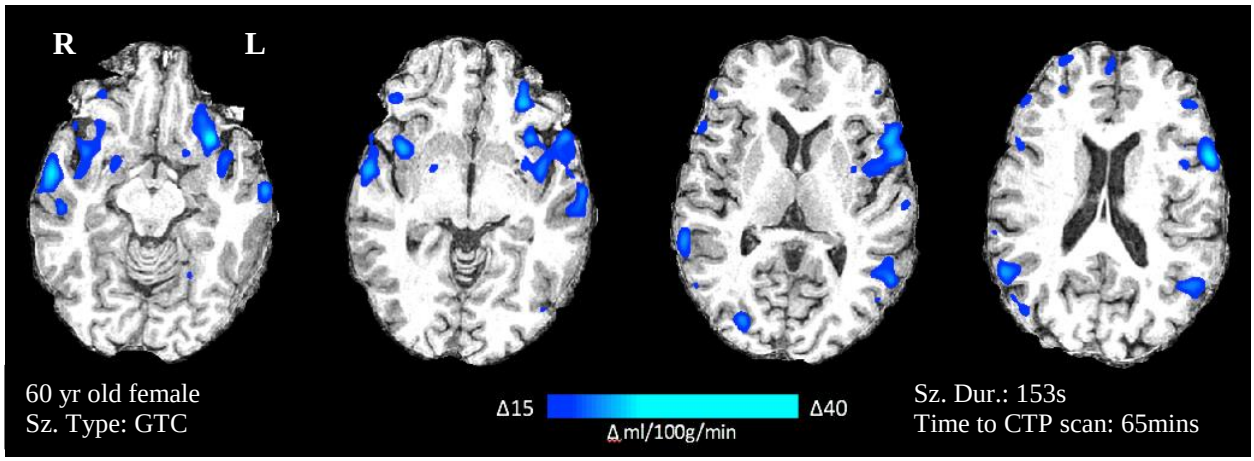

Figure A.4: Example of localizing hypoperfusion seen on sCTP through comparing a patient's postictal CTP CBF maps to the patient's baseline CTP CBF maps. Data are shown for Patient 4 and are superimposed on T1-weighted images.

A.4 Discussion

This study examined the feasibility of the quantitative subtraction of CBF maps collected using two different modalities, ASL and CTP. Although both modalities measure CBF, the algorithms used to calculate the CBF data are significantly different between them. I believe that the observed global hypoperfusion is artefactual in nature and likely the result of the incompatibility of cross-modality comparison.

In ASL, arterial blood water is magnetically labeled below the slice of interest by applying a 180 degree radiofrequency inversion pulse to create an endogenous tracer. The result of the radiofrequency inversion pulse is the inversion of the net magnetization of the hydrogen atoms in blood water (i.e., water molecules within the arterial blood are labeled magnetically). After a period of time, the "tracer" flows into the slice of interest and exchanges with tissue water. The inflowing inverted spins within the blood water alters and reduces the total tissue magnetization, and consequently the MR signal and image intensity. An image is taken at this time and is conventionally called the *tag image*. The experiment is repeated without labeling the arterial blood to create a *control image*. The control and the tag images are then subtracted to produce a perfusion image; the difference in magnetization between the control and tag images is proportional to the regional CBF (Petcharunpaisan, et al., 2010).

In contrast, calculations for CTP are made based on the central volume principle, which relates CBF, CBV, and MTT:

$$CBF = \frac{CBV}{MTT}$$

CTP intensities are expressed in Hounsfield Units (HU) and are linearly proportional to the efficiency of x-ray attenuation. An overview of the CTP image processing and theory was

provided in Chapter 1. Briefly, for each CTP scan, time-density curves (TDC) for the arterial input function (AIF) and venous output function (VOF) were obtained from the internal carotid artery. Parametric maps of CBF were calculated by deconvolution of tissue TDC's and the AIF. Perfusion weighted maps were created by averaging the cine CTP images over the duration of the first pass of contrast (d'Esterre, 2013).

Having two baselines for the same patient collected using two different modalities allowed us to test subtraction of one patient's postictal CTP from three different baselines: 1) ASL from 100 healthy controls, 2) patient's baseline ASL, and 3) patient's baseline CTP (Figure A.5). An intra-modality comparison (method 3) displayed the least widespread hypoperfusion that was lateralizing to the same hemisphere as the presumed seizure onset zone.

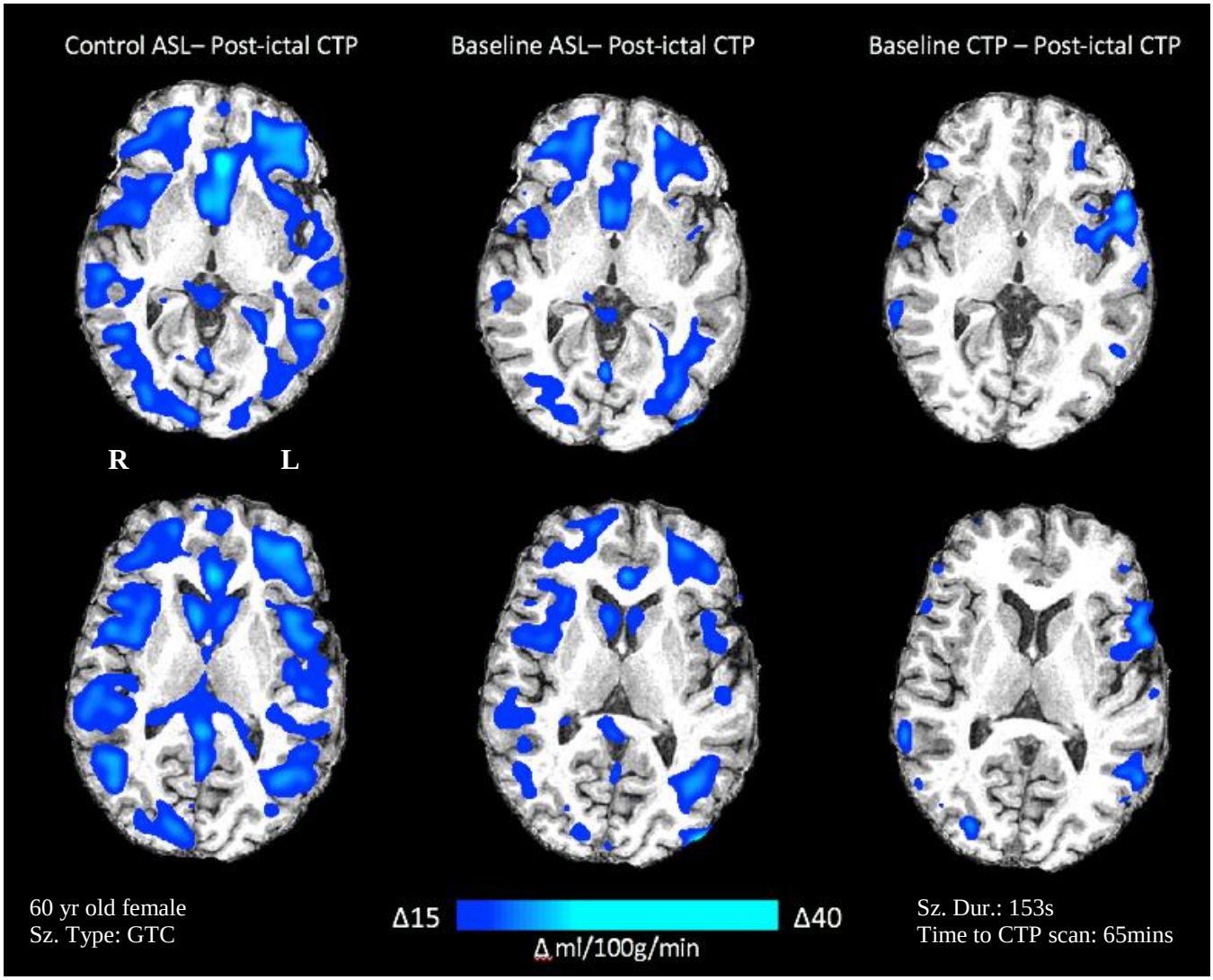

Figure A.5: Example of hypoperfusion using three different subtraction methods. Localizing hypoperfusion was only found in the intra-modality subtraction method. Data are shown for patient 4 and are superimposed on T1-weighted images.

The inherent differences between ASL and CTP make a direct quantitative subtraction between the two CBF datasets difficult. Differences in resampling and registration techniques between the two modalities may produce global differences that exceed the threshold of 15 ml/100g/min, as illustrated in Figure A.5. There may also be difficulties in compensating for the significant differences in dimensions between the two modalities. ASL images were collected with voxel dimensions of 1.87 mm x 1.875 mm x 5.00 mm, whereas the CTP voxels were 0.45 mm x 0.45 mm x 5.00 or 1.25 mm. Thus, the solution of re-slicing images into common voxel dimensions may compound perfusion artifacts that may have led to the observed global hypoperfusion.

Additionally, direct linear registration of the dynamic CBF maps from ASL and CTP onto a high resolution T1-weighted images may be poor. If both pre- and postictal modalities are CT, then registration is simple and reliable. This is because each scan includes a full anatomical image dataset, and these (postictal and baseline) may be efficiently and accurately co-registered to each other. Thereafter, the same transformation may be applied to the CBF data, which thereby inherits the accuracy of the anatomical registration. Because this characteristic of a common space during collection does not apply between the T1-weighted images and the ASL or CTP CBF maps, a direct linear registration of a low resolution dynamic map to a high resolution anatomical map must be applied.

Upon visual inspection, the quality of registration of each CTP and ASL onto the T1-weighted images was determined to be poor as slices and structures did not align optimally between the images. Despite this, registering two CTP scans onto an MRI demonstrated localized hypoperfusion more clearly than using a baseline ASL scan. Indeed, the superior

approach for detecting localized hypoperfusion between a baseline and postictal state was found to be an intra-modality comparison.

Collecting both the baseline and postictal scans using one modality, CTP, was deemed to be the optimal method of collection. In summary, CTP-ASL comparisons demonstrated poor localization, whereas the CTP-CTP comparison was localizing.

A.5 Conclusion

A quantitative comparison between postictal CTP and baseline ASL scans was not feasible. Differences in dimensionality, temporal resolution, and algorithms underlying the collection of CBF measurements by these methods produced patterns of apparent non-lateralized global hypoperfusion that is likely artefactual in nature. A comparison between three subtraction methods was made for one patient who had both ASL and CTP baseline scans (Figure A.5). An intra-modality comparison of baseline CTP to postictal CTP was the only comparison method that showed localized hypoperfusion.

APPENDIX B: Determining Electrode Artifacts

B.1 Introduction

A limitation of using ASL to collect baseline, and especially postictal CBF measurements, was the necessity to remove EEG electrodes prior to scanning. The EEG electrodes used at our center are not MR compatible and pose a safety concern for patients. In addition to the limited scanner availability, the need to remove EEG electrodes makes collecting postictal ASL scans more logistically difficult especially given the time sensitive nature of the transient postictal hypoperfusion phenomenon. Removing electrodes consistently added at least 20 minutes to postictal scanning acquisition. Furthermore, after a postictal CTP or ASL study, each patient's EEG electrodes needs to be reapplied so that they can continue with their clinical investigations, namely continuous video-EEG monitoring. This requires coordination with after-hours EEG technologists to come to our center and re-hook the EEG electrodes as soon as possible after completion of the postictal blood flow measurement. Indeed, although CTP has the benefit of 24/7 availability, the need to remove electrodes prior to scanning limits the study availability to the on-call hours of EEG technologist (0800-2200) because of the need to re-hook patients.

Because CTP employs radiation instead of magnetization to collect images, the EEG electrodes used at our center are CT compatible (International, 2011). Indeed, a proposed benefit of CTP was that EEG electrodes may not need to be removed as they do not propose any safety concerns to patients, allowing the postictal scans to be easier and more logistically feasible to collect.

Although the electrodes are CT compatible, they could depreciate the quality of the images by introducing various artifacts resulting from the electrode metal. Artifacts, in the

context of imaging, is something in an image that does not correspond to a physical feature in the test object (International, 2011). There are many types of CT artifacts including noise, beam hardening, scatter, motion, cone beam, helical, ring, and metal artifacts.

To investigate whether EEG electrodes cause artifacts on collected CBF images, a phantom with EEG electrodes attached was scanned. Additionally, one patient was scanned with electrodes on to further determine the significance of any artifacts on quantitative analysis.

B.2 Materials & Methods

B.2.1 *Phantom Electrode Placement*

A uniform spherical phantom (9 cm diameter) filled with 0.1% sodium azide was used to examine the potential artifacts from EEG electrodes on collected CTP images. Ambu® Neuroline Cup EEG electrodes, made of silver/silver chloride, were taped onto a phantom following the 10/20 electrode placement system (Figure B.1). Electrodes wires were moved outside of the scanner head rest during image acquisition to avoid excessive wire bundling.

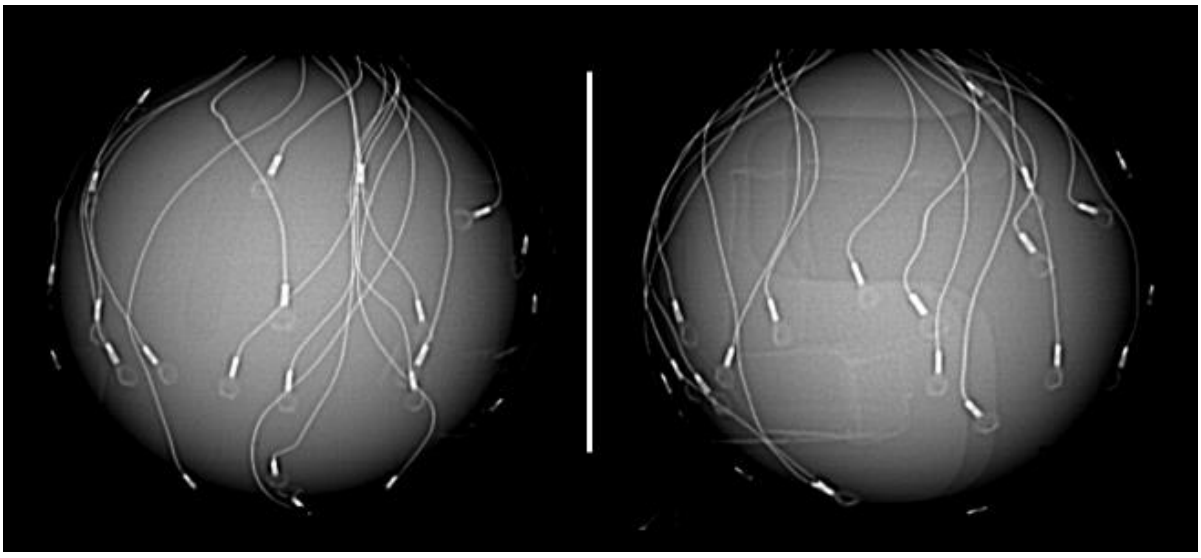

Figure B.1: Scout images collected showing the phantom and electrode set-up used to determine EEG electrodes artifacts on collected CT images. EEG electrodes were placed onto the phantom following the conventional 10/20 placement system. Left and right images are showcasing different angles of the phantom.

B.2.2 *Phantom CTP Acquisition*

CTP images were acquired using the protocol described in Ch.2, section 2.2.4 except no contrast agent was used for the phantom study; thus, no perfusion images could be generated. Notably, clinical CT scanners have a maximum CT number in CT images of 3071 HU except when

an extended CT scale is used (Coolens and Childs, 2003). Thus, all metallic objects will be set to 3071 HU, which underestimates the true CT value (i.e. maximum X-ray attenuation).

B.2.3 *Participants, Study Protocol, and CTP Acquisition*

One patient was recruited and studied using the criteria followed in Ch.2, section 2.2.1 except electrodes were not removed during CTP scanning in both postictal and baseline images. EEG electrodes were placed following the conventional 10/20 system. During CTP acquisition, the electrode cords were placed outside of the head rest in effort of alleviating additional electrode artifacts. The CTP data were co-registered to the anatomical CT average images and T1-weighted high-resolution images to define the seizure onset zone based on postictal hypoperfusion.

B.2.4 *CTP Co-Registration*

Baseline CTP and postictal CTP CBF images were co-registered (spatially normalized) to each patient's baseline CT anatomical average map and T1-weighted high-resolution images using a freely available software package (FSL: FMRIB Software Library, Release 5.0, University of Oxford). The MRI scan was used as an attempt to gather additional anatomical information as the average CT maps were affected by the artifacts resulting from the electrodes.

To register the CBF images onto the CT anatomical images, I performed a linear registration of the higher resolution postictal anatomical CT images to the baseline anatomical CT images. This process used a 12-parameter affine transform that accommodates scaling, shearing, translation and rotation to improve alignment. Registration was verified by visual inspection and minor manual adjustments were made as required. Because the anatomical CT images and the CBF CT images share a collective space, the same transformations may be applied to the CBF data,

thereby allowing the CBF images to inherit the same accuracy as the anatomical registration. After spatial normalization, the CTP quantification maps were smoothed by a 4-mm full-width-half-maximum Gaussian kernel to improve signal to noise and reduce small-scale registration errors.

To register onto the T1-weighted images, CTP CBF maps were linearly registered to the T1-weighted images using the same software and 12-parameter processing. A normalized mutual information metric was also selected. Normalized mutual information is one of five metrics available in FSL and allows images with different contrasts to be registered. Registration was verified through visual inspection of the images. After spatial normalization to the T1-weighted images, the CTP quantification maps were smoothed by a 4-mm full-width-half-maximum Gaussian kernel to improve signal to noise and reduce small-scale registration errors.

B.2.5 *Subtraction Analysis for Comparing Postictal CTP and Baseline CT Perfusion Data*

CTP scans were obtained within 51 minutes following a seizure (postictal) and following a seizure-free period of >24 hr (baseline). After spatial normalization and smoothing of CTP quantification maps, a global minimum of 0 ml/100g/min and maximum of 100 ml/100g/min was applied to baseline and postictal CBF maps to reduce artifactual hyperperfusion resulting from vessel artifacts. A subtraction CBF map (baseline minus postictal) was generated for each patient. The resulting subtraction map was superimposed onto the patient's CT anatomical average map or T1-weighted images to identify the anatomical brain areas with postictal CBF reductions of at least 15 ml/100g/min.

B.3 Results

B.3.1 *Patient Demographics*

One patient participated in the study. Their demographics and details of other clinical investigations including EEG onset, ictal SPECT, and structural imaging data are summarized in Table B.1.

Table B.1:Summary of demographics and clinical investigations of participating patients.

Patient ID	**Age**	**Sex**	**Seizure Duration (s)**	**Seizure Type**	**Time to Postictal CTP (mins)**
5	44	F	70	Focal impaired aware	51
	EEG Onset		**Interictal SPECT**		**MRI**
	Lt mid temporal		Hypoperfusion in Lt anterior temporal and Lt orbitofrontal		Normal

B.3.2 *Phantom Artifacts*

Three reviewers visually assessed the quality of the phantom images to determine further pursuit of a clinical trial. The preliminary results from the phantom revealed dark streaking artifacts developing from peripheral areas (assumed to be the electrodes). The streaking artifacts resulting from the metallic electrodes were deemed to be minor (Figure B.2) and a clinical trial was later pursued to delineate the severity of these artifacts.

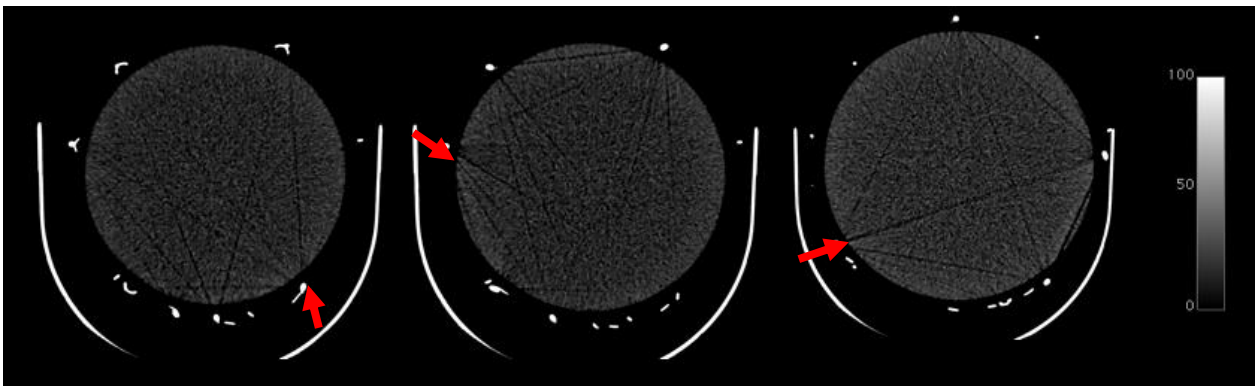

Figure B.2: Preliminary phantom results displaying multiple slices where streaking from the EEG electrodes placed on the phantom surface can be observed. Arrows depict origins of streaking in line with electrode locations. Voxel units are in HU.

B.3.3 *Qualitative Evaluation of EEG Electrode Artifacts*

Contrary to the phantom results, the streaking observed in the clinical trial of scanning with electrodes on was more apparent. Although electrode wires were placed outside of the headrest as much as possible during collection, it is apparent in Figure B.3A that there was wire bundling that caused excessive flaring and scatter effects on the periphery. The CBF perfusion maps displayed less apparent streaking than the CT average maps (Figure B.3B), however these artifacts negatively impacted quantitative (subtraction) CBF analysis.

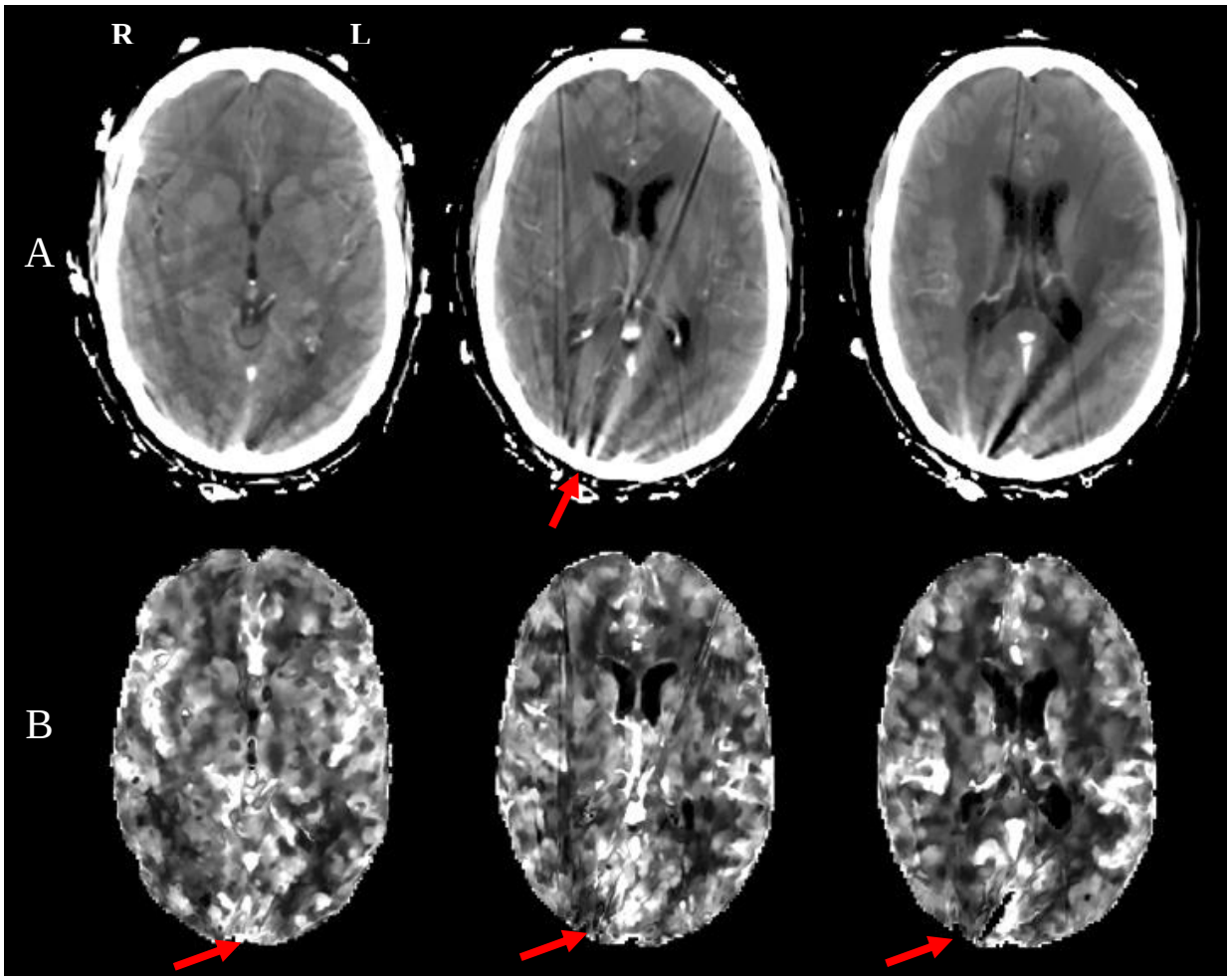

Figure B.3: CT images collected where EEG electrodes remained on during scanning. A. axial slices of the CT anatomical average map. B. axial slices of the postictal dynamic CT CBF quantification perfusion maps. Arrows depict origins of streaking. Data are shown for patient 5.

B.3.4 *Evaluation of EEG Electrode Artifacts on Subtraction Analysis*

Both postictal and baseline scans were acquired with electrodes remaining on. These quantitative CBF maps collected using CTP was compared by performing a subtraction analysis (baseline minus postictal). Upon visual inspection of the CBF maps, significant streaking artifacts were already observed. When subtraction analysis was performed, no localizing postictal hypoperfusion was seen. When a cross-modality registration (CT maps onto anatomical MR scans) was performed, no lateralizing or localizing hypoperfusion was seen (Fig. B.4A). When images remained within one modality for registration (CT), the superior slices predominately displayed hypoperfusion on the left hemisphere (Figure B.4B), which was concordant with the patient's clinical diagnosis of left temporal lobe epilepsy. However, many of these clusters of hypoperfusion were seen in the white matter and were deemed to be artifactual.

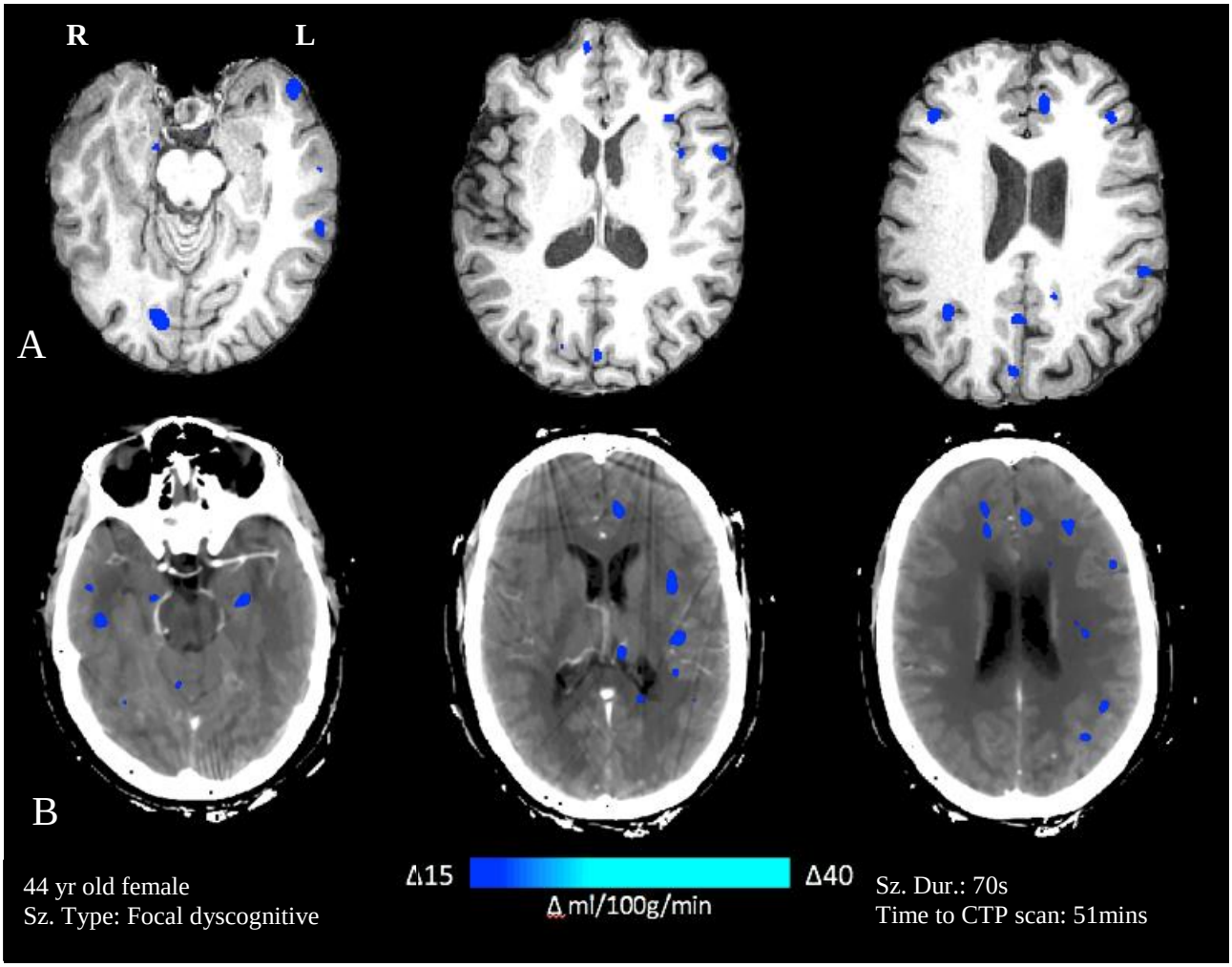

Figure B.4: Example of quantitatively comparing the postictal CBF measurements to baseline CBF measurements with electrodes on. Subtraction results are superimposed onto A. T1-weighted images and B. the CT anatomical average map. Data are shown for patient 5.

B.4 Discussion

The aim of this study was to investigate the effects of artifacts arising from the presence of metallic EEG electrodes on CTP images. A phantom with conventional EEG electrodes placed using the 10/20 system was initially used to determine the severity of the streaking artifacts. The streaks were deemed to be minor and a clinical trial was pursued. One patient participated and had both baseline and postictal CTP scans collected with EEG electrodes on.

Standard metallic disk EEG electrodes (Ambu® Neuroline Cup, silver/silver chloride) were used in this study and was deemed to be the dominant contributor of observed artifacts. Metal streak artifacts are caused by multiple mechanisms relating to either the metal itself, or the metal edges. The metal itself can cause beam hardening, scatter effects, and Poisson noise (Boas, 2012). Beam hardening and scattering results in dark streaks between metal, with surrounding bright streaks (example Figure B.3.A). The metal edges can cause streaks due to undersampling and motion. Indeed, keeping electrodes on during image acquisition produced substantial streaking CT artifacts that reduced image qualities and the potential to perform additional quantitative analysis.

Additional quantitative analysis was hampered by the artifacts artificially increasing or decreasing voxel values of CBF measurements that aligned with electrode streaks. Although both baseline and postictal scans were collected with electrodes placed following the same convention, the theory of the streaks cancelling one another out was nulled for numerous reasons. First, the scans were collected a week apart and the patient underwent an electrode change during that time. Although technicians would still be placing electrodes following the 10/20 system, it is unlikely that the placement of electrodes would have been in the exact same

spot to produce precisely the same artifact that could be cancelled out. Second, the patient's placement in the head rest would have been different and shifted as well, thus the slices acquired in the baseline vs postictal state would be slightly different. Taking these effects into consideration, this resulted in the CBF maps having hyper- or hypointense voxels resulting from electrodes in different areas between scans. As a result, the generated subtraction map would show these voxels with hyperintense differences as areas of artificial hypoperfusion. Although applying a smoothing kernel may negate some of these artifact noise, the hypoperfusion pattern for this patient remained non-localizing. Indeed, the artifacts resulting from the EEG electrodes make further quantitative analysis infeasible.

Several techniques have been proposed for metal artifact reduction which are based on the principle that projection data involving or near metal is less accurate and thus uses the non-metal data to construct over the metal portions of the image. Metal pixels are then deleted from the reconstructed image on each iteration. These kinds of technique try to look through the metal to see soft tissue instead of around the metal. However, this also means that any features that can only be seen looking through the metal will be lost, and structures within a few millimeters of metal are blurred out. Another disadvantage is that these techniques often work with the raw projection data from the scanner which is often stored in a proprietary format, and therefore not always accessible. For my purposes, the raw projection images were not accessible, and I could not employ many of these experimental techniques.

A future effort may be to try clinically employing non-metal EEG electrodes that are thus CT-compatible instead of deleting the artifacts post-processing. One study described 23 critically ill adults who underwent CTP scans with conductive plastic electrodes (Das, et al., 2009). All

were assessed to have had excellent image quality without significant CT artifacts. In contrast, another study investigated 13 children who underwent CTP scanning with conductive plastic electrodes (Abend, et al., 2015). Researchers observed artifacts but not attributable to the leads, rather it was the wires that inadvertently remained connected (Figure B.5A). The artifacts observed when wires were removed were very subtle, and significantly better compared to using metal electrodes (Figure B.5B and Figure B.5C). Thus, it was concluded that plastic electrodes do not produce problematic CT artifacts as long as the wires are properly disconnected.

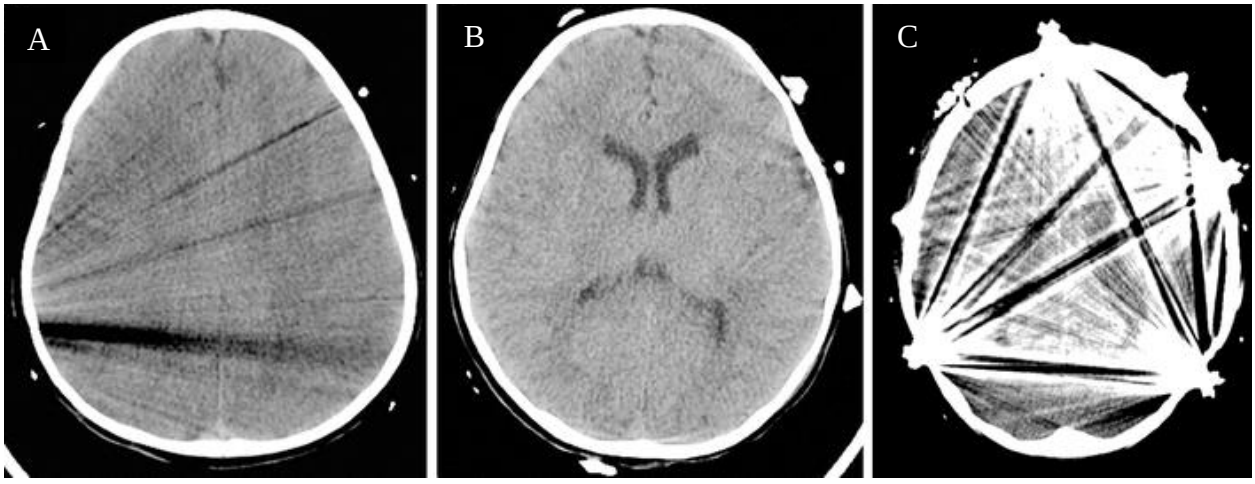

Figure B.5: CT image of a 1.5-year-old girl undergoing EEG monitoring. A) demonstrates artifacts attributable to the wires that remained connected and not the leads. B) demonstrates mild beam-hardening artifact under plastic electrodes. C) demonstrates extensive artifacts from a different patient scanned with metal scalp electrodes to compare. Adapted from (Abend, et al., 2015).

B.5 Conclusion

In summary, a quantitative comparison between a postictal CTP scan and a baseline CTP scan with EEG electrodes on the patient during acquisition was not feasible for the study. Although there were no safety concerns, significant streaking artifacts causing hyper- or hypointense CBF measurements in voxels made further quantitative analysis via a subtraction comparison non-localizing. Based on available literature, plastic electrodes show promising results and may be employed for future efforts to improve logistical feasibility and ease of postictal CBF data collection.

APPENDIX C: Pipeline Development

C.1 Introduction

The development of the finalized pipeline used in this thesis involved many trials to determine optimal registration, thresholding, smoothing, clustering, and intensity normalization parameters as well as overall methods of quantitatively comparing pre- versus postictal CBF data. Described below are the developed methods of each post-processing step prior to the finalized pipeline described in Chapter 2.

C.2 Registration

Amongst all the post-processing steps involved, accurate registration is one of the most important steps, perhaps second to the production of CBF maps. If registration is inaccurate then all subsequent post-processing analysis will be faulty. For this project, registering postictal CBF images into the baseline anatomical space was required. This registration process was necessary for further analyses as the postictal and baseline CBF images needed to be aligned to a common space. The baseline images served as the fixed image, and the postictal images served as the moving image to be transformed as close as possible to the fixed image. The challenge of how to accurately register a low-resolution image with little distinguishing anatomical features to a higher resolution anatomical image needed to be addressed. The following sections describe the registration methodologies that were tested.

C.2.1 Assessing Registration Quality

Registration quality was visually evaluated in each instance by myself and several imaging experts. There currently is no conventional systematic method of quantitatively evaluating quality of image registration. When visually evaluating registration quality, factors

considered included alignment of brain edges and accurate overlap of several key inner cortex structures such as the ventricles, thalami, and caudate.

C.2.2 Direct Linear Registration

Following the original subtraction ASL pipeline, the first registration attempt involved direct linear registration of the postictal quantitative CBF maps onto the baseline anatomical average map. Postictal CBF maps were brain extracted using the BET brain extraction toolbox from FSL (BET – FSL v2.1). Subsequently, CBF maps were registered onto each patient's baseline average maps using an affine transformation (12 degrees of freedom) from the FSL FLIRT toolbox (FLIRT – FSL v5.5). Internal structures were observed to be misaligned between the postictal CBF map and baseline average map (and consequently baseline CBF map), specifically the ventricles and subcortical structures. This was especially apparent when registering 5 mm thick slices.

C.2.3 Direct Non-Linear Registration

Non-linear methods of registration were attempted using Advanced Normalization Tools (ANTs), which includes powerful non-linear registration algorithms. Unlike linear registration which functions by aligning centers and orientations through rotations, non-linear registration works on the principles of matching boundaries and internal structures by warping the data. When postictal CBF maps were non-linearly registered to the baseline average map, the edges of the brain were aligned; however, the internal structures of the postictal CBF images were substantially warped compared to the baseline images. Non-linear registration methods also took much longer to complete compared to linear registration.

C.2.3.1 Two-Step Registration: Non-Linear Registration Following Linear Registration

Direct use of non-linear registration of CBF maps to anatomical data may have been too dramatic given the large number degrees of freedom involved and the reduction of defining landmark anatomical features in the CBF data**.** It was proposed to first perform linear registration to roughly align datasets in terms of centers, orientations, and account for any scale factors, then to perform non-linear registration for finer alignments. Compared to previous methods, there were no obvious structural misalignments, which increased our confidence in this method. However, the process was complex and lengthy with many parameters that could be further adjusted.

C.2.4 Linear Registration with Matrix Transformation

Each postictal and baseline acquisition contained a CBF map and an anatomical average map collected in the same space. To take advantage of this element, it was proposed to directly linearly register the higher resolution anatomical maps to each other and produce a transformation matrix. The direct linear registration of anatomical maps was significantly better compared to direct linear translation of CBF maps to anatomical space since both are high resolution scans with detailed anatomical landmarks. Given that the postictal CBF map is collected in the same space as the postictal average map, the transformations necessary to register the postictal average map to the baseline average map can thus be applied to the postictal CBF map. This method produced similar results to the aforementioned two-step registration and took significantly less time. It also involved less transformations applied to the postictal images thus limiting the influence registration may have on the location of any future perfusion changes.

C.2.5 Summary and Conclusions of Registration

In summary, linearly registering the postictal anatomical to the baseline anatomical scans, producing a transformation matrix, and applying those transformation to the postictal CBF data provided the best registration method in terms of anatomical accuracy and time (see section C.2.4).

C.3 Thresholding

Subtracting CBF images is challenging due to the presence of large vessels which cannot be perfectly registered and if not removed, produce very large discrepancies in the subtraction CBF map. The general range of healthy CBF measurements is approximately 60 CBF units in grey matter, and 25 CBF units in white matter (de Lucas, et al., 2008). When viewing the CBF measurements of vessels, they can exceed 300 CBF units. In contrast, voxels within the ventricles which should theoretically provide a value of 0 CBF units oftentimes report negative values. These extremes are clearly outside the boundaries of normal physiological CBF measurements. Thus, in an effort to minimize the effects of vessels and intensity artifacts, multiple methods of thresholding of the CBF data were attempted.

C.3.1 Global Thresholding to Zero

Following the original postictal ASL subtraction pipeline, the first attempt at thresholding the CBF data was to apply a global threshold where voxels above 100 CBF units and below 0 CBF units were set to 0 CBF units. This would theoretically null hyperintense vessels and voxels that were beyond physiological values. Using this method while performing a subtraction analysis created more artifacts in the final cluster map. Registration of the CBF data into the same anatomical space is not perfect and oftentimes the vessels between two images can be misaligned. If the vessel was artificially thresholded to 0 CBF units in one scan, and it is overlaid over an area of normal tissue on the other scan, the subtraction between the two would result in a larger difference that is artifactual but would pass the absolute threshold of 15 CBF units. Thus, globally thresholding hyperintense or hypointense voxels to 0 CBF units was not optimal for performing a subtraction analysis.

C.3.2 Localized Thresholding

The goal of the vessel filtering algorithm is to replace hyperintense voxels representing vessels with the median CBF values of the surrounding tissue. For this application, pixels with a CBF greater than 100 CBF units were identified to be a vessel. This was based on literature values of average white matter and grey matter CBF measurements being between 20 – 60 CBF units; thus, perfusion values above 100 were deemed to be artifactual in nature.

To identify tissue (non-vessel) pixels in a region, a histogram cutoff value was used for a 2D window size of 19 x 19 voxels. A ROI containing a vessel cross section surrounded by normal tissue would have a corresponding CBF histogram displaying a spike at the higher end of CBF values, representing the vessel. The histogram percentile cutoff can be set and adjusted to exclude these vessel pixels to isolate the non-vessel CBF values. Once the CBF threshold and percentile threshold is applied, the median value of the CBF values is identified and replaces the voxels that were initially identified as a vessel. This process is iterated over the entire new image, and the final effect is that the algorithm replaces vessel voxels with the median CBF value of the surrounding (non-vessel) tissue.

Although applying this localized filtering algorithm removed hyperintense vessel voxels and created CBF data that were more uniform in value, it ultimately did not create a significant difference when performing the subtraction analysis compared to applying a global thresholding (described below). sCTP cluster maps were near identical and applying the localized thresholding algorithm was considerably more difficult to perform.

C.3.3 Global Min and Max Thresholding

In an effort to minimize the effects of hypo- or hyperintense voxels in the CBF data after subtracting between two images, applying a global minimum of 0 CBF units and global maximum of 100 CBF units to the CBF images was proposed. This meant that all voxels below 0 CBF units were revalued to 0, and all voxels above 100 CBF units were revalued to 100. Although these thresholds were arbitrarily chosen, they were selected on the basis that values beyond this range would not be physiological.

Especially compared to globally thresholding hypo- or hyperintense voxels to 0 CBF units (see section C.3.1), this method of thresholding provided results that had significantly less scattering of hypoperfused clusters after subtraction. This method is more robust and resistant to small registration errors because slight misalignment of hyperintense voxels to normal voxels will provide smaller differences (e.g., comparing 80 CBF units to 100 CBF units vs. 80 CBF units to 0 CBF units) that would be later filtered out by the 15 CBF units threshold or the cluster filter.

C.3.4 Summary and Conclusion of Thresholding

In summary, applying a global minimum and maximum was most resistant to slight registration errors and provided the least artifactual scattering from hypo- or hyperintense voxels. It provided similar results to the localized vessel filtering algorithm but took less time and was significantly less complex (see section C.3.2) and was thus used for the final pipeline.

C.4 Quantitative Comparison Analysis: Absolute Subtraction vs. Percent Decrease

Ultimately, this project sought to detect localized perfusion changes between the baseline images and the postictal images. Two main comparative methods were investigated: a subtraction (baseline minus postictal), whereby the remaining clusters represented absolute decreases in blood flow, or a division (postictal divided by baseline), whereby the remaining clusters represented a fractional or percent decrease. The subtraction method was ultimately chosen and described in more detail in Chapter 2. This section will describe the attempt at representing clusters of hypoperfusion as a percent decrease.

C.4.1 Percent Decrease Method

The rationale for representing clusters as a percent decrease over an absolute value was so that a universal threshold can be applied to view results between patients. In the subtraction method, a minimum of 15 CBF units is applied for viewing as this represents an approximate 30% decrease from average baseline CBF values and what was observed as postictal hypoperfusion in animal studies. However, each patient will have different baseline CBF dynamics, thus it is possible that one patient will require a higher threshold (e.g., 20 CBF units) than another patient to show localized CBF changes. Thus, using a minimum threshold of 15 CBF units and stating that this represents a 30% decrease in CBF values is a broad assumption. By representing clusters as a fraction with voxels having a value between 0 – 1, using a minimum threshold of 0.3 would guarantee an accurate change of at least 30% relative to the patient's specific baseline, making it more theoretically better to compare CBF changes between patients.

C.4.1.1 Division Pipeline Development

Similar to the subtraction pipeline, postictal and baseline CBF data were registered, thresholded to have a global minimum and maximum of 0 and 100 CBF units respectively, and smoothed. Division was performed by dividing the postictal CBF data by the baseline data, and subsequently subtracting from a binary map $\left(1 - \frac{postictal}{baseline}\right)$ to represent postictal hypoperfusion. Although the ventricles should theoretically have CBF values of 0 units, ventricular values ranged from 0 to 5 CBF units. In the case of subtraction analysis, a 15 CBF unit threshold was used, thus eliminated ventricular. However, the division method could highlight these voxels in some cases and result in false localization of clusters that 30%. To circumvent this issue, the ventricles were masked and removed from the division maps. Finally, cluster filtering was applied similar to the subtraction analysis but with different threshold values (e.g., clusters ≥ 400 voxels and exceeding a ratio of 0.3).

C.4.2 Division Results

The division method of comparison was functional and provided clusters that overlaid in similar regions as the subtraction method. However, it was noted that there were more clusters in division maps than subtraction maps. Figure C.1. shows an example of the results obtained from subtraction versus division for patient 1. Both methods overlap and show areas of hypoperfusion in the left temporal region, which is concordant with the location of the presumed SOZ. However, the division analysis revealed additional clusters in the left frontal white matter and right temporal lobe, both of which were not detected in other modalities and are ultimately seen as discordant locations. It was suspected that comparing images using a division method was more susceptible to smaller perfusion changes compared to performing subtraction analysis. The

increased number of operations involved in the division versus subtraction analysis may also contribute to image acquisition errors being compounded throughout the pipeline as dividing is slightly more complex.

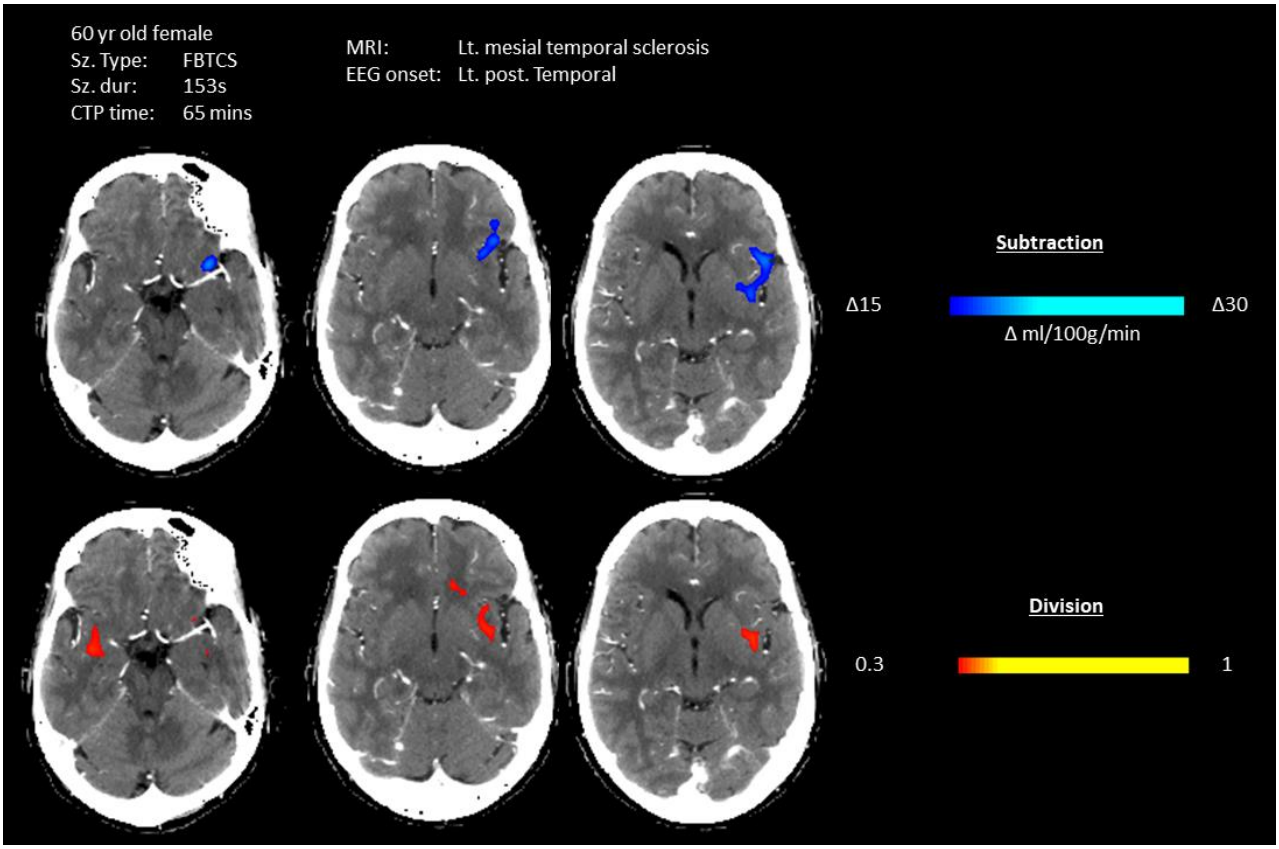

Figure C.1: A comparison of the subtraction method versus the division method of comparison for patient 1. Left temporal clusters are observed in both which are concordant with the presumed SOZ, however division maps showed additional clusters in the left sided white matter and right temporal lobe which were not observed in other modalities.

C.4.3 Summary and Conclusion of Quantitative Comparison Method

Ultimately, the subtraction method was chosen as the final method of comparison. Although the division method provided similar localizing results in most patients, it was found to be noisier and produced additional clusters in areas that were discordant with other diagnostic modalities.

C.5 Smoothing

All brain images are inherently noisy due to errors associated with image acquisition. In addition to image acquisition errors, there are also errors caused by image registration, segmentation, and other post-processing steps like performing a subtraction. Thus, it is necessary to smooth out the segmentation before any statistical analysis is performed. Upon performing a subtraction of unsmoothed images, there will be significant noise. To circumvent this, postictal and baseline CBF images were each smoothed prior to subtraction. Gaussian kernel smoothing was used and is a common technique employed in brain imaging.

C.5.1 3 mm vs. 4 mm. vs 5 mm. vs 6 mm

The degree of Gaussian smoothing needed to be determined. The challenge was finding the balance between smoothing enough to produce clean images with significant localizing clusters but not too much, which could result in the loss of significant clusters. Gaussian kernels with varying spatial full width at half maximum (FWHM) values were tested. The 3mm FWHM Gaussian filter retained widespread clusters of hypoperfusion that were felt to represent noise. In contrast, the 6mm FWHM Gaussian filter retained significant localizing clusters whilst eliminating excessive noise (Fig. C.2). For some patients, a 6mm FWHM Gaussian filter was too aggressive, resulting in the elimination of all areas of hypoperfusion. These patients often had either focal aware seizures or a shorter seizure, which were associated with smaller perfusion changes. Thus, a 6mm FWHM Gaussian filter was optimal for eliminating noise for the majority of patients, whilst still highlighting clean localizing clusters. However, in some cases a lower degree of spatial smoothing was necessary to account for smaller postictal perfusion changes.

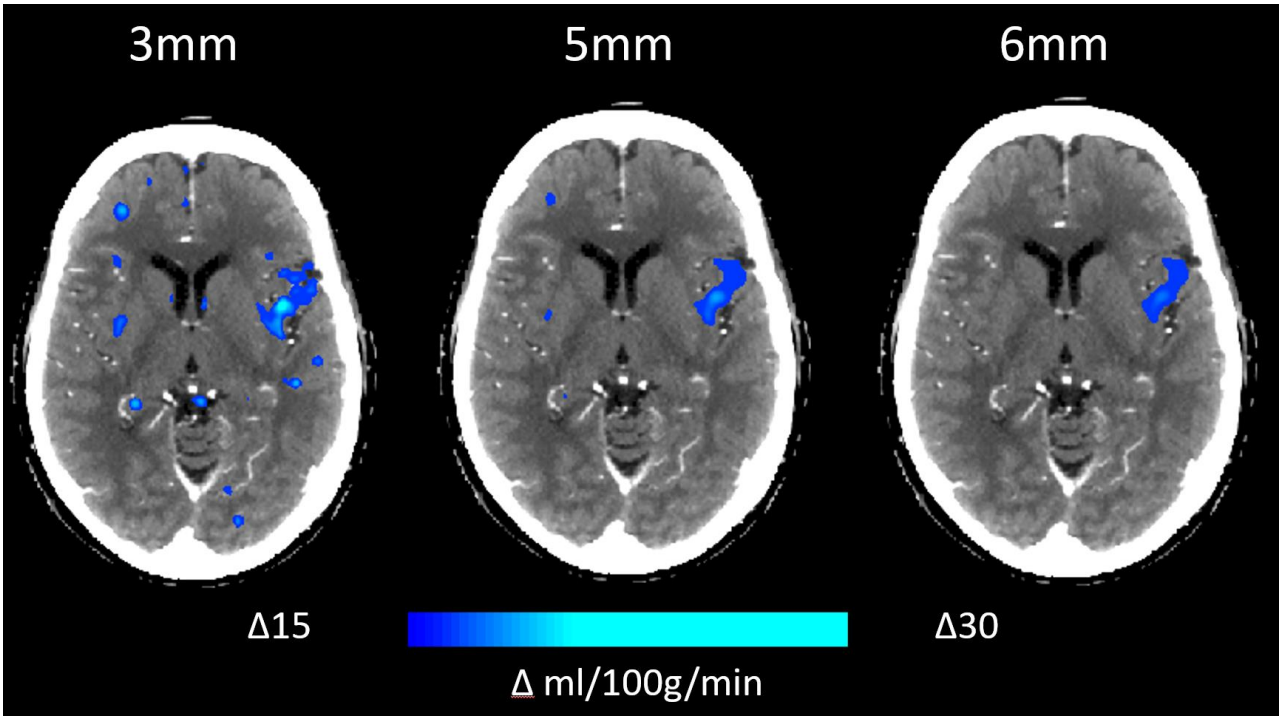

Figure C.2: Comparison of Gaussian kernels of various spatial FWHM for smoothing the sCTP map. sCTP clusters (blue) are overlaid on the patient's CT anatomical average map. Data are shown for patient 1.

C.5.2 Summary and Conclusion of Smoothing

A 6 mm FWHM Gaussian filter was optimal for the majority of the patients and best eliminated noise while adequately displaying localizing clusters of hypoperfusion. A 5 mm FWHM Gaussian filter may be used as needed for patients with smaller perfusion changes. In the cohort used in this thesis, a 5 mm spatial filtering was used to observe clusters of hypoperfusion for 3 out of 13 patients.

C.6 Clustering

In the context of this thesis, a cluster is defined as a group of voxels that are touching by at least one face in one of the three dimensions. As mentioned in smoothing, all brain images are inherently noisy. Despite application of smoothing kernels, the resulting subtraction map continued to display collections of very small and low intensity clusters. These clusters can often be ignored as they did not influence localization given the insignificance of both cluster size and intensity. Despite this, to better clean subtraction maps, a cluster filter was applied whereby a threshold value (e.g., magnitude of CBF change) and a cluster size threshold are set. The threshold value ultimately determines the size of the clusters. Higher threshold values result in smaller clusters, as more voxels would not pass the threshold to stay connected. After setting a threshold value, a cluster size threshold is set. Together, clusters of a certain intensity and certain size will remain. The challenge was finding the optimal balance between these thresholds: a filter that is too stringent may eliminate physiological clusters. Thus, the aim was to determine whether a low threshold value with higher cluster size thresholds was better, or whether a higher threshold value with lower cluster size threshold, or some variation in between.

C.6.1 Optimizing Value and Cluster Threshold

Various combinations of the two thresholds were tested. In general, combinations of low threshold values paired with higher cluster size thresholds provide the most best results. High threshold values and high cluster size was too aggressive as no clusters would remain. Low threshold and low cluster size was too permissive, and no changes would be seen if viewing the maps on a 15 CBF unit minimum. Threshold values were initially set at 5 CBF units, and incrementally increased to 25 CBF units. These thresholds were paired with an associated cluster

size of 500 voxels, and incrementally decreased to 300 voxels. The size of a significant cluster was usually in the several thousands in three-dimensional space. Thus, filtering clusters based on several hundred voxels was not encroaching on physiological clusters.

C.6.2 Summary and Conclusion of Clustering

In summary, a threshold value of 15 CBF units in combination with a cluster size threshold of 400 voxels was used. This combination was found to eliminate insignificant clusters in the majority of patients while retaining presumed physiological clusters. Similar to the challenge in smoothing, an overly high cluster size threshold could not be used to accommodate more subtle perfusion changes for some patients. Although more aggressive combinations would function well with patients with larger perfusion changes, it would ultimately result in empty subtraction maps with patients with more subtle changes. Thus, this combination of thresholds was chosen to function for all patients but is arguably less optimal for patients with large perfusion changes.

C.7 Intensity Normalization

After comparing the postictal and baseline CTP CBF maps qualitatively (see Ch.2, section 2.2.6 for review process), the intensity scales of each scan needed to be adjusted significantly to match intensities to account for global differences. To further pursue a quantitative comparison by subtracting the two images, it was determined that a form of intensity normalization would be necessary to account for the global differences between the two maps (See Ch.3, section 3.4). Various methods of normalizing the intensities were tried, and many more exist. This section highlights the methods that were tested in this thesis. The goal was to find a scaling factor to globally shift the postictal intensities to the same range as the baseline data, hypothetically eliminating global differences and allowing subsequent subtraction analysis to be performed.

C.7.1 Normalizing Global Mean

The global mean was calculated for baseline (M1) and postictal (M2) CBF maps. The difference in means (ΔM) was calculated ($\Delta M = M1 - M2$) and added to the postictal data in a voxel-wise manner. This resulted in the postictal CBF data having the same mean as the baseline data. This method was an improvement over subtraction analysis performed without intensity normalization as clusters, especially those observed along the midline, were oftentimes removed and overall perfusion changes were more focal.

C.7.2 Normalizing Global Mean and Standard Deviation

Given that the postictal maps are expected to be focally hypoperfused, this would result in a lower global mean and larger standard deviation relative to the baseline data. We attempted to account for both differences by normalizing both the mean and the standard deviation.

The global mean was calculated for baseline (M1) and postictal (M2) CBF maps. The difference in means (ΔM) was calculated ($\Delta M = M1 - M2$) and added to the postictal data in a voxel-wise manner ($\widetilde{Post}$). Standard deviation was calculated for baseline (σ_1) and $\widetilde{Post}$ (σ_2). A ratio (α) of the standard deviation was calculated ($\alpha = \frac{\sigma_1}{\sigma_2}$). Finally, the normalized postictal scan was produced as follows:

$$Post_{Norm.} = M1 + \alpha(\widetilde{Post} - M1)$$

This method was used for this thesis. Normalizing both the mean and standard deviation highlighted localized perfusion changes the best compared to other methods. Certain clusters were eliminated whereas others became significant enough to pass the threshold. Interestingly, those clusters that appeared were often concordant with clinical data, further confirming that intensity normalization is a necessary step when comparing CBF data between two different time points to fully highlight perfusion differences.

C.7.3 Z-Score Normalization

We also attempted to convert CBF values into Z-scores and normalize intensities in this scale. Postictal and baseline maps were registered into a collective space. Hypo- and hyperintense voxels were thresholded to 0 following section C.3.1 to avoid significantly increasing the calculation of the mean global CBF value. The global mean and standard deviation was calculated for each data set. The Z-score was calculated for each voxel using the following formula:

$$Z - score = \frac{[image] - Global\ Mean}{Global\ Standard\ Deviation}$$

A subtraction was then performed with the Z-score converted images. There were multiple challenges with this method. First, the original threshold of 15 CBF units could not be applied as all voxels were Z-scores. Second, the inclusion of positive and negative Z-scores made it difficult to apply any viewing threshold, making the Z-score subtraction maps non-localizing. Lastly, the maps were completely non-localizing with widespread changes observed throughout the entire brain; this may be due to any compounding of image acquisition errors because of the increased number of operations (similar to the division method), or it could be that converting CBF values to Z-scores simply does not delineate perfusion changes as clearly.

C.7.4 Normalizing White Matter Mean and Standard Deviation

Previous methods included calculating mean CBF for the entire brain; however, white matter and grey matter have different perfusion ranges. Thus, calculating one global mean is not truly representative of either of these distinct tissue types. From the previous postictal ASL study, it was initially thought that focal postictal perfusion changes should not occur in the white matter and only grey matter was expected to be hypoperfused. Extrapolating from this assumption, normalizing based on the consistency of white matter can be used to globally shift the grey matter into the same intensity ranges to further identify focal perfusion changes. The idea was to see if there are any global differences in the white matter of the two scans; if there was, then a scaling factor would be determined and applied directly to the grey matter to globally shift the values.

Postictal and baseline CBF maps were registered into a collective space. The Hounsfield units of the anatomical average map has a consistent range throughout the entire white matter. Thus, using the anatomical average map, a white matter mask was produced by thresholding

between 0 – 20 CBF units for each dataset resulting in the white matter being isolated. The mean and standard deviation of the white matter for baseline (M1) and postictal (M2) CBF maps were calculated. The difference in means (ΔM) was calculated and used as a scaling factor to shift the grey matter of the postictal CBF data to the baseline CBF data ($\Delta M = M1 - M2$). Images were then subtracted, smoothed, and given a cluster filter. The global differences between the white matter were minimal, and thus did not serve well as a scaling factor for grey matter changes. Results from this method were similar to a direct subtraction with no intensity normalization applied.

C.7.5 Revisiting ASL data: Cases of Postictal Hyperperfusion

After establishing that performing intensity normalization based on global mean and standard deviation was advantageous, the subtraction ASL data from a previous study from the Federico laboratory was briefly revisited. There were two patients in the ASL cohort that showed post-ictal hyperperfusion because a subtraction of baseline minus postictal gave a null result, however a subtraction of postictal minus baseline resulted in observable perfusion differences. Although the pipelines are slightly different, the CTP pipeline was adjusted to suit the ASL data for reanalyzing these two cases.

Figure C.3A shows the original figure with postictal hyperperfusion resulting from the ASL pipeline (Gaxiola-Valdez, et al., 2017). Figure C.3B shows the ASL results using the adjusted CTP pipeline, where no intensity normalization was performed. Through this modified pipeline, performing a baseline minus postictal subtraction showed no significant CBF changes, but postictal minus baseline revealed regions of hyperperfusion similar to the original analysis. Figure C.3.C shows the results of running the CTP pipeline on the ASL data with intensity

normalization. Interestingly, the previously observed areas of hyperperfusion are eliminated, and performing the baseline minus postictal subtraction resulted in a small cluster of hypoperfusion in the frontal region, which is concordant with the presumed SOZ. This suggests that the patients potentially displaying postictal hyperperfusion may not be doing so, and that the dynamic range of resting CBF values can influence the subtraction pipeline. To account for these baseline fluctuations, a form of intensity normalization should be considered.

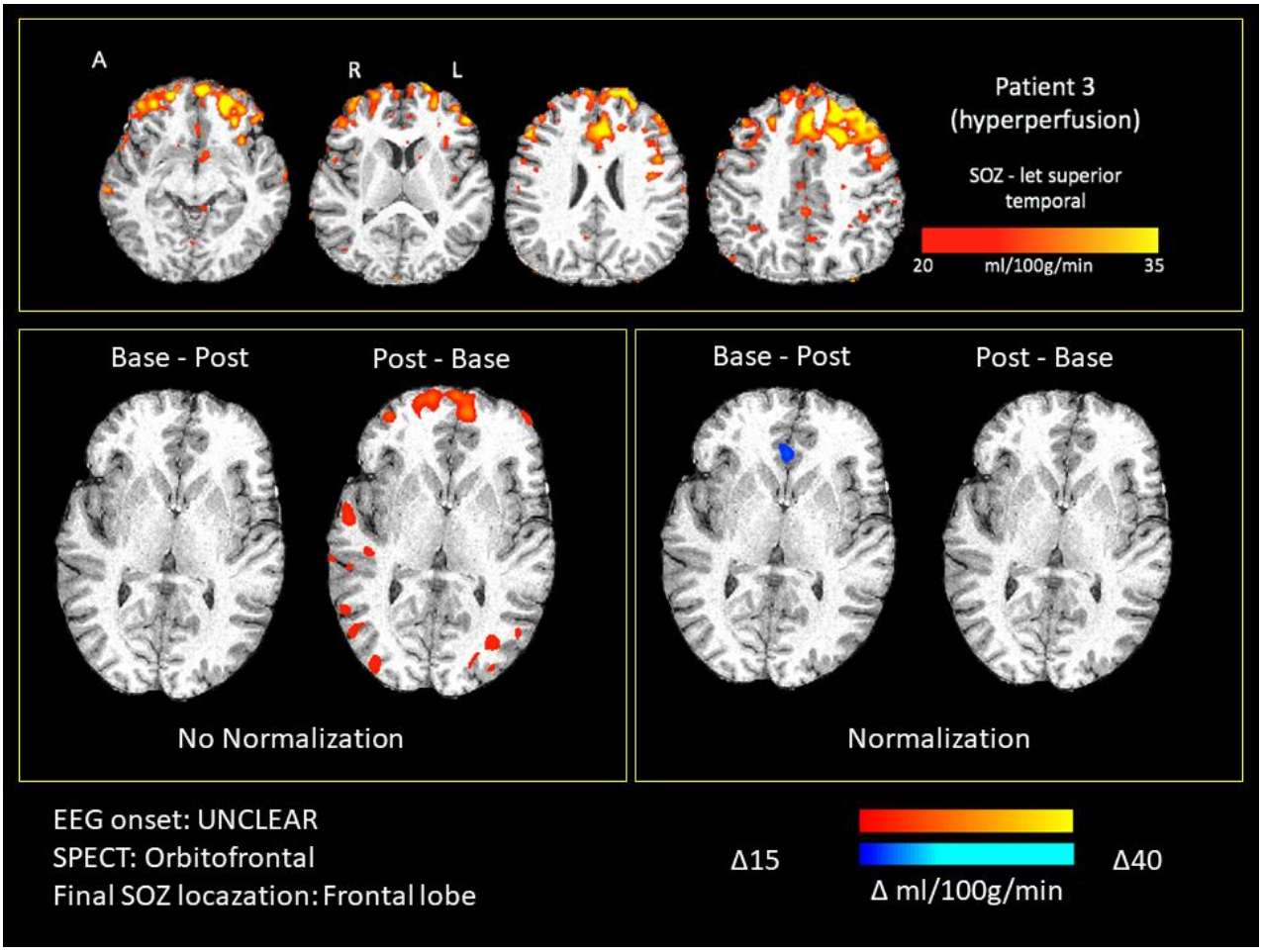

Figure C.3: A patient classified as displaying postictal hyperperfusion was reanalyzed and intensity normalization was performed. A. The original figure displaying patient 3 showing postictal hyperperfusion. B. The results of the modified CTP pipeline on the ASL data without normalization, showing similar changes to the original. C. The results of performing intensity normalization on ASL data. Hyperperfusion clusters were eliminated and instead, hypoperfusion corresponding to a similar region as the clinical consensus was observed.

C.7.6 Summary and Conclusion of Normalizing

Intensity normalization is common in pre- and post-processing image studies and there may be a more complex model to better perform a similar function. For this project, normalizing based on global CBF mean and standard deviation provided the optimal results in accounting for fluctuating baseline CBF values and highlighting perfusion differences.

C.8 Overall Pipeline Conclusion

In summary, a number of variations in the analysis of post-processing CTP images were investigated. In the end, the CTP pipeline used in this thesis involved the following steps:

1. CBF maps were given a global threshold of a minimum of 0 CBF units and maximum of 100 CBF units.
2. Postictal CBF intensities were normalized to the global mean and standard deviation of the baseline CBF intensities.
3. Postictal CBF data were spatially registered to the baseline data by first registering the postictal anatomical average map to the baseline average map, producing a transformation matrix, and applying that matrix to the postictal CBF data.
4. A mask of hyperintense vessels and ventricles of each CBF scan was created.
5. CBF maps were smoothed using a 6 mm FWHM Gaussian filter. Patients with very small perfusion changes used 5 mm smoothing as needed.
6. A voxel-by-voxel based subtraction analysis was performed: Baseline CBF minus postictal CBF
7. Vessels and ventricles were removed from the subtraction map using the mask created from step 4.
8. Cluster filtering was applied at a threshold value of 15 and cluster size threshold of 400 voxels.

Many of these steps can be further optimized, particularly registration or method of intensity normalization. The current pipeline provides confidence that the phenomenon of

postictal hypoperfusion can be quantitatively detected using CTP and provides the framework for further post-processing optimization.

References

Abend, N.S., Dlugos, D.J., Zhu, X., Schwartz, E.S. (2015) Utility of CT-compatible EEG electrodes in critically ill children. Pediatr Radiol, 45:714-8.

Abou-Khalil, B.W. (2010) When should corpus callosotomy be offered as palliative therapy? Epilepsy Curr, 10:9-10.

Abou-Khalil, B.W., Siegel, G.J., Sackellares, J.C., Gilman, S., Hichwa, R., Marshall, R. (1987) Positron emission tomography studies of cerebral glucose metabolism in chronic partial epilepsy. Ann Neurol, 22:480-6.

Altrichter, S., Pendse, N., Wissmeyer, M., Jagersberg, M., Federspiel, A., Viallon, M., Seeck, M., Lovblad, K.O. (2009) Arterial spin-labeling demonstrates ictal cortical hyperperfusion in epilepsy secondary to hemimegalencephaly. J Neuroradiol, 36:303-5.

Asadi-Pooya, A.A., Sharan, A., Nei, M., Sperling, M.R. (2008) Corpus callosotomy. Epilepsy Behav, 13:271-8.

Berg, A.T., Berkovic, S.F., Brodie, M.J., Buchhalter, J., Cross, J.H., van Emde Boas, W., Engel, J., French, J., Glauser, T.A., Mathern, G.W., Moshe, S.L., Nordli, D., Plouin, P., Scheffer, I.E. (2010) Revised terminology and concepts for organization of seizures and epilepsies: report of the ILAE Commission on Classification and Terminology, 2005-2009. Epilepsia, 51:676-85.

Berkovic, S.F., Mulley, J.C., Scheffer, I.E., Petrou, S. (2006) Human epilepsies: interaction of genetic and acquired factors. Trends Neurosci, 29:391-397.

Bien, C.G., Szinay, M., Wagner, J., Clusmann, H., Becker, A.J., Urbach, H. (2009) Characteristics and surgical outcomes of patients with refractory magnetic resonance imaging-negative epilepsies. Arch Neurol, 66:1491-9.

Boas, F.E., Fleishmann, D. (2012) CT Artifacts: Causes and reduction techniques. Imaging in medicine.

Boscolo Galazzo, I., Storti, S.F., Del Felice, A., Pizzini, F.B., Arcaro, C., Formaggio, E., Mai, R., Chappell, M., Beltramello, A., Manganotti, P. (2015) Patient-specific detection of cerebral blood flow alterations as assessed by arterial spin labeling in drug-resistant epileptic patients. PLoS One, 10:e0123975.

Brahim, A., Ramirez, J., Gorriz, J.M., Khedher, L., Salas-Gonzalez, D. (2015) Comparison between Different Intensity Normalization Methods in 123I-Ioflupane Imaging for the Automatic Detection of Parkinsonism. PLoS One, 10:e0130274.

Bromfield, E.B., Cavazos, J.E., Sirven, J.I. (2006) An introduction to epilepsy. West Hartfort. American Epilepsy Society.

Cao, H., Sen, P.K., Peery, A.F., Dellon, E.S. (2016) Assessing agreement with multiple raters on correlated kappa statistics. Biom J, 58:935-43.

Choy, M., Wells, J.A., Thomas, D.L., Gadian, D.G., Scott, R.C., Lythgoe, M.F. (2010) Cerebral blood flow changes during pilocarpine-induced status epilepticus activity in the rat hippocampus. Exp Neurol, 225:196-201.

Coolens, C., Childs, P.J. (2003) Calibration of CT Hounsfield units for radiotherapy treatment planning of patients with metallic hip prostheses: the use of the extended CT-scale. Phys Med Biol, 48:1591-603.

d'Esterre, C.D. (2013) Improving acute stroke management with CT perfusion imaging: Approaches to treatment guidance and brain tissue salvage: University of Western Ontario.

Das, R.R., Lucey, B.P., Chou, S.H., Espinosa, P.S., Zamani, A.A., Dworetzky, B.A., Bromfield, E.B., Lee, J.W. (2009) The utility of conductive plastic electrodes in prolonged ICU EEG monitoring. Neurocrit Care, 10:368-72.

de Lucas, E.M., Sanchez, E., Gutierrez, A., Mandly, A.G., Ruiz, E., Florez, A.F., Izquierdo, J., Arnaiz, J., Piedra, T., Valle, N., Banales, I., Quintana, F. (2008) CT protocol for acute stroke: tips and tricks for general radiologists. Radiographics, 28:1673-87.

de Tisi, J., Bell, G.S., Peacock, J.L., McEvoy, A.W., Harkness, W.F., Sander, J.W., Duncan, J.S. (2011) The long-term outcome of adult epilepsy surgery, patterns of seizure remission, and relapse: a cohort study. Lancet, 378:1388-95.

Devous, M.D., Sr., Thisted, R.A., Morgan, G.F., Leroy, R.F., Rowe, C.C. (1998) SPECT brain imaging in epilepsy: a meta-analysis. J Nucl Med, 39:285-93.

Di Bonaventura, C., Bonini, F., Fattouch, J., Mari, F., Petrucci, S., Carni, M., Tinelli, E., Pantano, P., Bastianello, S., Maraviglia, B., Manfredi, M., Prencipe, M., Giallonardo, A.T. (2009) Diffusion-weighted magnetic resonance imaging in patients with partial status epilepticus. Epilepsia, 50 Suppl 1:45-52.

Duncan, J.S., Sander, J.W., Sisodiya, S.M., Walker, M.C. (2006) Adult epilepsy. Lancet, 367:1087-100.

Duncan, R., Patterson, J., Roberts, R., Hadley, D.M., Bone, I. (1993) Ictal/postictal SPECT in the pre-surgical localisation of complex partial seizures. J Neurol Neurosurg Psychiatry, 56:141-8.

Duncan, S., Gillen, G., Adams, F.G., Duncan, R., Brodie, M.J. (1992) Interictal HM-PAO SPECT: a routine investigation in patients with medically intractable complex partial seizures? Epilepsy Res, 13:83-7.

Dymond, A.M., Crandall, P.H. (1976) Oxygen availability and blood flow in the temporal lobes during spontaneous epileptic seizures in man. Brain Res, 102:191-6.

Engel, J., Jr., Brown, W.J., Kuhl, D.E., Phelps, M.E., Mazziotta, J.C., Crandall, P.H. (1982) Pathological findings underlying focal temporal lobe hypometabolism in partial epilepsy. Ann Neurol, 12:518-28.

Engel, J., Jr., Wiebe, S., French, J., Sperling, M., Williamson, P., Spencer, D., Gumnit, R., Zahn, C., Westbrook, E., Enos, B. (2003) Practice parameter: temporal lobe and localized neocortical resections for epilepsy. Epilepsia, 44:741-51.

Fabene, P.F., Marzola, P., Sbarbati, A., Bentivoglio, M. (2003) Magnetic resonance imaging of changes elicited by status epilepticus in the rat brain: diffusion-weighted and T2-weighted images, regional blood volume maps, and direct correlation with tissue and cell damage. Neuroimage, 18:375-89.

Farrell, F.W., Jr., Taveras, J.M. (1974) Angiographic stain produced by seizures. Neuroradiology, 8:49-53.

Farrell, J.S., Colangeli, R., Wolff, M.D., Wall, A.K., Phillips, T.J., George, A., Federico, P., Teskey, G.C. (2017) Postictal hypoperfusion/hypoxia provides the foundation for a

unified theory of seizure-induced brain abnormalities and behavioral dysfunction. Epilepsia, 58:1493-1501.

Farrell, J.S., Gaxiola-Valdez, I., Wolff, M.D., David, L.S., Dika, H.I., Geeraert, B.L., Rachel Wang, X., Singh, S., Spanswick, S.C., Dunn, J.F., Antle, M.C., Federico, P., Teskey, G.C. (2016) Postictal behavioural impairments are due to a severe prolonged hypoperfusion/hypoxia event that is COX-2 dependent. Elife, 5.

Feichtinger, M., Eder, H., Holl, A., Korner, E., Zmugg, G., Aigner, R., Fazekas, F., Ott, E. (2007) Automatic and remote controlled ictal SPECT injection for seizure focus localization by use of a commercial contrast agent application pump. Epilepsia, 48:1409-13.

Fisher, R.S., Cross, J.H., D'Souza, C., French, J.A., Haut, S.R., Higurashi, N., Hirsch, E., Jansen, F.E., Lagae, L., Moshe, S.L., Peltola, J., Roulet Perez, E., Scheffer, I.E., Schulze-Bonhage, A., Somerville, E., Sperling, M., Yacubian, E.M., Zuberi, S.M. (2017) Instruction manual for the ILAE 2017 operational classification of seizure types. Epilepsia, 58:531-542.

Fisher, R.S., Schachter, S.C. (2000) The postictal state: a neglected entity in the management of epilepsy. Epilepsy Behav, 1:52-9.

Gaxiola-Valdez, I., Singh, S., Perera, T., Sandy, S., Li, E., Federico, P. (2017) Seizure onset zone localization using postictal hypoperfusion detected by arterial spin labelling MRI. Brain, 140:2895-2911.

Gelfand, J.M., Wintermark, M., Josephson, S.A. (2010) Cerebral perfusion-CT patterns following seizure. Eur J Neurol, 17:594-601.

Gibbs, F.A.L., W. G.; Gibbs, E. L. (1934) Cerebral blood flow preceding and accompnaying epiletic seizures in man. Archives of Neurology and Psychiatry, 32:257-272.

Goffin, K., Dedeurwaerdere, S., Van Laere, K., Van Paesschen, W. (2008) Neuronuclear assessment of patients with epilepsy. Semin Nucl Med, 38:227-39.

Grond, M., von Kummer, R., Sobesky, J., Schmulling, S., Rudolf, J., Terstegge, K., Heiss, W. (2000) Early x-ray hypoattenuation of brain parenchyma indicates extended critical hypoperfusion in acute stroke. Stroke, 31:133-9.

Guo, X., Xu, S., Wang, G., Zhang, Y., Guo, L., Zhao, B. (2015) Asymmetry of cerebral blood flow measured with three-dimensional pseudocontinuous arterial spin-labeling mr imaging in temporal lobe epilepsy with and without mesial temporal sclerosis. J Magn Reson Imaging, 42:1386-97.

Hauf, M., Slotboom, J., Nirkko, A., von Bredow, F., Ozdoba, C., Wiest, R. (2009) Cortical regional hyperperfusion in nonconvulsive status epilepticus measured by dynamic brain perfusion CT. AJNR Am J Neuroradiol, 30:693-8.

Hendrikse, J., Petersen, E.T., Golay, X. (2012) Vascular disorders: insights from arterial spin labeling. Neuroimaging Clin N Am, 22:259-69, x-xi.

Ho, S.S., Berkovic, S.F., McKay, W.J., Kalnins, R.M., Bladin, P.F. (1996) Temporal lobe epilepsy subtypes: differential patterns of cerebral perfusion on ictal SPECT. Epilepsia, 37:788-95.

Hufnagel, A., Weber, J., Marks, S., Ludwig, T., De Greiff, A., Leonhardt, G., Widmann, G., Stolke, D., Forsting, M. (2003) Brain diffusion after single seizures. Epilepsia, 44:54-63.

Immonen, A., Jutila, L., Muraja-Murro, A., Mervaala, E., Aikia, M., Lamusuo, S., Kuikka, J., Vanninen, E., Alafuzoff, I., Ikonen, A., Vanninen, R., Vapalahti, M., Kalviainen, R. (2010) Long-term epilepsy surgery outcomes in patients with MRI-negative temporal lobe epilepsy. Epilepsia, 51:2260-9.

International, A. 2011. Standard Guide for Computer Tomography (CT) Imaging.

Janszky, J., Janszky, I., Schulz, R., Hoppe, M., Behne, F., Pannek, H.W., Ebner, A. (2005) Temporal lobe epilepsy with hippocampal sclerosis: predictors for long-term surgical outcome. Brain, 128:395-404.

Kastrup, A., Li, T.Q., Glover, G.H., Moseley, M.E. (1999) Cerebral blood flow-related signal changes during breath-holding. AJNR Am J Neuroradiol, 20:1233-8.

Kim, B.S., Lee, S.T., Yun, T.J., Lee, S.K., Paeng, J.C., Jun, J., Kang, K.M., Choi, S.H., Kim, J.H., Sohn, C.H. (2016) Capability of arterial spin labeling MR imaging in localizing seizure focus in clinical seizure activity. Eur J Radiol, 85:1295-303.

Kim, S.H., Lim, S.C., Kim, J., Son, B.C., Lee, K.J., Shon, Y.M. (2017) Long-term follow-up of anterior thalamic deep brain stimulation in epilepsy: A 11-year, single center experience. Seizure, 52:154-161.

Konig, M. (2003) Brain perfusion CT in acute stroke: current status. Eur J Radiol, 45 Suppl 1:S11-22.

Konstas, A.A., Goldmakher, G.V., Lee, T.Y., Lev, M.H. (2009) Theoretic basis and technical implementations of CT perfusion in acute ischemic stroke, part 2: technical implementations. AJNR Am J Neuroradiol, 30:885-92.

Kwan, P., Sander, J.W. (2004) The natural history of epilepsy: an epidemiological view. J Neurol Neurosurg Psychiatry, 75:1376-81.

la Fougere, C., Rominger, A., Forster, S., Geisler, J., Bartenstein, P. (2009) PET and SPECT in epilepsy: a critical review. Epilepsy Behav, 15:50-5.

Lee, J.J., Lee, S.K., Lee, S.Y., Park, K.I., Kim, D.W., Lee, D.S., Chung, C.K., Nam, H.W. (2008) Frontal lobe epilepsy: clinical characteristics, surgical outcomes and diagnostic modalities. Seizure, 17:514-23.

Lim, Y.M., Cho, Y.W., Shamim, S., Solomon, J., Birn, R., Luh, W.M., Gaillard, W.D., Ritzl, E.K., Theodore, W.H. (2008) Usefulness of pulsed arterial spin labeling MR imaging in mesial temporal lobe epilepsy. Epilepsy Res, 82:183-9.

Luders, H.O., Najm, I., Nair, D., Widdess-Walsh, P., Bingman, W. (2006) The epileptogenic zone: general principles. Epileptic Disord, 8 Suppl 2:S1-9.

Maehara, T., Shimizu, H. (2001) Surgical outcome of corpus callosotomy in patients with drop attacks. Epilepsia, 42:67-71.

Masterson, K., Vargas, M.I., Delavelle, J. (2009) Postictal deficit mimicking stroke: role of perfusion CT. J Neuroradiol, 36:48-51.

Mathews, M.S., Smith, W.S., Wintermark, M., Dillon, W.P., Binder, D.K. (2008) Local cortical hypoperfusion imaged with CT perfusion during postictal Todd's paresis. Neuroradiology, 50:397-401.

Mayer, T.E., Hamann, G.F., Baranczyk, J., Rosengarten, B., Klotz, E., Wiesmann, M., Missler, U., Schulte-Altedorneburg, G., Brueckmann, H.J. (2000) Dynamic CT perfusion imaging of acute stroke. AJNR Am J Neuroradiol, 21:1441-9.

McHugh, M.L. (2012) Interrater reliability: the kappa statistic. Biochem Med (Zagreb), 22:276-82.

McIntosh, A.M., Kalnins, R.M., Mitchell, L.A., Fabinyi, G.C., Briellmann, R.S., Berkovic, S.F. (2004) Temporal lobectomy: long-term seizure outcome, late recurrence and risks for seizure recurrence. Brain, 127:2018-30.

Meldrum, B.S., Nilsson, B. (1976) Cerebral blood flow and metabolic rate early and late in prolonged epileptic seizures induced in rats by bicuculline. Brain, 99:523-42.

Michalak, Z., Lebrun, A., Di Miceli, M., Rousset, M.C., Crespel, A., Coubes, P., Henshall, D.C., Lerner-Natoli, M., Rigau, V. (2012) IgG leakage may contribute to neuronal dysfunction in drug-refractory epilepsies with blood-brain barrier disruption. J Neuropathol Exp Neurol, 71:826-38.

Michalak, Z., Obari, D., Ellis, M., Thom, M., Sisodiya, S.M. (2017) Neuropathology of SUDEP: Role of inflammation, blood-brain barrier impairment, and hypoxia. Neurology, 88:551-561.

Miyaji, Y., Yokoyama, M., Kawabata, Y., Joki, H., Kushi, Y., Yokoi, Y., Sasame, J., Seki, S., Mori, K., Kamide, T., Tamase, A., Shima, H., Nomura, M., Kitamura, Y., Tanaka, F. (2014) Arterial spin-labeling magnetic resonance imaging for diagnosis of late seizure after stroke. J Neurol Sci, 339:87-90.

Morris, G.L., 3rd, Mueller, W.M. (1999) Long-term treatment with vagus nerve stimulation in patients with refractory epilepsy. The Vagus Nerve Stimulation Study Group E01-E05. Neurology, 53:1731-5.

Nakasu, Y., Nakasu, S., Morikawa, S., Uemura, S., Inubushi, T., Handa, J. (1995) Diffusion-weighted MR in experimental sustained seizures elicited with kainic acid. AJNR Am J Neuroradiol, 16:1185-92.

Nelson, K.P., Edwards, D. (2015) Measures of agreement between many raters for ordinal classifications. Stat Med, 34:3116-32.

Newton, M.R., Greenwood, R.J., Britton, K.E., Charlesworth, M., Nimmon, C.C., Carroll, M.J., Dolke, G. (1992) A study comparing SPECT with CT and MRI after closed head injury. J Neurol Neurosurg Psychiatry, 55:92-4.

Nguyen, D., Kapina, V., Seeck, M., Viallon, M., Fedespiel, A., Lovblad, K.O. (2010) Ictal hyperperfusion demonstrated by arterial spin-labeling MRI in status epilepticus. J Neuroradiol, 37:250-1.

Noachtar, S., Borggraefe, I. (2009) Epilepsy surgery: a critical review. Epilepsy Behav, 15:66-72.

Otsubo, H., Hwang, P.A., Gilday, D.L., Hoffman, H.J. (1995) Location of epileptic foci on interictal and immediate postictal single photon emission tomography in children with localization-related epilepsy. J Child Neurol, 10:375-81.

Pendse, N., Wissmeyer, M., Altrichter, S., Vargas, M., Delavelle, J., Viallon, M., Federspiel, A., Seeck, M., Schaller, K., Lovblad, K.O. (2010) Interictal arterial spin-labeling MRI perfusion in intractable epilepsy. J Neuroradiol, 37:60-3.

Penfield, W. (1939) Epilepsy and the Cerebral Lesions of Birth and Infancy. Can Med Assoc J, 41:527-34.

Petcharunpaisan, S., Ramalho, J., Castillo, M. (2010) Arterial spin labeling in neuroimaging. World J Radiol, 2:384-98.

Piliszek, A., Witkowski, G., Sklinda, K., Szary, C., Ryglewicz, D., Dorobek, M., Walecki, J. (2016) Comprehensive imaging of stroke - Looking for the gold standard. Neurol Neurochir Pol, 50:241-50.

Pizzini, F.B., Farace, P., Manganotti, P., Zoccatelli, G., Bongiovanni, L.G., Golay, X., Beltramello, A., Osculati, A., Bertini, G., Fabene, P.F. (2013) Cerebral perfusion alterations in epileptic patients during peri-ictal and post-ictal phase: PASL vs DSC-MRI. Magn Reson Imaging, 31:1001-5.

Pollock, J.M., Deibler, A.R., Whitlow, C.T., Tan, H., Kraft, R.A., Burdette, J.H., Maldjian, J.A. (2009) Hypercapnia-induced cerebral hyperperfusion: an underrecognized clinical entity. AJNR Am J Neuroradiol, 30:378-85.

Regesta, G., Tanganelli, P. (1999) Clinical aspects and biological bases of drug-resistant epilepsies. Epilepsy Res, 34:109-22.

Rigau, V., Morin, M., Rousset, M.C., de Bock, F., Lebrun, A., Coubes, P., Picot, M.C., Baldy-Moulinier, M., Bockaert, J., Crespel, A., Lerner-Natoli, M. (2007) Angiogenesis is associated with blood-brain barrier permeability in temporal lobe epilepsy. Brain, 130:1942-56.

Rosenow, F., Luders, H. (2001) Presurgical evaluation of epilepsy. Brain, 124:1683-700.

Rowe, C.C., Berkovic, S.F., Austin, M.C., McKay, W.J., Bladin, P.F. (1991) Patterns of postictal cerebral blood flow in temporal lobe epilepsy: qualitative and quantitative analysis. Neurology, 41:1096-103.

Royter, V., Paletz, L., Waters, M.F. (2008) Stroke vs. status epilepticus. A case report utilizing CT perfusion. J Neurol Sci, 266:174-6.

Ryvlin, P., Bouvard, S., Le Bars, D., De Lamerie, G., Gregoire, M.C., Kahane, P., Froment, J.C., Mauguiere, F. (1998) Clinical utility of flumazenil-PET versus [18F]fluorodeoxyglucose-PET and MRI in refractory partial epilepsy. A prospective study in 100 patients. Brain, 121 (Pt 11):2067-81.

Salmenpera, T.M., Duncan, J.S. (2005) Imaging in epilepsy. J Neurol Neurosurg Psychiatry, 76 Suppl 3:iii2-iii10.

Sanelli, P.C., Lev, M.H., Eastwood, J.D., Gonzalez, R.G., Lee, T.Y. (2004) The effect of varying user-selected input parameters on quantitative values in CT perfusion maps. Acad Radiol, 11:1085-92.

Schmidt, D., Schachter, S.C. (2014) Drug treatment of epilepsy in adults. BMJ, 348:g254.

Shelly, S., Maggio, N., Boxer, M., Blatt, I., Tanne, D., Orion, D. (2017) Computed Tomography Perfusion Maps Reveal Blood Flow Dynamics in Postictal Patients: A Novel Diagnostic Tool. Isr Med Assoc J, 19:553-556.

Shin, W.C., Hong, S.B., Tae, W.S., Kim, S.E. (2002) Ictal hyperperfusion patterns according to the progression of temporal lobe seizures. Neurology, 58:373-80.

Sierra-Marcos, A., Carreno, M., Setoain, X., Lopez-Rueda, A., Aparicio, J., Donaire, A., Bargallo, N. (2016) Accuracy of arterial spin labeling magnetic resonance imaging (MRI) perfusion in detecting the epileptogenic zone in patients with drug-resistant neocortical epilepsy: comparison with electrophysiological data, structural MRI, SISCOM and FDG-PET. Eur J Neurol, 23:160-7.

Sillanpaa, M. (2000) Long-term outcome of epilepsy. Epileptic Disord, 2:79-88.

Spanaki, M.V., Spencer, S.S., Corsi, M., MacMullan, J., Seibyl, J., Zubal, I.G. (1999) Sensitivity and specificity of quantitative difference SPECT analysis in seizure localization. J Nucl Med, 40:730-6.

Spencer, S., Huh, L. (2008) Outcomes of epilepsy surgery in adults and children. Lancet Neurol, 7:525-37.

Spencer, S.S., Berg, A.T., Vickrey, B.G., Sperling, M.R., Bazil, C.W., Shinnar, S., Langfitt, J.T., Walczak, T.S., Pacia, S.V., Multicenter Study of Epilepsy, S. (2005) Predicting long-term seizure outcome after resective epilepsy surgery: the multicenter study. Neurology, 65:912-8.

Stefan, H., Bauer, J., Feistel, H., Schulemann, H., Neubauer, U., Wenzel, B., Wolf, F., Neundorfer, B., Huk, W.J. (1990) Regional cerebral blood flow during focal seizures of temporal and frontocentral onset. Ann Neurol, 27:162-6.

Stewart, S.B., Koller, J.M., Campbell, M.C., Perlmutter, J.S., Black, K.J. (2015) Additive global cerebral blood flow normalization in arterial spin labeling perfusion imaging. PeerJ, 3:e834.

Storti, S.F., Boscolo Galazzo, I., Del Felice, A., Pizzini, F.B., Arcaro, C., Formaggio, E., Mai, R., Manganotti, P. (2014) Combining ESI, ASL and PET for quantitative assessment of drug-resistant focal epilepsy. Neuroimage, 102 Pt 1:49-59.

Sugita, K., Kamida, T., Matsuta, H., Shimomura, T., Fujiki, M. (2014) Usefulness of pulsed arterial spin-labeling MRI for localizing a seizure focus: a surgical case. Seizure, 23:318-20.

Takano, A., Shiga, T., Kobayashi, J., Adachi, I., Nakamura, F., Koyama, T., Katoh, C., Morita, K., Tsukamoto, E., Tamaki, N. (2001) Thalamic asymmetry on interictal SPECT in patients with frontal lobe epilepsy. Nucl Med Commun, 22:319-24.

Tang, W., Hu, J., Zhang, H., Wu, P., He, H. (2015) Kappa coefficient: a popular measure of rater agreement. Shanghai Arch Psychiatry, 27:62-7.

Tao, J.X., Baldwin, M., Hawes-Ebersole, S., Ebersole, J.S. (2007) Cortical substrates of scalp EEG epileptiform discharges. J Clin Neurophysiol, 24:96-100.

Tao, J.X., Ray, A., Hawes-Ebersole, S., Ebersole, J.S. (2005) Intracranial EEG substrates of scalp EEG interictal spikes. Epilepsia, 46:669-76.

Tellez-Zenteno, J.F., Dhar, R., Wiebe, S. (2005) Long-term seizure outcomes following epilepsy surgery: a systematic review and meta-analysis. Brain, 128:1188-98.

Van Paesschen, W. (2004) Ictal SPECT. Epilepsia, 45 Suppl 4:35-40.

Van Paesschen, W., Dupont, P., Van Heerden, B., Vanbilloen, H., Mesotten, L., Maes, A., Van Driel, G., Mortelmans, L. (2000) Self-injection ictal SPECT during partial seizures. Neurology, 54:1994-7.

van Vliet, E.A., da Costa Araujo, S., Redeker, S., van Schaik, R., Aronica, E., Gorter, J.A. (2007) Blood-brain barrier leakage may lead to progression of temporal lobe epilepsy. Brain, 130:521-34.

Wall, A.K. (2017) Seizure-induced brainstem hypoxia as a possible mechanism of sudden unexpected death in epilepsy: University of Calgary.

Wang, Y., Majors, A., Najm, I., Xue, M., Comair, Y., Modic, M., Ng, T.C. (1996) Postictal alteration of sodium content and apparent diffusion coefficient in epileptic rat brain induced by kainic acid. Epilepsia, 37:1000-6.

Weil, S., Noachtar, S., Arnold, S., Yousry, T.A., Winkler, P.A., Tatsch, K. (2001) Ictal ECD-SPECT differentiates between temporal and extratemporal epilepsy: confirmation by excellent postoperative seizure control. Nucl Med Commun, 22:233-7.

Weinand, M.E., Carter, L.P., el-Saadany, W.F., Sioutos, P.J., Labiner, D.M., Oommen, K.J. (1997) Cerebral blood flow and temporal lobe epileptogenicity. J Neurosurg, 86:226-32.

Wiest, R., von Bredow, F., Schindler, K., Schauble, B., Slotboom, J., Brekenfeld, C., Remonda, L., Schroth, G., Ozdoba, C. (2006) Detection of regional blood perfusion changes in epileptic seizures with dynamic brain perfusion CT--a pilot study. Epilepsy Res, 72:102-10.

Wolf, R.L., Alsop, D.C., Levy-Reis, I., Meyer, P.T., Maldjian, J.A., Gonzalez-Atavales, J., French, J.A., Alavi, A., Detre, J.A. (2001) Detection of mesial temporal lobe hypoperfusion in patients with temporal lobe epilepsy by use of arterial spin labeled perfusion MR imaging. AJNR Am J Neuroradiol, 22:1334-41.

Yarnell, P.R. (1975) Todd's paralysis: A cerebrovascular phenomenon? Stroke, 6:301-3.

Yune, M.J., Lee, J.D., Ryu, Y.H., Kim, D.I., Lee, B.I., Kim, S.J. (1998) Ipsilateral thalamic hypoperfusion on interictal SPECT in temporal lobe epilepsy. J Nucl Med, 39:281-5.

Zaknun, J.J., Bal, C., Maes, A., Tepmongkol, S., Vazquez, S., Dupont, P., Dondi, M. (2008) Comparative analysis of MR imaging, ictal SPECT and EEG in temporal lobe epilepsy: a prospective IAEA multi-center study. Eur J Nucl Med Mol Imaging, 35:107-15.

Zhong, J., Petroff, O.A., Prichard, J.W., Gore, J.C. (1995) Barbiturate-reversible reduction of water diffusion coefficient in flurothyl-induced status epilepticus in rats. Magn Reson Med, 33:253-6.

Ziegelitz, D., Starck, G., Mikkelsen, I.K., Tullberg, M., Edsbagge, M., Wikkelso, C., Forssell-Aronson, E., Holtas, S., Knutsson, L. (2009) Absolute quantification of cerebral blood flow in neurologically normal volunteers: dynamic-susceptibility contrast MRI-perfusion compared with computed tomography (CT)-perfusion. Magn Reson Med, 62:56-65.